MANGANESE BASED OXIDATIVE TECHNOLOGIES FOR WATER/WASTEWATER TREATMENT

A Dissertation

by

ISHAN DESAI

Submitted to the Office of Graduate and Professional Studies of
Texas A&M University
in partial fulfillment of the requirements for the degree of

DOCTOR OF PHILOSOPHY

Chair of Committee,	Bryan Boulanger
Co-Chair of Committee,	Bill Batchelor
Committee Members,	Karthi Karthikeyan
	Thomas McDonald
	Marc Mills
	Julian Sandino
Head of Department,	Robin Autenrieth

December 2013

Major Subject: Civil Engineering

ABSTRACT

Manganese is a commonly occurring mineral found in soil and sediments that takes part in chemical reactions in groundwater and soil systems. It plays a significant role in controlling the environmental fate and transport of organic and inorganics by facilitating redox reactions. The reactivity of manganese oxides with some emerging contaminants like 4-tert octylphenol (OP) in aqueous systems is yet to be explored. Additionally, manganese's use within treatment systems designed to remove trace organics is yet to be fully developed.

This research work explores the reactivity of manganese oxide to degrade OP in aqueous systems. The rate equation has been determined by conducting experiments at various conditions of oxide and organic loading as well as different pH's. The reaction order was found to be ≈ 1.1 for both oxide as well as the organic. The reactivity was much higher under acidic conditions. The presence of metals and humic acids greatly reduced the reactivity. The primary reaction by-product observed in the system was 4-(2,4,4-trimethylpentan-2yl)benzene-1,2-diol. Magnetic manganese ferrites were further created in the laboratory using a novel combustion method in order to blend the catalytic properties of manganese with the magnetic and structural properties of ferrites. These laboratory prepared catalysts were thoroughly characterized using XRD, SEM, TEM, HR-TEM, and BET. Their magnetic properties have also been studied. These manganese ferrites offer the potential to enhance hydroxyl radical production within catalytic ozonation systems. Thus their catalyst effectiveness was determined by measuring R_{ct},

ozone exposure, hydroxyl radical production, and ozone decomposition. The effect of catalyst type, catalyst dosage, pre-ozonation, pH, and presence of dissolved organic matter (DOM) on the hydroxyl radical production during catalytic ozonation was also explored. An increase in ozone dosage, catalyst dosage, and PVA content enhanced organic removal in the system. Organic removal was lower at a decreased system pH, in the presence of DOM, and with increasing levels of Mn incorporated into the catalyst. Pre-ozonation of the catalyst at lower dosages did not have an effect on the system, though extensive pre-ozonation greatly reduced catalyst activity. Overall, R_{ct} and organic removal were not correlated.

To my family

ACKNOWLEDGEMENTS

I would first of all like to express my deep gratitude to my advisor Dr. Bryan Boulanger for his guidance and supervision throughout the research project. I gratefully acknowledge him for the freedom and flexibility that he gave me in performing my research. He has always provided attention to my research and my wellbeing and has always supported me in various ways when I needed him. I would also like to thank my family: my mother, my father and my wife Unnati, for encouraging me to pursue research. Thanks to my Grandma, Uncle, Aunt, Kunal, and my extended family for loving and caring for me.

Dr. Bill Batchelor, Dr. Thomas McDonald, Dr. R. Karthikeyan, Dr. Marc Mills and Dr. Julian Sandino kindly served on my committee. Dr. Batchelor has always inspired me through his excellent teaching. Special thanks to Dr. McDonald for letting me use his facilities during the early part of my PhD. I am also grateful to Dr. R. Karthikeyan for all his valuable advice and support. Dr. Sandino's continual support and interest is greatly appreciated. I would extend my heartfelt thanks to Dr. Marc Mills who mentored me during my research participation at US EPA. I thank him for all his support and acknowledge him for the faith he had in me.

Many a thanks to Dr. Michael Elovitz for some great discussions and advice he provided on my work. He has helped me to understand approaching a problem in so many different ways. Thanks also to Dr. Mallikarjuna Nadagouda for helping me with

some particle characterization work. Dr. Raghuraman Venkatapathy and Adam Balz's help in the laboratory is also greatly appreciated.

A number of fellow students and associates contributed to this work through their support and friendship. Thanks to Dr. Pranav Nagarnaik, Dr. Kavitha Dasu, Dr. Ruth Marfil-Vega, Kidus Tadele, and Brian Crone, for all their help in the laboratory and/or their willingness to share ideas related to the project.

Financial support from the Oak Ridge Institute of Science and Engineering (ORISE) is gratefully acknowledged.

NOMENCLATURE

pCBA	p-chlorobenzoic acid
PVA	Polyvinyl alcohol
CI	Confidence Interval
SOP	Standard Operating Procedure
XPS	X-ray photoelectron spectroscopy
XRD	X-Ray Diffraction
SEM	Scanning electron microscope
TEM	Tunneling electron microscope
UV/Vis	Ultraviolet–visible spectroscopy
FTIR	Fourier Transform Infrared Spectroscopy
BET	Brunauer-Emmett-Teller
GC	Gas chromatography
LC	Liquid chromatography
ICP	Inductively coupled plasma
MS	Mass spectrometry
QTOF	Quadrupole time-of-flight mass
HPLC	High-performance liquid chromatography
OP	Octylphenol
AP	Alkylphenol
APEO	Alkylphenol ethoxylate

NP	Nonylphenol
OPEO	Octylphenol ethoxylate
NPEO	Nonylphenol ethoxylate
DI Water	Deionized water
WWTP	Waste water treatment plant
$MnFe_2O_4$	Manganese ferrite
$NaMnO_4$	Sodium manganate
NaOH	Sodium hydroxide
$MnCl_2$	Manganese chloride
MnO_2	Manganese oxide
N_2	Nitrogen
$NaNO_3$	Sodium nitrate
Ca^{2+}	Calcium (II) ions
Fe^{3+}	Iron (II) ions
Mg^{2+}	Magnesium(II) ions
Cu^{2+}	Copper (II) ions
Mn^{2+}	Manganese (II) ions
Zn^{2+}	Zinc(II) ions
Cr^{3+}	Chromium(III) ions
TiO_2	Titanium dioxide
Al_2O_3	Aluminium oxide
CeO_2	Cerium(II) oxide

SiO_2	Silica
O_3	Ozone
r_{init}	Initial reaction rate
pH_{zpc}	pH of zero point charge
$Mn(NO_3)_2$	Manganese nitrate
$Fe(NO_3)_3$	Iron nitrate
HCl	Hydrochloric acid
H_3PO_4	Phosphoric acid
NOM	Natural organic matter
R_{ct}	$\frac{\int[\cdot OH]dt}{\int[O_3]dt}$
ZFC	Zero field-cooling
FC	Field-cooling

TABLE OF CONTENTS

Page

LIST OF FIGURES

Page

LIST OF TABLES

Page

1. INTRODUCTION

Manganese is a commonly occurring mineral found in soil and sediments that takes part in chemical reactions in groundwater and soil systems (*1*). Manganese is found in several oxidation states in the environment (including +2, +3 and +4) and plays a significant role in controlling the environmental fate and transport of organic and inorganics by facilitating redox reactions.

Catalytic and non-catalytic manganese based oxidative treatment technologies are demonstrated to oxidize phenols (*2*), aniline (*3*), triclosan (*4*), chlorophene (*4*), fluoroquinoline antibacterial agents (*5*), antibacterial N-oxides (*6*), 17-alpha-ethinylestradiol (*7*), estradiol (*8*), lincosamide (*9*), atrazine (*10*), bisphenol A (*11*), tetrabromobisphenol A (*12*), oxytetracycline (*13*), estrogens (*14*), chlorophenols (*15*), pentachlorophenols (*16*), tetrachlorophenols (*17*) and trichlorophenols (*17*) within aqueous systems.

Additionally, manganese based catalysts enhance ·OH radical production in ozonation systems (*18-34*). Enhancing ·OH radical production in ozonation systems provides the benefit of being able to target organics that are recalcitrant to molecular ozone alone.

With the discovery of low amounts of pharmaceuticals and personal care products in drinking water, wastewater effluents, and environmental waters, there is an increased interest in developing catalytic and non-catalytic manganese based treatment systems to target trace organic removal. Therefore, the goal of this PhD research was to

develop a greater understanding of manganese based technologies for removal of trace organics from aqueous solutions. Specifically, this research centered on the use and development of heterogeneous manganese based catalysts for aqueous phase 1) removal of a model recalcitrant trace organic (4-tert alklyphenol) and 2) enhancement of ·OH radicals production during catalytic ozonation (which applies to a broader range of trace organics). Three topics were explored to meet the established goal of this dissertation. The three topics included:

Topic 1: aqueous phase oxidation of 4-tert-octylphenol by manganese oxides

Topic 2: synthesis and characterization of manganese ferrites; and

Topic 3: effectiveness of manganese ferrites as ozonation catalysts

While the three topics stand alone as individual lines of research, the three lines are linked together through the use of manganese based treatment technologies. As a whole, the collective results of this research aid in developing a better understanding of manganese's use within treatment systems designed to remove trace organics. Additionally, each investigation helps clarify the underlying science behind each topic of exploration. A brief description of the activities and hypothesis explored within each topic are presented below. Full details of carried out research within each topic are found in the subsequent chapters within this dissertation.

Topic 1 research explored oxidation of 4-tertiary octylphenol (octylphenol, OP) within an aqueous system in the presence of manganese oxide. Topic 1 research was carried out in order to set a foundation for future experimental approaches, while also

addressing the efficacy of using manganese oxides as a treatment technology to remove OP from aqueous systems. OP was selected as the model trace organic target compound for Topic 1 research because OP is an endocrine active detergent metabolite that has been widely observed and reported in treated effluents and environmental waters.

The *primary hypothesis* explored during **Topic 1** research is that *manganese oxide removes OP from aqueous systems through oxidation and the removal is dependent on various factors including pH, temperature and ionic strength.* Therefore, the effect of pH, temperature, ionic strength, reaction kinetics, and metabolite formation when OP reacts with manganese oxides was evaluated. Finally, the effect of co-solutes (humic acid and metals) on the reaction was examined. Topic 1 research will be submitted as a paper to *Chemosphere* entitled, "Oxidation of 4-tertiary octylphenol by manganese oxides in aqueous solutions" in Chapter 2.

Topic 2 research explored the synthesis and characterization of magnetic manganese ferrites. The purpose of creating the magnetic manganese ferrites was for their planned use as ozonation catalysts. Their magnetic properties allow for their recovery from the treatment system. Magnetic manganese ferrites were prepared by mixing manganese nitrate and iron nitrate in a stoichiometric ratio of 1:2. Polyvinyl alcohol was added to the mixed metal salt solution and the ratio of PVA: total nitrate salt added was varied from 1:1 up to 1:2 by weight.

The *primary hypothesis* explored during **Topic 2** research is that *PVA is required to create magnetic manganese ferrites.* The resulting particles were characterized by X-Ray diffraction (XRD), X-ray photoelectron spectroscopy (XPS), scanning electron

microscope (SEM), tunneling electron microscope (TEM), and Ultraviolet–Visible spectroscopy (UV/Vis). Topic 2 research will be submitted as a paper to the Journal of Nanoparticle Research entitled, "Synthesis and characterization of magnetic manganese ferrites using a combustion method" in Chapter 3. A four page extended abstract for Topic 2 research was submitted to and presented at the TechConnect World Summit and Innovation Conference 2013 in Washington DC in May of 2013.

Research carried out in support of **Topic 3** evaluated the effectiveness of the use of the prepared magnetic manganese ferrites as ozonation catalysts by exploring the ratio of ·OH exposure to the O_3 exposure $[\frac{\int[\cdot OH]dt}{\int[O3]dt}]$ (also referred to as R_{ct}) generated in an ozonation system with and without the catalysts present. The research postulated that generation of higher R_{ct} values using the catalysts would demonstrate higher rates of hydroxyl radical production. Therefore, the *primary hypothesis* explored during **Topic 3** research is that *the magnetic manganese ferrites increase* R_{ct}.

Topic 3 research focused on the ability of novel magnetic manganese ferrite catalysts to transform ozone into hydroxyl radicals and evaluated the effect of catalyst type, catalyst dosage, pre-ozonation of the catalysts, system pH, and humic acid on the transformation efficiency using parachlorobenzoic acid (pCBA) as a probe compound. pCBA is resistant to degradation by ozone, but degrades slowly in the presence of ·OH. Topic 3 research will be submitted as a paper to *Environmental Science & Technology* entitled, "Magnetic manganese ferrites as catalysts during aqueous solution ozonation" in Section 4.

Section 2, 3, and 4 of this dissertation contain complete papers which will be submitted for external publication following peer review. Section 5 presents the overall summary of the combined research, key findings, and interpretations of the research outcomes concerning the initially stated hypotheses explored in this dissertation research.

2. OXIDATION OF 4-TERT-OCTYLPHENOL BY MANGANESE OXIDES IN AQUEOUS SOLUTION (TOPIC 1)

2.1 Introduction

Alkylphenol ethoxylates (APnEO) are a class of non-ionic surfactants that are widely use in the production of plastics, elastomers, textiles, agricultural chemicals, paper, cleaners, and laundering products. Nonylphenol ethoxylate (NPnEO) and octylphenol ethoxylate (OPnEO) are the two most significant groups of APnEOs. Octylphenol (OP) is the main biodegradation product of OPnEO. OP enters the environment predominantly through the degradation and disposal of OPnEO based products. Reported concentrations of OP in environmental waters range from non-detectable to as high as 1440 ng/L in river water (*35*) and 1700 ng/L in treated effluents (*36*) .

Presence of OP in environmental systems is of concern because OP is a biologically active compound that is known to mimic the action of natural hormones in exposed organisms (*37*). In vitro studies have demonstrated the ability of OP to bind with estrogen receptors and alter their functioning in fish, birds and mammals (*38-42*). OP also caused a prolonged suppression of testosterone synthesis and an increase in uterine weight in exposed rats (*43, 44*). Sharpe and his coworkers (*45*) observed the malfunction and malformation of testicular size and sperm production in rats whose mothers were exposed to OP via drinking water during periods of gestation and lactation.

Presence of OP in the environment has led to observed effects on the reproductive systems of aquatic organisms living in water bodies receiving estrogenic wastewater effluents and/or runoff. OP was found to reduce reproductive success of male fish and alter the mating behavior by acting on the neuroendocrine system (*46*). OP was shown to be both genotoxic and estrogenic in fish. The exposed fish showed spermatogenesis with some fish developing oocytes in their testes (*40*). In vitro studies have revealed that OP is 10-20 fold more potent than all the other alkylphenols (*38*). Therefore, developing an understanding of the fate and degradation of OP in the environment is an area of interest because of the noted adverse effects of OP on exposed organisms.

Due to this surfactants low aqueous solubility and a high octanol-water partition coefficient (log K_{ow} = 4.12), OP has a tendency to sorb to soils and sediments (*47, 48*). OP has also been shown to degrade through hydroxide radical reaction, photolysis, UV-photodegradation, and photocatalyic interaction with mineral surfaces. Ning *et al*. studied the reaction kinetics of OP with both molecular ozone and hydroxyl radical and identified reaction products (*49, 50*). OP photolysis was also explored using a solar simulator (*51*). Transformation of OP under UV irradiation is also reported (*52*). Oxidation of OP by photoinduced Fe(III) (*53*), UV/TiO_2 and UV/TiO_2/$S_2O_8^{2-}$ (*54*) and ferrate(VI) (*55*) is also demonstrated in the literature.

While iron and titanium oxides have been demonstrated to oxidize OP, the interaction of OP with manganese oxides is currently not known. However, manganese oxides have been shown to degrade a number of other organic compounds including

phenols (*2*) and substituted phenols (*15, 16, 56*), aniline (*3, 57*), triclosan (*4*), chlorophene (*4*), fluoroquinoline antibacterial agents (*5*), antibacterial N-oxides (*6*) , steroid hormones (*7, 14, 58, 59*), lincosamide (*9*), atrazine (*10*), bisphenol A (*11*), tetrabromobisphenol A (*12*), and oxytetracycline (*13*). The reaction products from these studies were oxidized organic and reduced manganese (Mn^{2+}). Manganese oxides are one of the strongest oxidants available in natural waters, soils, and sediments. Therefore, evaluating the interaction of OP with manganese oxides is important in order to understand the fate and transformation of OPs in environmental waters.

The objective of this study was to evaluate reaction kinetics of manganese oxides with OP. Influence of pH, temperature, and ionic strength on the reaction rate was also evaluated. The effect of humic acid and metal co-solutes on the reaction of OP and manganese oxide was also examined. Finally, research was carried out to identify byproducts of the reaction of OP with manganese oxides.

2.2 Materials and Methods

2.2.1 Chemicals

Sodium permanganate monohydrate (≥97% purity), sodium hydroxide (97% purity), manganese chloride (98% purity), 4-(tert-octyl) phenol (97% purity), and L-ascorbic acid (reagent grade) were purchased from Sigma-Aldrich and used as received. Dichloromethane (OmniSolv, ACS, high purity grade) and methanol (EMD Chemicals, ACS, HPLC Grade) were used for preparing GC/MS standards and spiking solution

respectively. All experiments were performed using reagent-grade water (>18 MΩ-cm resistivity). Solution pH was maintained using acetate (pH 4-5); 3-(N-morpholino)propanesulfonic acid (MOPS) (pH 6.5-8) and 2-(Cyclohexylamino)ethanesulfonic acid (CHES) (pH 9-10) buffer systems.

2.2.2 Preparation and characterization of manganese oxide

Manganese oxide was prepared according to the method described in Murray *et al.* (*60*). Their method details the preparation of the oxide using sodium permanganate and manganese chloride under basic conditions to create a kinetically favored reaction. Briefly, 160 mL of 0.1 M $NaMnO_4$ and 320 ml of 0.1 M NaOH were mixed with 3.28 L of N_2 purged reagent water. 240 mL of 0.1 mM $MnCl_2$ was then added dropwise to this mixture. Manganese oxide particles formed during the reaction were allowed to settle and the supernatant was washed several times and replaced with reagent grade water until the supernatant conductivity fell below 2 μS cm^{-1}. The oxide particles were then stored in suspension within a glass amber bottle at 4°C.

In order to determine the concentration and composition of the oxide particle in suspension, three 1 mL samples were heated until dried and the weight of the particles was recorded. A subsample of the dried oxide was analyzed by an X-ray diffractometer (XRD) and a BET surface analyzer. A Bruker D8 XRD (CuKα radiation; 40 kV, 40 mA) fitted with a LynxEYE detector was used for data collection. The BET surface area was determined by N_2 adsorption using a Beckman Coulter SA 3100 surface area and pore size analyzer.

2.2.3 Analytical methods

The concentration of 4-tert octylphenol (OP) in reaction solutions was determined using a HPLC (Thermo Electron Corporation) equipped with a diode-array detector operating at a UV wavelength of 224 nm. Chromatography was performed on a Hypersil Green PAH (5 µm, 4.6 mm x 100 mm) at a flow rate of 1 mL/min under isocratic conditions with the solvent in the ratio of 70:30 acetonitrile: reagent water containing 0.2% glacial acetic acid. Quantitation was achieved using a five point external calibration curve. Blanks, calibration check standards, and matrix spikes were utilized to ensure quality assurance/quality control of generated concentration data. For product identification, samples were injected into an Accela Ultra-High Pressure Liquid Chromatography (UPLC) system coupled to a heated electrospray ionization source (HESI) LTQ Discovery Ion-Trap/Orbitrap mass spectrometer (Thermo Scientific, San Jose, CA). UPLC analysis was performed using a C18 column (Thermo Hypersil 50x2.1 cm, 1.9um) at a column temperature of 26 ^{o}C with an injection volume of 75 µL. A gradient mixture was applied as a mixture of acetonitrile, methanol and 0.02% formic acid or 10 mM ammonium hydroxide in DI water at a variable flow rate. Separate conditions were selected based on the ionization method utilized during the mass analysis. UPLC conditions are summarized in Table 2-1.

Reaction byproducts were identified based upon fragmentation patterns from multiple mass spectra analyses (MS^n). XCalibur (version 2.0.7) was used for data acquisition and for identifying unknowns. An initial chromatographic scan was performed in full MS-only mode for each unknown sample solution to identify

chromatographic peaks of interest. Isolated mass peaks from the initial chromatographic scan were then subjected to a series of collision-induced dissociation (CID) experiments using a peak-picking algorithm. The most intense chromatographic peak mass was isolated and fragmented by applying a collision energy. An appropriate collision energy was determined iteratively prior to further analysis. MS^3 CID analysis was then performed on the most intense and second most intense daughter fragment masses. Further MS^n experiments were performed until no further detection of fragment ions could be observed.

Table 2- 1 UPLC conditions

Negative Ionization Mode					
Solvent A: 10 mM NH_4OH					
Solvent B: Methanol					
Solvent C: Acetonitrile					
Gradient Table					
No	Time (min)	A%	B%	C%	Flow Rate (µL/min)
0	0.00	55.0	35.0	10.0	400.0
1	1.00	40.0	45.0	15.0	450.0
2	4.50	20.0	65.0	15.0	500.0
3	9.50	5.0	80.0	15.0	500.0
4	10.00	35.0	50.0	15.0	500.0

Positive Ionization Mode					
Solvent A: 0.02% Formic acid					
Solvent B: Methanol					
Solvent C: Acetonitrile					
Gradient Table					
No	Time (min)	A%	B%	C%	Flow Rate (µL/min)
0	0.00	55.0	35.0	10.0	400.0
1	1.00	40.0	45.0	15.0	450.0
2	4.50	20.0	65.0	15.0	500.0
3	9.50	5.0	80.0	15.0	500.0
4	10.00	35.0	50.0	15.0	500.0

The concentration of Mn^{2+} ions in reaction solutions was determined using a Perkin Elmer DRCII inductively coupled plasma mass spectrometry (ICP-MS). All the samples were digested with 1% (v/v) HNO_3 prior to analysis and stored at 4°C in vials. The concentration of Mn^{2+} in solution was evaluated using a five point external calibration curve.

2.2.4 Batch reactor setup

All glassware was washed with 2% (v/v) HNO_3 and carefully rinsed with reagent-grade water. A 3 mM OP stock solution was prepared in methanol due to the high solubility of OP in the solvent. The stock solution of the organic was stored in a glass bottle and preserved in a freezer at -10°C. Preliminary experiments were performed to assess the effect of laboratory light on the reaction and to determine the effect of dissolved O_2 on the reaction rates. The preliminary results indicated that within the reaction time laboratory lighting and dissolved oxygen did not have any effect on the reaction rates. Therefore, all of the experiments were performed in triplicate in 250 mL glass amber bottles in the presence of O_2 and under ambient light conditions.

Each batch reactor used within the experiments consisted of an Erlenmyer flask filled with buffered reagent grade water at a fixed ionic strength of 0.01 M $NaNO_3$. The vessel was then spiked with manganese oxide to achieve a specified oxide concentration. The reactor solution was stirred using a Teflon coated magnetic stirrer for an hour before the reaction's initiation. This process ensured that oxide surfaces were equilibrated at the

specified pH and ionic strength conditions. The reaction was initiated by adding a spiked solution of OP into the flask to achieve an initial specified OP concentration.

Subsamples were drawn at intermediate time points and quenched using excess 0.1 M L-ascorbic acid. L-ascorbic acid converts the oxide to Mn^{2+} ions in order to stop the reaction and this quenching method releases both the adsorbed OP and Mn^{2+} generated in the process into the solution. Additional experiments were also carried out to evaluate the extent of adsorption of OP on the oxide surface. In these adsorption experiments, the reaction was also quenched by micro-centrifuging the sample at a speed of 14,000 rpm for 2 minutes to separate out the oxide particles from the reaction solution. The supernatant from this quenching method was separated out and analyzed and the difference in OP concentrations observed between the two quenching methods gave us the percent adsorption of the organic onto the surface of manganese oxide.
In separate control experiments OP solutions with and without L-ascorbic acid were examined in absence of any manganese oxide at different time intervals to assess OP stability in the solutions. OP was stable throughout the timeframes evaluated in this study with and without the presence of ascorbic acid. All experiments were performed with at least three replicated samples per analysis point.

2.3 Results and Discussion

2.3.1 Manganese oxide characterization

The concentration of the oxide solution was found to be ~ 0.01 M. A portion of the suspension was freeze-dried and characterized using X-Ray Diffraction (XRD). The XRD spectra indicated that the particles were MnO_2 and resembled the natural mineral, birnessite. The particles had significant amorphous character. The BET surface area of the created MnO_2 was 355 m^2/g.

2.3.2 Determination of order of the reaction with respect to organic, oxide, and pH

During our initial evaluation of OP reaction with excess MnO_2 at a pH of 4.6, OP adsorption onto the manganese oxide surface was found to account for < 2% of the total organic present in the solution. Such low surface coverage was also reported for phenol compounds onto both manganese oxide and iron oxide (*2, 61*). Therefore, ascorbic acid quenching was used throughout the batch kinetic experiments. This initial evaluation also indicated that the reaction between the oxide and organic was fast in the initial stages but deviated from the pseudo first order conditions as the reaction proceeded. This finding indicates that few active sites exist on the oxide or the active sites are altered as the reaction proceeds. This observed behavior of manganese oxide with other organics is reported in the literature (*2-4*).

The mechanism behind the oxidation of OP in this study was inferred by measuring the generation of [Mn^{2+}] ions in the reaction solution. The results

demonstrate that there was an increase in the concentration of [Mn^{2+}] ions in the solution as the reaction proceeded indicating that OP is oxidizing through reductive dissolution of Mn(IV) oxides. During the experiments, however, the concentration of [Mn^{2+}] ions did not increase proportionately to OP removal. This finding indicates that [Mn^{2+}] ions generated in the process are either adsorbed to the surface of the manganese oxides or the reaction did not follow a 1:1 stoichiometry.

Stone *et al.* (*2*) presents a reaction scheme for the dissolution process of manganese oxides in presence of organics, which can be briefly summarized as the diffusion of organic into the boundary of the oxide layer and a momentary formation of an organic-oxide complex. During the dissolution process electron transfer takes place at the surface of the complex and then the subsequent separation of oxidized and reduced products evolve into the solution. Because this reaction chemistry was also anticipated for the reaction between OP and manganese oxides, an initial rate method was used to determine the reaction order. One advantage of using this method to determine reaction order is that complications arising due to product interferences as the reaction proceeds are avoided (*62*).

The reaction orders were determined by carrying out experiments at a pH of 4.6 and ionic strength of 0.01 M $NaNO_3$ at three different loadings of MnO_2 (100 µM, 300 µM and 500 µM) and OP (40 µM, 30 µM and 20 µM). The slope of the plot of ln(initial reaction rate) versus ln[OP] gave the reaction order with respect to the oxide. Similarly the slope of the plot of ln(initial reaction rate) versus ln [oxide] gave the reaction order with respect to OP.

Figure 2- 1 Determination of order with respect to organic

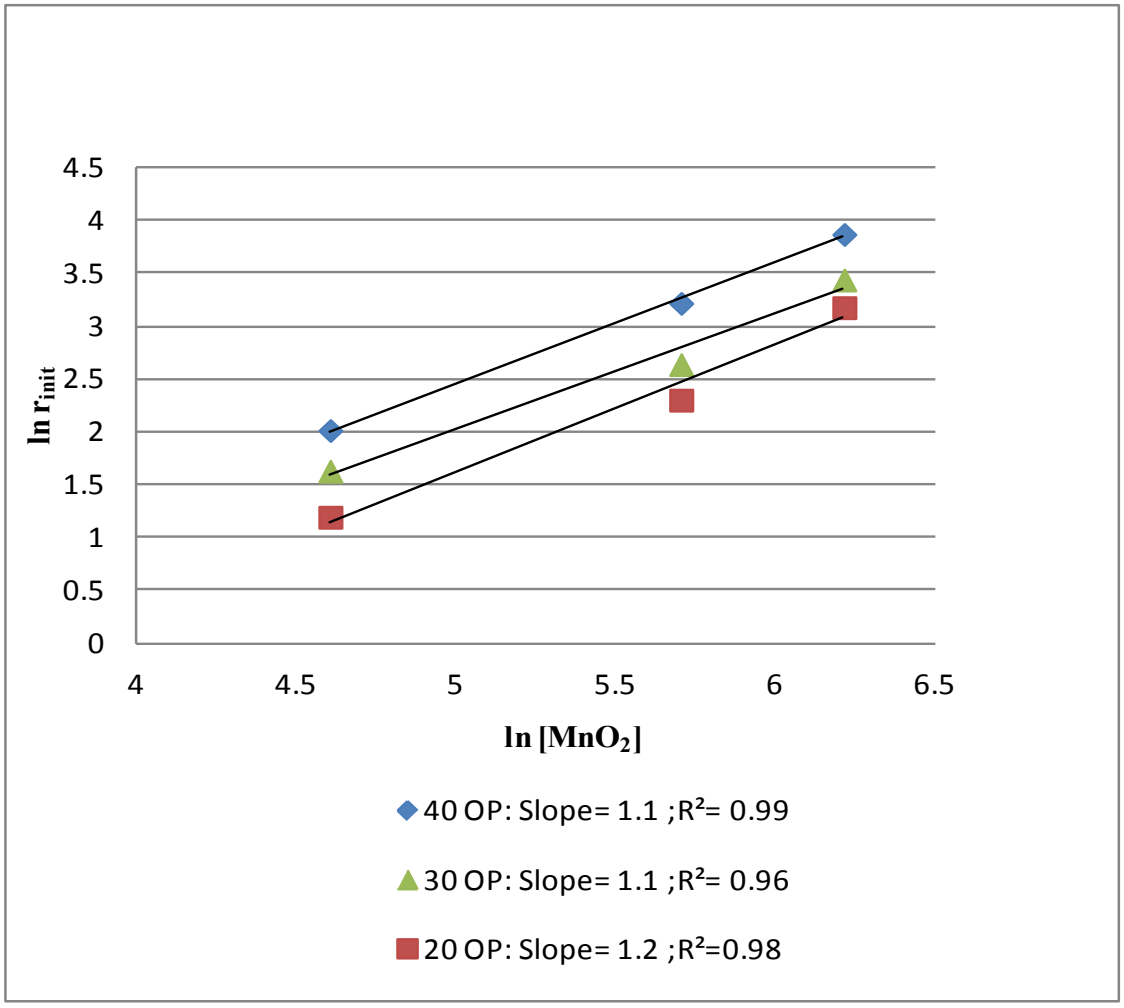

As can be observed from Figures 2-1 and 2-2, the average order with respect to both the organic and oxide is 1.13 and 1.16, respectively.

Figure 2- 2 Determination of order with respect to oxide

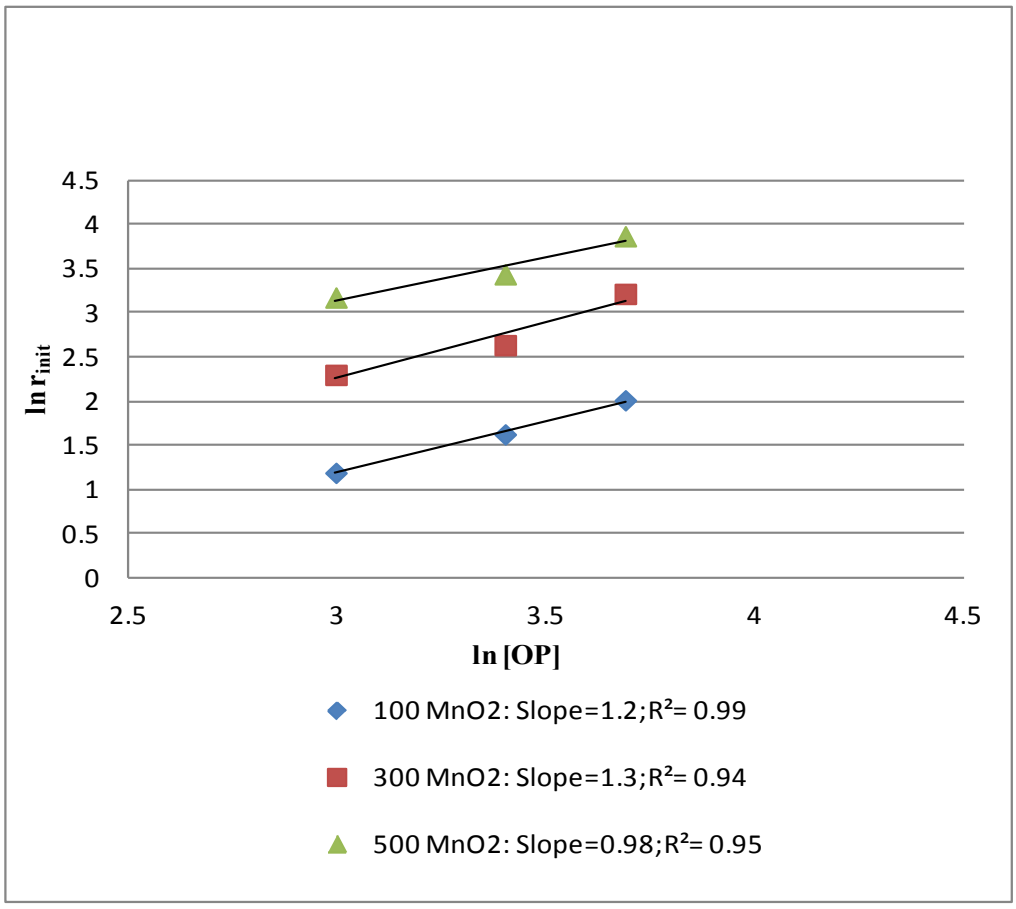

Results presented in Figure 2-3 demonstrate how the initial reaction rates decreased linearly as the pH increased. By evaluating the slope of the linear decrease, the order with respect to pH was found to be constant with a value of 0.65.

Stone *et al.* (*2*) in their study with substituted phenols had reported that their order with respect to pH was not constant, but had decreased from 1.3 to 0.45 between pH 7 and pH 4.4. This study had used an organic:oxide ratio between 1.6 and 2.8. Another study with triclosan and chlorophene; however, found the reaction order with

Figure 2- 3 Determination of order with respect to pH

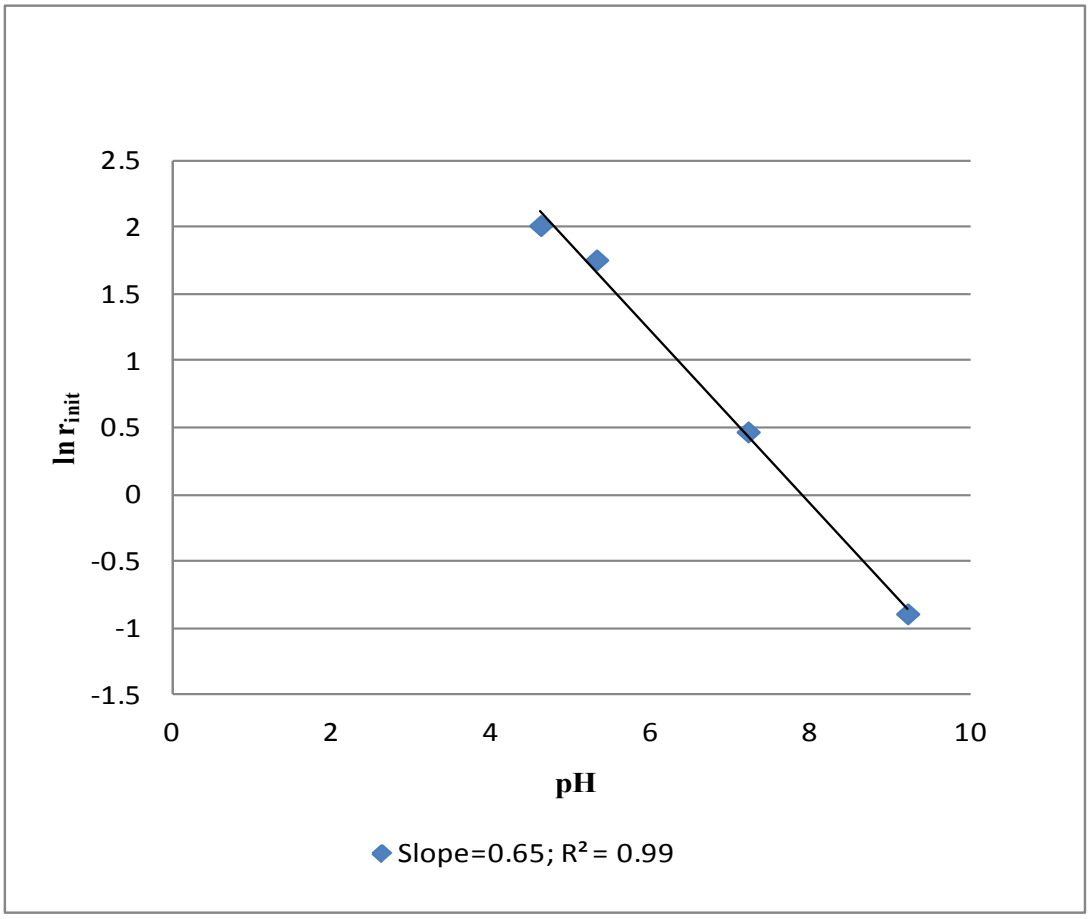

respect to pH to be constant for both organics (*4*). Their organic:oxide ratio was 0.1, a value lower than the previous study. These authors suggested that a different organic:oxide ratio, as well as the method of manganese oxide preparation, were the contributing factors behind the different trends in orders observed. In our reported study, an organic:oxide ratio of 0.4 was used to determine the order with respect to the pH. A constant order with respect to pH indicates that the reaction mechanism does not change

as a function of pH within our experimental range. Moreover, the observed trend can be explained by the changes in speciation of both OP and manganese oxides with pH. These changes affects not only the interaction between them, but also the redox potentials of the reacting species (*57*). OP has a pK_a value close to 10.7 (*62*) and over the entire range of experimental pH the protonated OP is the dominant species. At a pH value close to 4.6 the concentration of protonated OP is 6 orders of magnitude more than the concentration of unprotonated OP. The pH_{zpc} of MnO_2 has been determined to be close to 2.4 (*60*). Thus, MnO_2 exhibits positive charge below this pH value and the surface becomes increasingly more negative as the pH increases. The decrease in pH from 8 to 4, results in reduction potential of MnO_2 half-reaction increasing from 0.76 to 0.99V as shown in Equation 2-1

$$\frac{1}{2}MnO_2(s) + 2H^+ + e^- \rightarrow \frac{1}{2}Mn^{2+}(aq) + H_2O \qquad (2\text{-}1)$$

The difference of surface charges will result in different electrostatic interaction between the oxide and the organic and an observed difference in rates during the process. Therefore, the highest rates are observed at lower pH's due to interaction between negatively charged oxide surface and the protonated organic species. As the pH increases, OP becomes less protonated and hence the interaction between the surfaces decreases.

To summarize the initial reaction rate of OP oxidation by MnO_2 can be described by the following equation:

$$r_{init} = k_{init}[OP]^{1.13}[MnO_2]^{1.16}[H^+]^{0.65} \quad (2\text{-}2)$$

2.3.3 Effect of co-solutes on the reaction rates

Metal co-solutes are known to inhibit the interaction of organic with mineral surfaces (Figure 2-4). Co-solute experiments were carried out for each of the metals at concentration of 0.01 M, pH of 4.6, [OP] = 40 µM, [MnO_2] = 100 µM and ionic strength = 0.01 M $NaNO_3$. At pH 4.6 the MnO_2 surface is negatively charged and the positively charged metals can bind electrostatically to block the active sites for the organic oxidation. The inhibition effect for the metals follows the trend [Mn^{2+}]> [Fe^{3+}] > [Cu^{2+}] > [Ca^{2+}] > [Mg^{2+}]. During the ascorbic acid quenching step a white precipitate formed only in the presence of Cu^{2+} and not with any of the other metal co-solutes. This precipitation reaction is extensively reported in the literature and is caused by the reduction of Cu^{2+} to Cu^{+1}. For Cu^{2+} as a co-solute, the effect of the precipitate on OP removal was not evaluated, but the system followed the same analytical procedures as the other experimental runs.

Mn^{2+} ions inhibited OP oxidation by as much as 83% in the first 15 minutes, providing evidence for the argument that the reaction of OP with MnO_2 deviated from pseudo first order conditions due to blocking of active sites by the Mn^{2+} ions generated in the process. Fe^{3+} ions also had a pronounced effect on the reaction rates and the removal of OP reduced by as much as 67% in first 15 minutes. Ca^{2+} showed a reduction

of 30% followed by Mg^{2+}, which inhibited the oxidation of OP by almost 25% in the same time frame.

Figure 2- 4 Effect of metal ions on OP removal

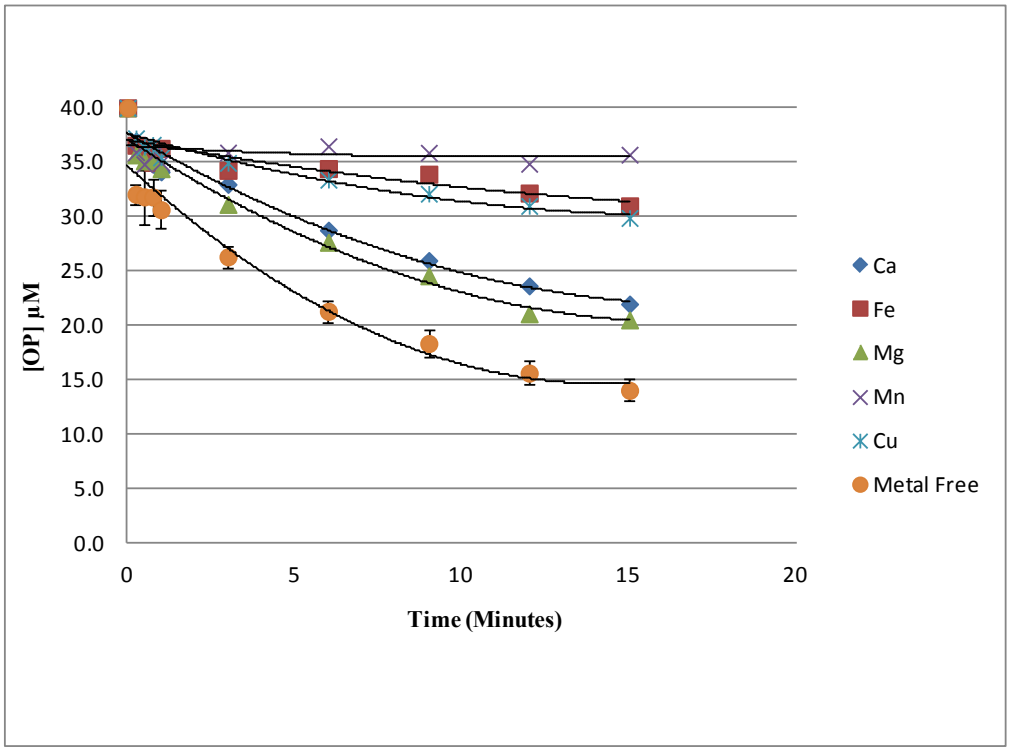

Because organic matter is known to inhibit the interaction of organics with mineral surfaces, experiments were also carried out to determine the effect of 5 mg/L and 10 mg/L humic acid on the oxidation of OP in the presence of MnO_2. Results presented in Figure 2-5 show that the presence of humic acid significantly inhibited the oxidation of OP at a pH of 4.6. In the presence of 5 mg/L and 10 mg/L of humic acid

the initial reaction rate decreased by 20% and 55%, respectively. Xu et al. (*14*) report that the oxidation of 17β-estradiol by MnO_2 is facilitated due to possible complexation of the humic acids with the Mn^{2+} ions. In another study of the oxidation of substituted anilines by MnO_2, humic acid was also found to suppress oxidation (*57*).

However, the Lin *et al.* (*11*) study exploring the reaction between Bisphenol-A and MnO_2 showed very weak inhibition of humic acid on organic removal. They suggested that either inhibition did not occur or that two interactions (facilitation and suppression) may have counterbalanced each other leading to negligible effect. Our data clearly demonstrates that suppression effect is predominant compared to facilitation (if facilitation even is present).

Figure 2- 5 Effect of humic acid on OP removal

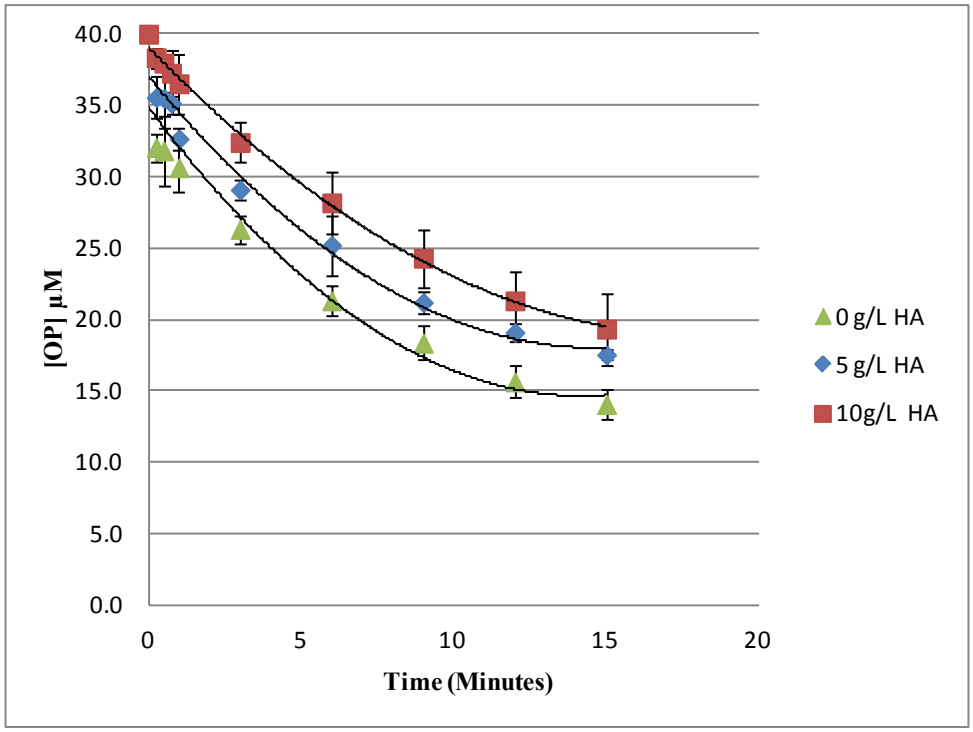

2.3.4 Reaction products

The identification of chemical transformation byproducts is an integral part of understanding the fate of chemicals during reaction processes. Liquid chromatography (LC) followed by accurate mass – mass spectroscopy (MS) is a detection technique used for screening byproducts. Identification of reaction byproducts is based upon observations of compound fragmentation patterns from multiple MS/MS analyses (MS^n). Only one byproduct peak not caused by background signal was observed in the system.

Figure 2- 6 LC/MS chromatography of the sample and background

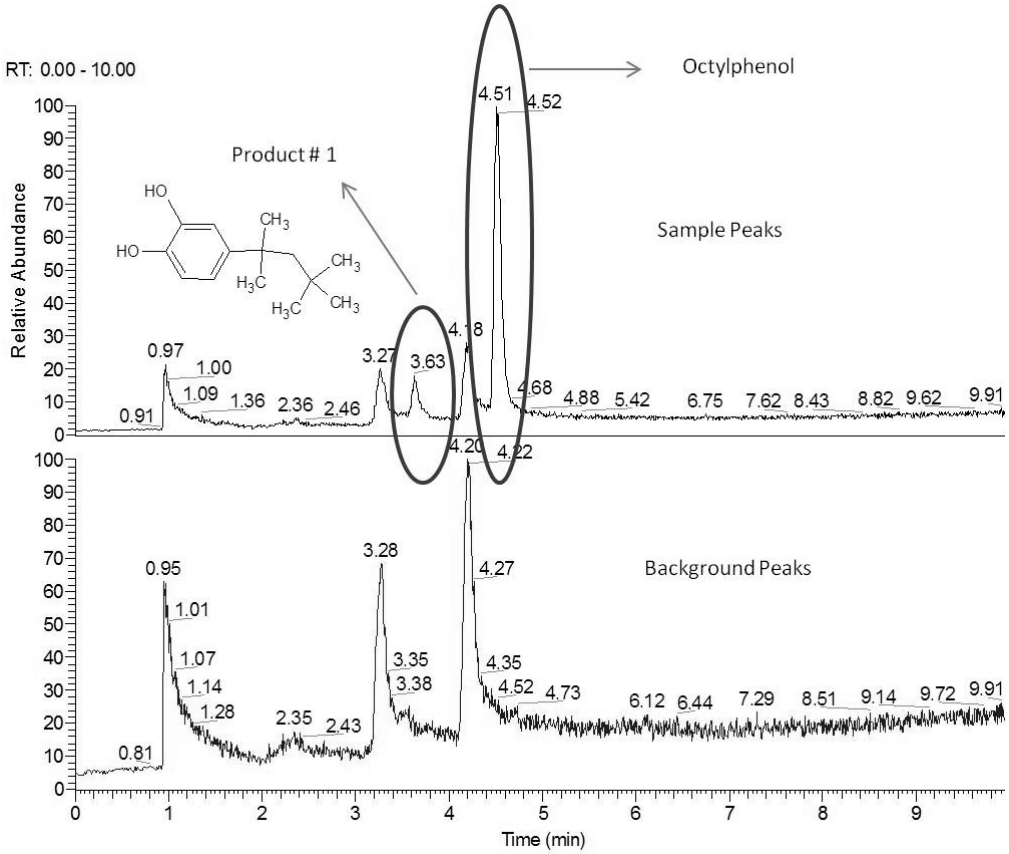

Figure 2-6 presents the resulting chromatogram observed when the system was operated in negative ionization mode using a full scan from 50-1000 m/z. Scans in the positive mode did not generate identifiable byproducts from the reaction. Analysis of the peak at 3.63 min (Figure 2-6) showed the byproduct to be a hydroxylation of the oxidized parent compound with a composition of $C_{14}H_{21}O_2$. Figure 2-7, provides the two potential structural compositions for the by-product. As the para position is already blocked by a large alkyl group ($-C_8H_{17}$), the most likely addition will take place at the ortho position due to steric hindrance at para position.

Figure 2- 7 Proposed structures of identified byproducts

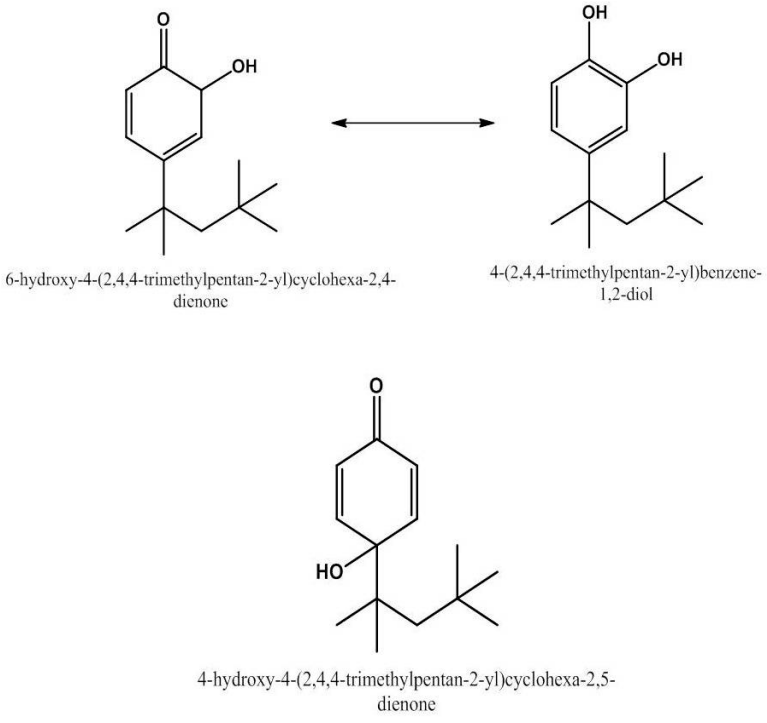

6-hydroxy-4-(2,4,4-trimethylpentan-2-yl)cyclohexa-2,4-dienone

4-(2,4,4-trimethylpentan-2-yl)benzene-1,2-diol

4-hydroxy-4-(2,4,4-trimethylpentan-2-yl)cyclohexa-2,5-dienone

The reaction mechanisms identified based upon the observed byproduct are listed in Figure 2-8. These reactions are similar to reactions of phenols with Mn-oxides as described by Stone *et al.*(*2*) The mechanism starts by the deprotonation of OP. The deprotonated OP then reacts with Mn^{+4} to from a phenoxy radical and Mn^{3+}. The formed phenoxinium ion reacts with Mn^{3+} to form major and minor OP byproducts and Mn^{2+}. The major and minor OP byproducts undergo hydrolysis to form the final byproducts observed in our reactions.

Figure 2- 8 Reaction mechanism

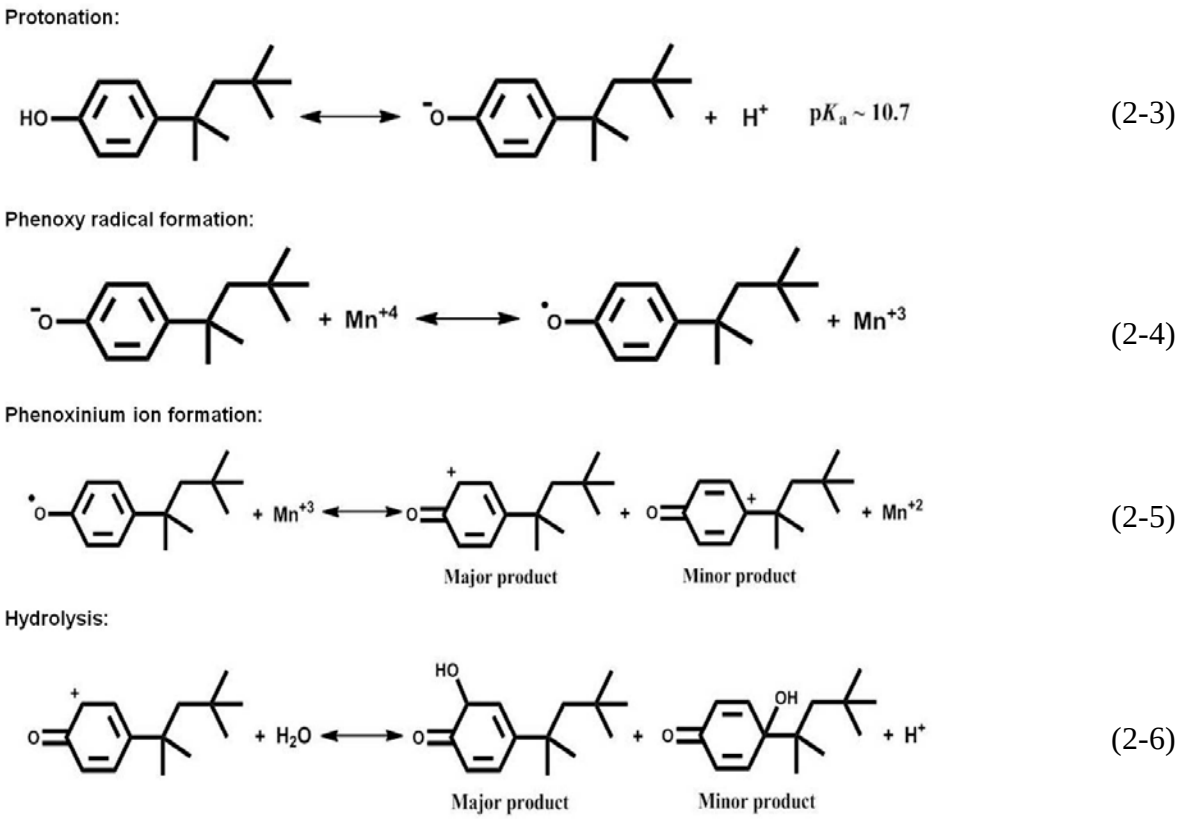

2.4 Conclusion

This study shows the reactivity of manganese oxide to degrade OP in aqueous systems. Abiotic degradation of OP in natural systems especially in soils where manganese oxides are present is a ubiquitous reaction pathway in the environment. Reaction rates increase under acidic conditions. The presence of metals and humic acids decreases the reactivity of manganese oxide in OP removal due to the competitive binding of the co-solutes for the active sites on the oxide. The disappearance of OP from the system is mainly due to a phenoxy radical formation and subsequent transformation by the transfer of electrons between the radical and the manganese oxides. Because estrogenicity is imparted to OP by the phenolic moiety, additional research should be carried out to determine whether the reaction byproducts will exhibit endocrine disruption in exposed organisms.

3. SYNTHESIS AND CHARACTERIZATION OF MAGNETIC MANGANESE FERRITES (TOPIC 2)

3.1 Introduction

Manganese ferrite particles are of interest because of their large surface to volume ratio and their many uses in the areas of biosensors (*63*) , electronics (*64*), and pharmaceutical delivery (*65*). Because the structural characteristics of manganese ferrite particles are controlled by their synthesis approach, different preparation methods have been explored. Reported synthesis methods include ceramic, co-precipitation, sol-gel, spray drying, freeze drying, and high temperature and pressure hydrothermal methods (*66-69*). In the ceramic method, metal oxides are mixed together by mechanical milling. This method does not yield fine particles and results in a wide distribution of particle sizes. Also, significant impurities are introduced due to the process of milling. Co-precipitation methods result in creating particles that are homogeneous, have defined stoichiometry, and a narrow distribution of particle size. Sol-gel techniques control particle size and size-distribution, but also help to control the shape of the particle. Spray-drying involves precipitation of concentrated cation solution by solvent evaporation, whereas in free-drying the concentrated solution is atomized into fine droplets (*70*). Hydrothermal methods are very promising methods to create manganese ferrites where particles are made from much smaller particles, such as clusters, molecules, ions, and atoms (*71*).

Manganese ferrite belongs to the class of ferrospinel, which are represented by the general formula AB_2O_4. Manganese ferrites also occur naturally as jacobsite. Different electrical, magnetic, and catalytic properties of ferrospinels are governed by the distribution of metals between the octahedral and tetrahedral sites. Manganese based ferrospinels show interesting catalytic properties in the oxidative dehydrogenation of hydrocarbons (*72*), oxidative gas phase CO oxidation (*73*), decomposition of peroxides (*74*), and oxidation of alkenes (*75*).

The purpose of this research was to synthesize and characterize manganese ferrite using a novel combustion method. This paper reports on the developed synthesis method involved mixing Mn and Fe salts with PVA followed by calcination. Characterization of the created manganese ferrites is also reported.

3.2 Methods and Materials

3.2.1 Preparation of magnetic manganese ferrites

Magnetic manganese ferrite was prepared by mixing $Mn(NO_3)_2$ and $Fe(NO_3)_3$ in the stoichiometric ratio of 1:2 within a ceramic crucible. Poly-vinyl alcohol (PVA) was added to the mixture according to NO_3:PVA ratios of 10:1; 5:1; 10:3; 2:1; 1:1; 1:1.5 and 1:2. The total weight of NO_3 in each NO_3:PVA composition was 10 g. Therefore, a prepared manganese ferrite with a label '$MnFe_2O_4$ PVA10' refers to a composition prepared with 10 g of total NO_3 salts, a Mn:Fe ratio of 1:2, and 10 g of added PVA.

100 mL DI water was added to dissolve the NO_3 salts. The solution was allowed to stand for 8 hours to ensure dissolution. 20 mL DI water was then added and the solution was mixed. The mixture was fired in a muffle furnace at 773K for a period of 60 minutes. After 60 minutes the furnace was turned off and allowed to cool. Once the furnace cooled down, the crucible was removed and the particles within the crucible were transferred into a 40 mL glass vial, capped, and stored at room temperature. Particles with different stoichiometric ratios of the two NO_3 salts were also created by varying the Mn percentage.

3.2.2 Characterization of magnetic manganese ferrites

All prepared samples were characterized using X-Ray Diffraction (XRD), X-ray photoelectron spectroscopy (XPS), Scanning electron microscope (SEM), Tunneling electron microscope (TEM), magnetic analysis, X-ray photoelectron spectroscopy (XPS), carbon analysis, pHzpc and BET surface area.

A PANalytical Xpert Pro theta-two theta diffractometer with Cu Kα radiation at 45kV and 40 mA (λ= 1.5406 Å) was used to identify the crystal phase of the created manganese ferrites. XRD pattern analysis was performed using the Jade+ software (version 7, MDI, Inc., Livermore, CA) according to ASTM D934-80 and using ICDD reference patterns (2002 PDF-2 release, International Center for Diffraction Data, Newtown Square, PA). The Brunauer-Emmett-Teller (BET) surface area, porosity and pore size distribution of ferrite nanoparticles were measured using a Tristar 3000 BET

surface analyzer (Micromeritics). The isoelectric point was determined with a zetasizer (3000HSA, Malvern).

A high-resolution transmission electron microscopy (HR-TEM, JEM-2010F, JEOL) with field emission-transmission gun at 200 kV was applied to analyze the morphology and crystallinity of the nanoparticles. The particles were dispersed in Milli-Q water using an ultrasonicator (2510R-DH, Bransonic) for more than 15 minutes and fixed on a carbon-coated copper grid (FCF400-Cu, EMS). Surface morphology of the ferrites was assessed using an environmental scanning electron microscope (ESEM, Philips XL 30 ESEM-FEG) at an accelerating voltage of 10-30 kV.

Magnetic measurements were performed using a Quantum Design SQUID magnetometer MPMS-XL in an applied field of 100 Oe in the 5-300 K temperature range. Magnetization data were measured at 300 K with the magnetic field varying from 0 to 7 T. Hysteresis were measured at 5 K with the magnetic field varying from 2 to -2 T. AC measurements were performed at 5 Oe oscillating magnetic field 5-300 K temperature range.

3.3 Results and Discussion

3.3.1 X-Ray diffraction

X-Ray diffraction (Figure 3-1) indicates that PVA was required to form pure manganese ferrite.

Figure 3- 1 XRD patterns at different PVA compositions

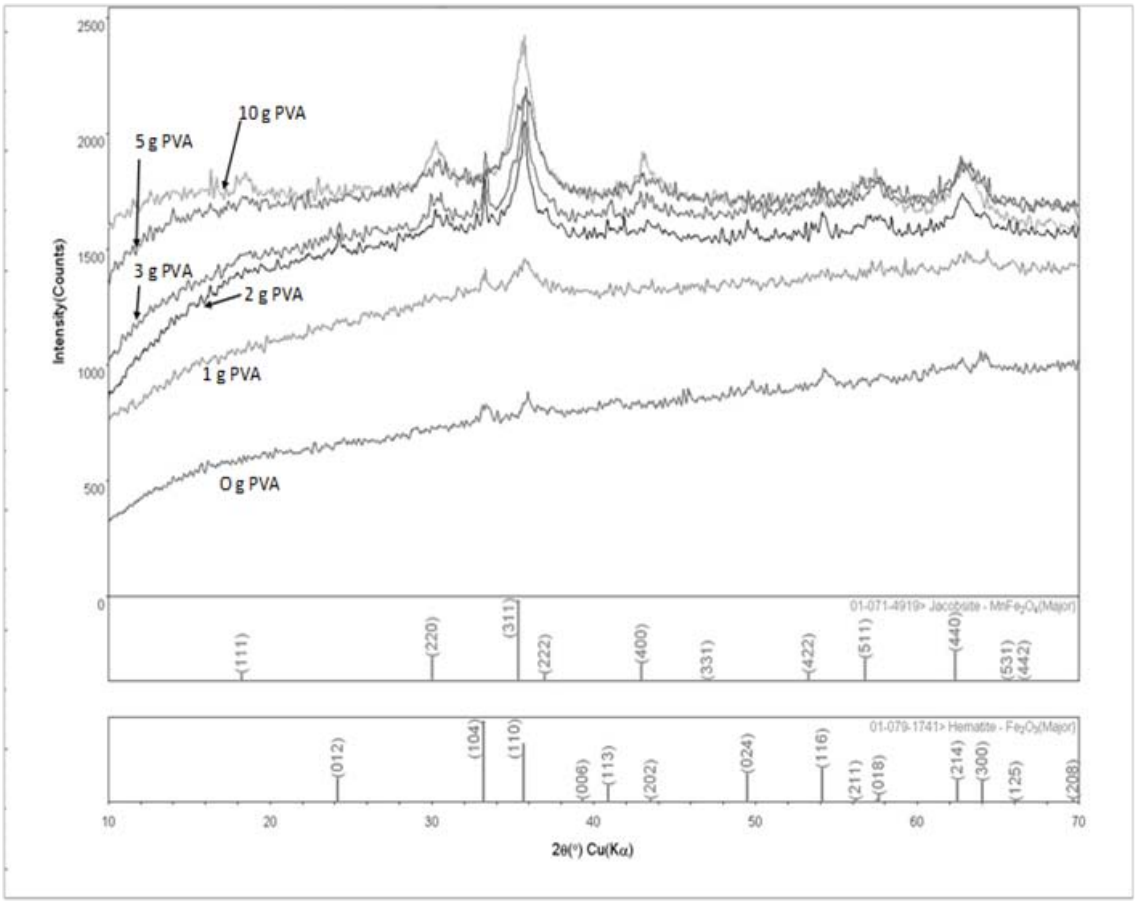

PVA acts as a fuel during synthesis helping to crystallize the manganese ferrite structure. At nitrates: PVA ratios above 1:1 peaks of a mixture of Fe_2O_3 and Mn-oxides were observed. Nitrates: PVA ratios below 1:1 resulted into complete conversion to $MnFe_2O_4$. Above this ratio (i.e. $MnFe_2O_4$ PVA10, $MnFe_2O_4$ PVA15 and $MnFe_2O_4$ PVA20), the XRD pattern observed matches Jacobsite (Figure 3-2). Observed peaks occur at $2\theta = 30.195^0$, 35.543^0, 43.217^0, 53.60^0, 57.067^0, 62.665^0 and 71.15^0 which

represent the Bragg reflections from the (220), (311), (400), (422), (511), (440) and (533) planes, respectively.

Figure 3- 2 XRD patterns showing complete conversion to manganese ferrites for different catalysts. (a) $MnFe_2O_4$ PVA10 (b) $MnFe_2O_4$ PVA15 and (c) $MnFe_2O_4$ PVA20

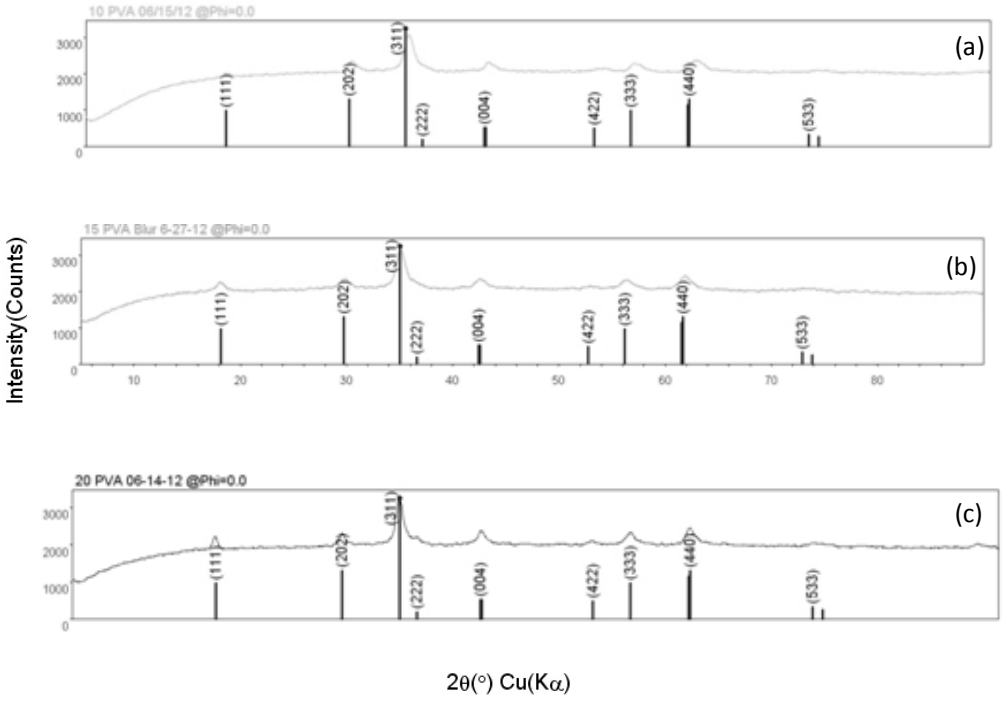

For further characterization, only compositions where there was a complete transformation to manganese ferrite were evaluated. The compositions are summarized in the Table 3-1.

Table 3-1 Summary of prepared catalysts

Catalyst	$Mn(NO_3)_2.xH_2O$ (gm)	$Fe(NO_3)_2.9H_2O$ (gm)	PVA (gm)
$MnFe_2O_4$ 10PVA	8.2	1.8	10
$MnFe_2O_4$ 15PVA	8.2	1.8	15
$MnFe_2O_4$ 20PVA	8.2	1.8	20
$Mn_{0.5}Fe_{2.5}O_4$ 15PVA	0.9	9.1	15
$Mn_{2.5}Fe_{0.5}O_4$ 15PVA	3.12	6.88	15

Table 3-2 Carbon content of prepared catalysts

Catalyst	% Carbon	BET Area
$MnFe_2O_4$ 10PVA	Non Detectable	48.8
$MnFe_2O_4$ 15PVA	0.14	57.4
$MnFe_2O_4$ 20PVA	0.22	39.9

3.3.2 Carbon composition and BET surface areas of synthesized manganese ferrites

Table 3-2 presents the carbon content analysis. A slight increase in the percentage of carbon was observed as PVA content increased. However, the carbon content was always less than 0.2% by weight. The BET surface area of the prepared catalysts is reported in Table 3-3. The BET surface area ranged from 46 m^2/g to 58 m^2/g depending upon the PVA amounts used during synthesis.

Table 3- 3 BET surface area of prepared catalysts

Catalyst	BET Area (m^2/g)
$MnFe_2O_4$ 10PVA	48.8
$MnFe_2O_4$ 15PVA	57.4
$MnFe_2O_4$ 20PVA	39.9
$Mn_{0.5}Fe_{2.5}O_4$ 15PVA	46.4
$Mn_{2.5}Fe_{0.5}O_4$ 15PVA	50.9

3.3.3 SEM-EDX analysis

Figure 3-3 shows the SEM images of (a) $MnFe_2O_4$ 10PVA (b) $MnFe_2O_4$ 15PVA (c) $MnFe_2O_4$ 20PVA (d) $Mn_{0.5}Fe_{2.5}O_4$ 15PVA (e) $Mn_{2.5}Fe_{0.5}O_4$. 15PVA. Prepared manganese ferrites were agglomerated and formed dense, flake-like structures ranging in size from nanometers to micrometers.

Figure 3- 3 SEM images of prepared catalysts. The different catalyst images are (a) $MnFe_2O_4$ 10PVA, (b) $MnFe_2O_4$ 15PVA, (c) $MnFe_2O_4$ 20PVA, (d) $Mn_{0.5}Fe_{2.5}O_4$ 15PVA, and (e) $Mn_{2.5}Fe_{0.5}O_4$ 15PVA.

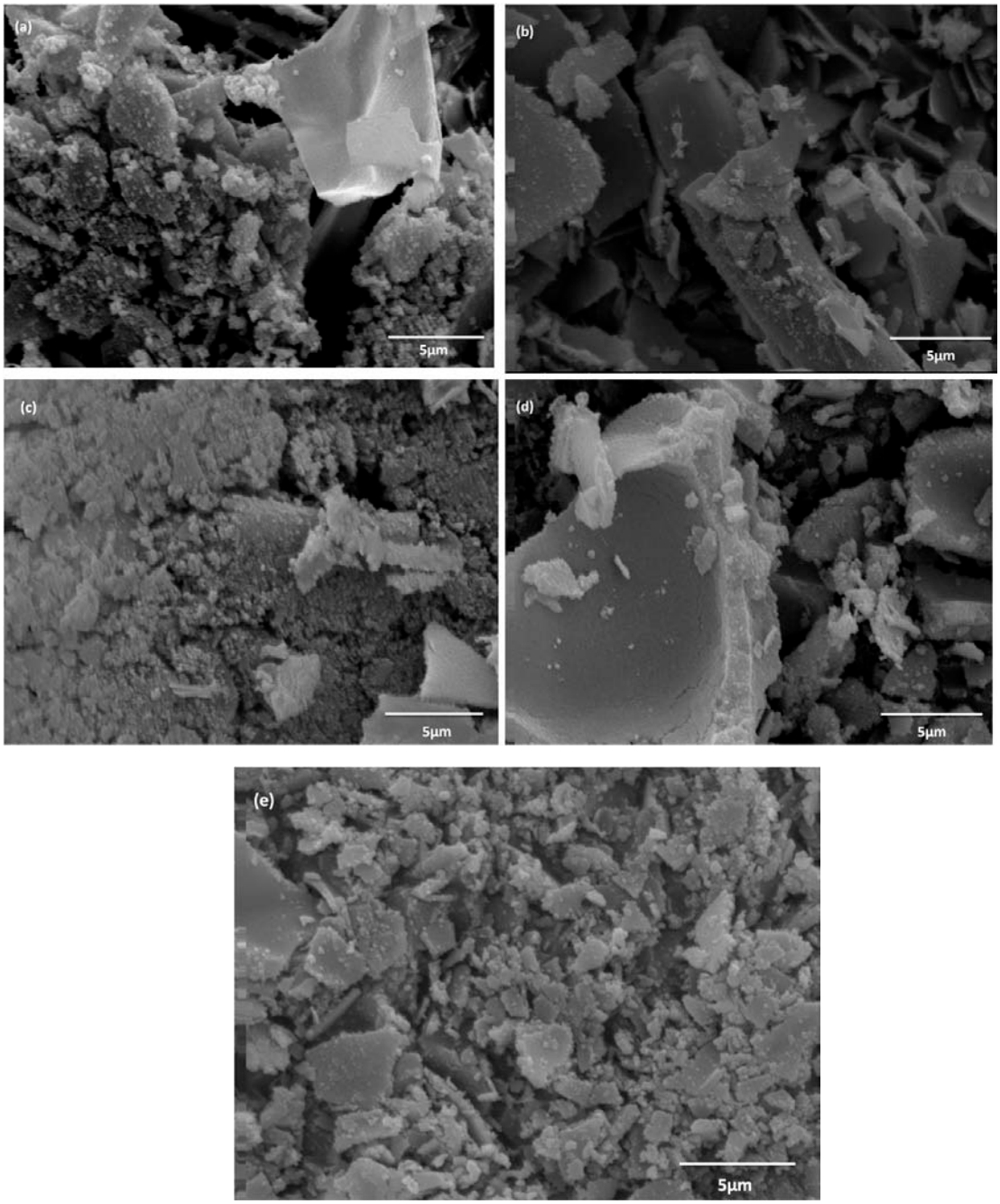

The formation of $Mn_xFe_{3-x}O_4$ was again confirmed with energy dispersive x-ray analysis (EDX) and is shown in Figure 3-4. Peak heights of manganese and iron vary according to the different stoichiometric ratios used in their preparation.

Figure 3- 4 EDX spectra at different Mn:Fe ratios. The three different catalysts are (a) $Mn_{0.5}Fe_{2.5}O_4$ 15PVA, (b) $MnFe_2O_4$ 15PVA, (c) $Mn_{2.5}Fe_{0.5}O_4$ 15PVA

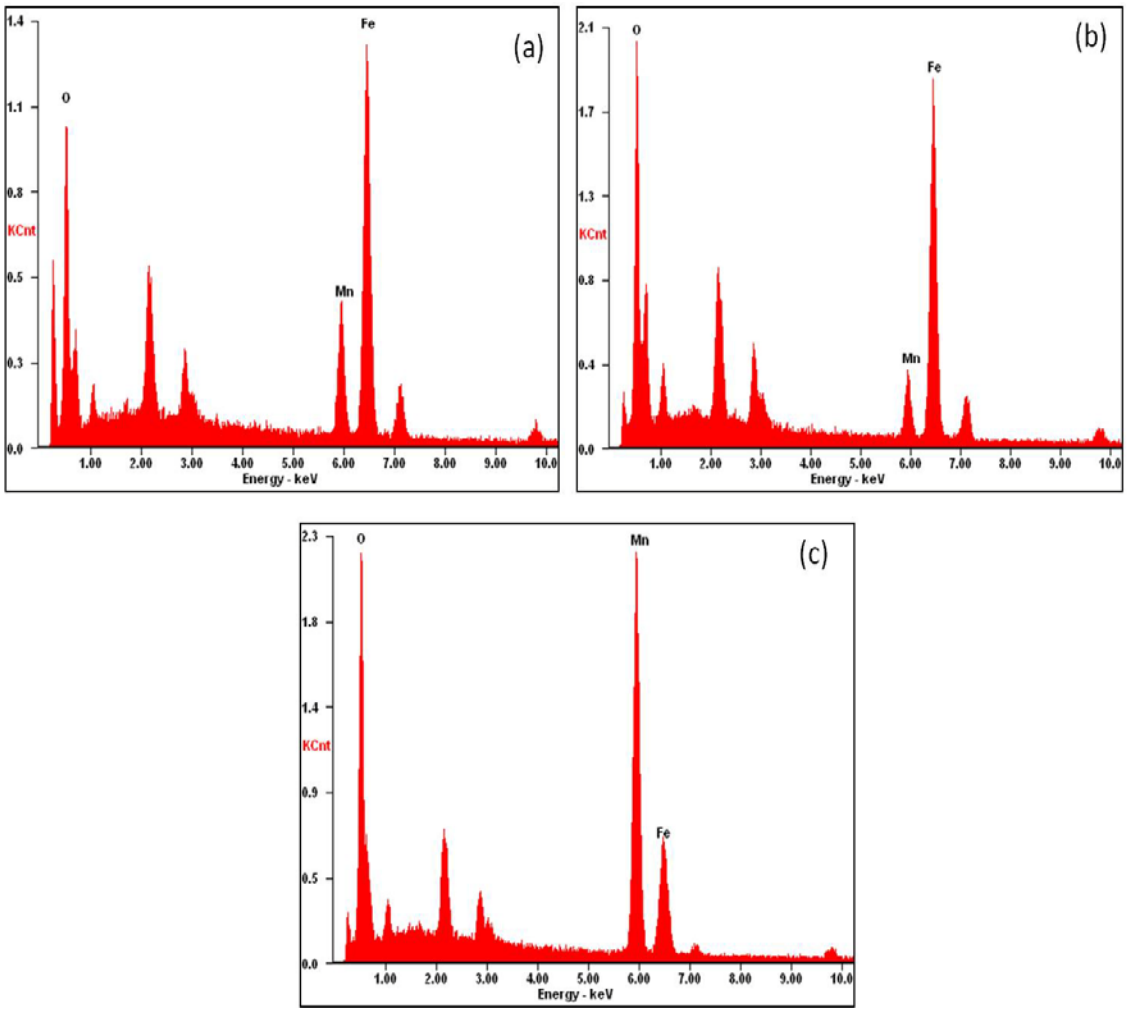

3.3.4. TEM analysis

TEM was used to analyze the particle size and shape. TEM images of the produced catalysts are shown in Figure 3-5. While the catalysts were variable in shape and size, the majority were spherical in nature with size ranging from 20 to 100 nm.

Figure 3- 5 TEM images of prepared catalysts. The different catalysts shown are (a) $MnFe_2O_4$ 10PVA, (b) $MnFe_2O_4$ 15PVA, (c) $MnFe_2O_4$ 20PVA, (d) $Mn_{0.5}Fe_{2.5}O_4$ 15PVA, and (e) $Mn_{2.5}Fe_{0.5}O_4$ 15PVA

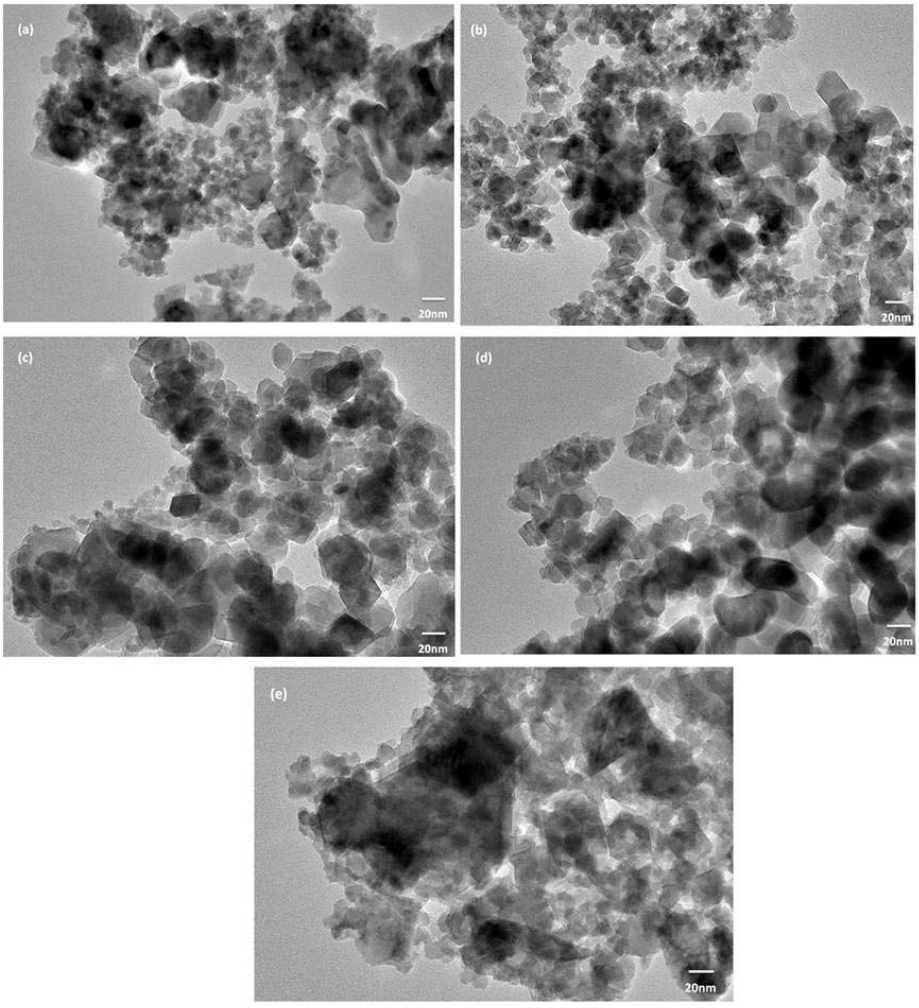

For both $MnFe_2O_4$ PVA10 and $MnFe_2O_4$ PVA15 samples, diffraction patterns of (111), (220), (311), (400), (411), and (440) plane for $MnFe_2O_4$ were observed by selected area electron diffraction (SAED) analysis. Therefore, the formation of magnetic $MnFe_2O_4$ nanoparticles is confirmed (*76*). The lattice spacing of the synthesized materials was investigated with HR-TEM analysis (Figure 3-6). The measured lattice spacing was 0.48 nm for (111) plane and 0.212 nm for (400) plane of $MnFe_2O_4$ PVA15 which provides another confirmation of the SAED analysis findings (*77*).

Figure 3- 6 HR-TEM and diffraction pattern of catalysts. The two catalysts shown are (a) $MnFe_2O_4$ 10PVA, (b) $MnFe_2O_4$ 15PVA

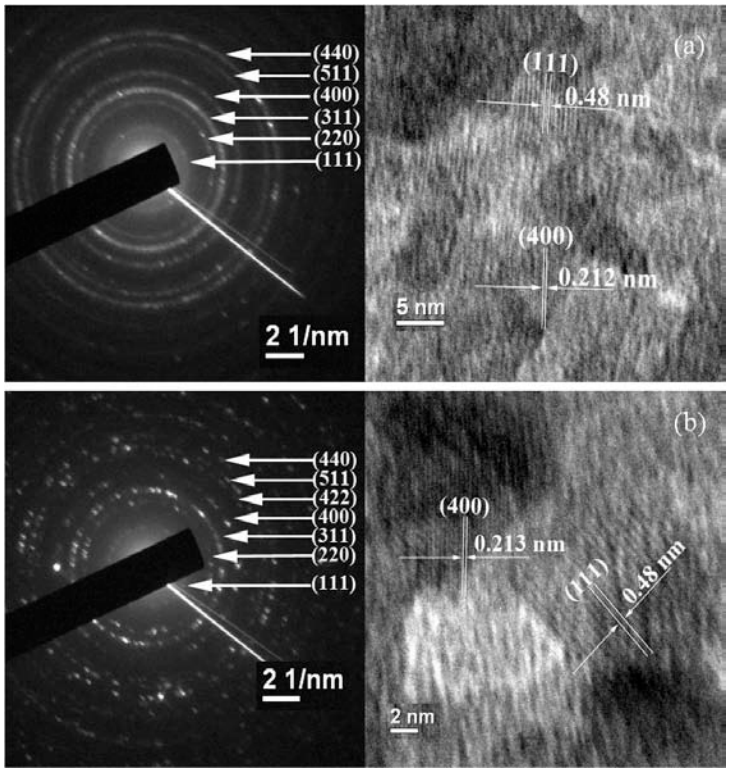

3.3.5 X-ray photoelectron spectroscopy

Figure 3-7 shows the XPS spectra for a representative sample of $MnFe_2O_4$ PVA15 catalyst. Figure 3-7(a) shows the C1s core level spectra measured by XPS. Two main peaks appeared at 284. 6 and 288.5 eV for C-C/C-H bonds and C-O bonds, respectively (*78*). Figure 3-7(b) shows two peaks of the O1s spectra at 529.9 and 531.5 eV corresponding to O^{2-} and OH^-, respectively. For $MnFe_2O_4$ PVA10, three peaks of the O1 spectra at 529.7, 530.5, and 532.5 eV were observed which indicate the binding energies of O^{2-}, O^-, and O_2^{2-}, respectively (*79*).

The peak of Fe ($2p_{3/2}$) at 710.5 eV was observed for all samples. The satellite peak between Fe($2p_{3/2}$) (710.9 eV) and Fe($2p_{1/2}$) (724.8 eV), indicates Fe_2O_3 (*80*). The Mn ($2p_{3/2}$) peak was observed for all samples around 641.7 eV of Mn^{3+} spectrum (*81*). The Fe(2p) and Mn(2p) spectra in Figure 3-6 clearly show defined peaks associated with the $MnFe_2O_4$ formation. The Fe($2p_{3/2}$) and Fe($2p_{1/2}$) binding energies appear at 711.9 eV and 725.1 eV in the XPS spectra, respectively. Furthermore, the Mn($2p_{3/2}$) and Mn($2p_{1/2}$) binding energies appear at 641.7 eV and 654.0 eV, respectively. These results are consistent with those in a previous study (*82*) and support the $MnFe_2O_4$ formulation. Furthermore, the presence of both Mn and Fe in the nanoparticles is confirmed by the results from energy dispersive X-ray (EDX) analysis.

Figure 3- 7 XPS analysis of $MnFe_2O_4$ 15PVA catalyst. The peaks for 4 different elements shown are a) C(1s), b) O(1s), c) Fe(2p), and d) Mn(2p). The presented results are characteristic of the XPS analysis observed for all samples. Differences in observed spectra between catalysts are discussed in the text

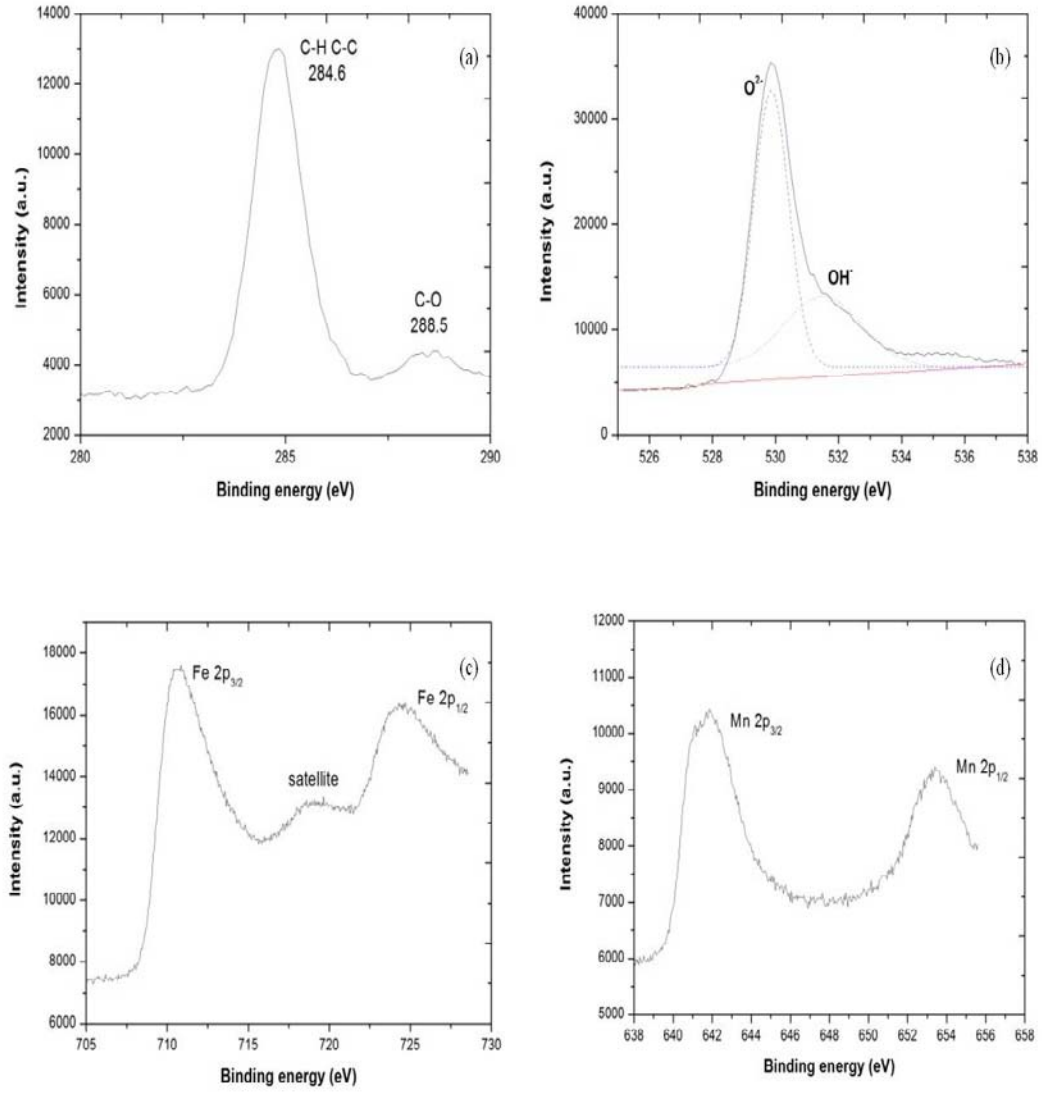

3.3.6 Magnetic analysis

The plot of magnetization versus field at T =300 K shown in Figure 3-8 reveals superparamagnetism for all the particles. The saturation magnetization values (Table 3-4) show that the values for most particles range between 46 and 52 emu/g except the $Mn_{2.5}Fe_{0.5}O_4$ 15PVA composition which shows lower saturation magnetization (19.6 emu/g). This indicates lower concentration of metal ion in this catalyst than in previous ones.

Table 3- 4 Saturation magnetization

Catalyst	Saturation magnetization (Ms) emu/g
$MnFe_2O_4$ 10PVA	52
$MnFe_2O_4$ 15PVA	49.6
$MnFe_2O_4$ 20PVA	46.9
$Mn_{0.5}Fe_{2.5}O_4$ 15PVA	52
$Mn_{2.5}Fe_{0.5}O_4$ 15PVA	19.6

Figure 3- 8 Magnetization versus magnetic field (Oe) at T =300 K. The different catalysts shown are (a) $MnFe_2O_4$ 10PVA, (b) $MnFe_2O_4$ 15PVA, (c) $MnFe_2O_4$ 20PVA, (d) $Mn_{0.5}Fe_{2.5}O_4$ 15PVA, and (e) $Mn_{2.5}Fe_{0.5}O_4$ 15PVA

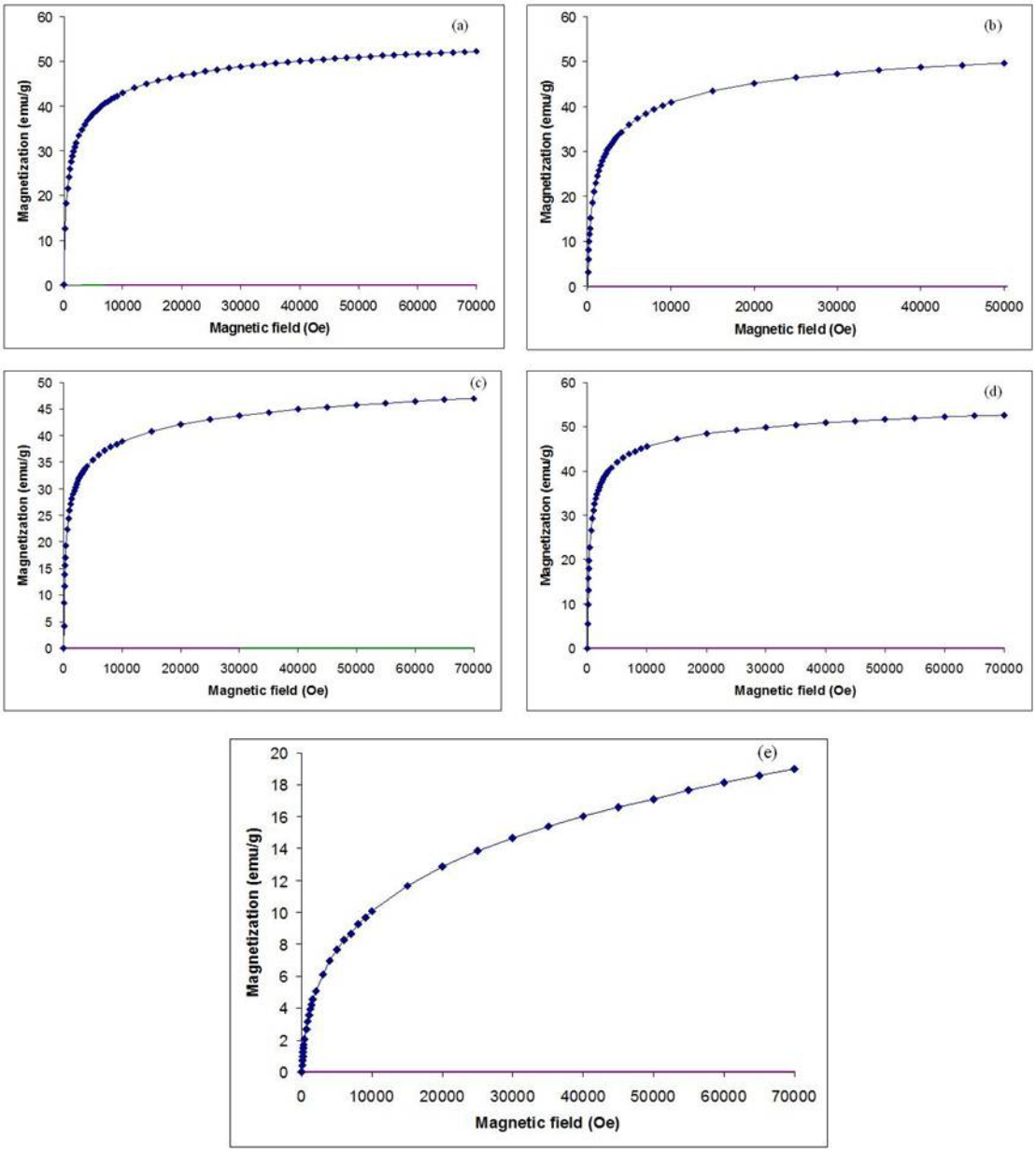

Figure 3- 9 Temperature dependence of the real χ' (full symbols) and imaginary χ" (open symbols) components of the AC susceptibility with oscillating field of 5 Oe at different frequencies. The different catalyst shown are (a) $MnFe_2O_4$ 10PVA, (b) $MnFe_2O_4$ 15PVA, (c) $MnFe_2O_4$ 20PVA, (d) $Mn_{0.5}Fe_{2.5}O_4$ 15PVA, (e) $Mn_{2.5}Fe_{0.5}O_4$ 15PVA

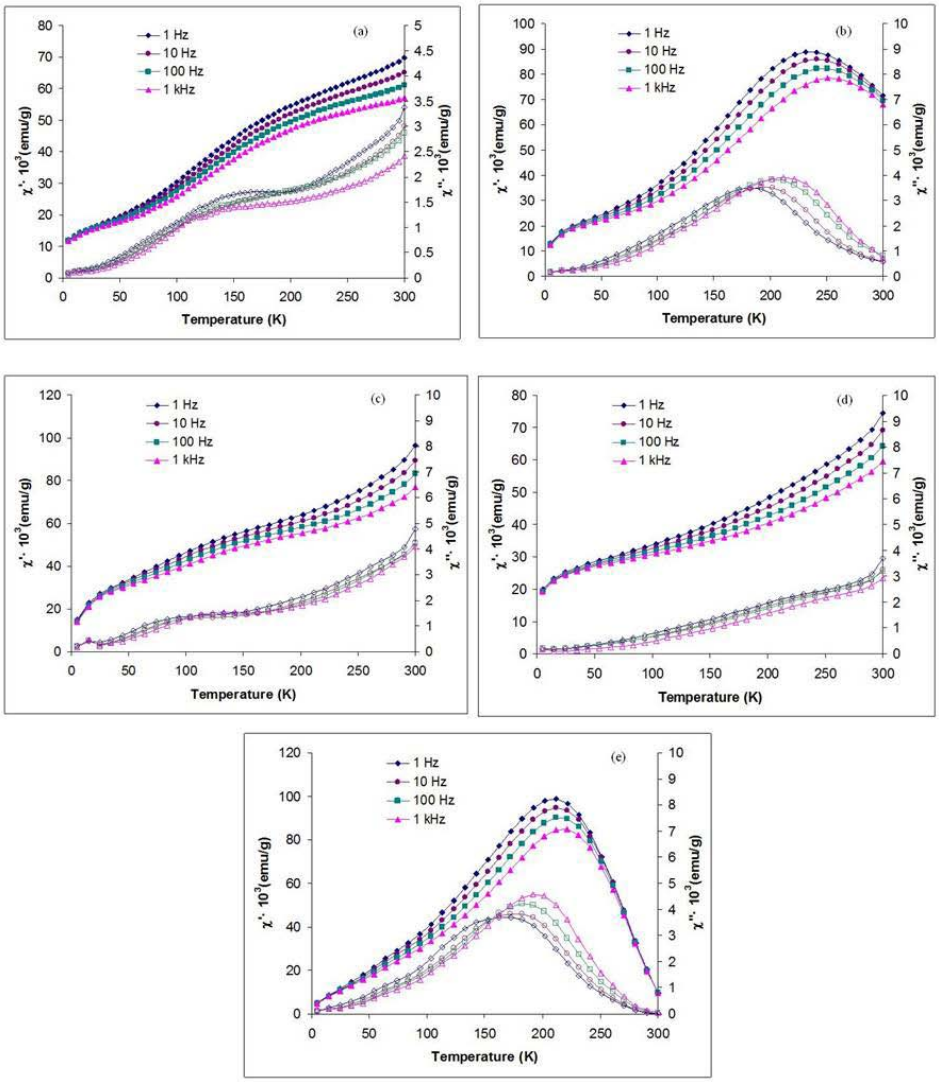

The AC magnetic measurement in which an AC field is applied to a sample and the resulting AC moment is measured indicates presence of two types of nanoparticle for

the $MnFe_2O_4$ 10PVA sample with blocking temperature 150K and over 300K (Figure 3-9). This is clearly visible from the temperature dependent AC susceptibility which shows a peak at about 150K and continual increase of χ" (imaginary component of AC magnetic susceptibility) over 300K (Figure 3-9).

Non-zero remnant magnetization and non-superposition of field-cooling (FC) and zero field-cooling (ZFC) curves also indicate the existence of nanoparticles with blocking temperature over 300K (Figure 3-10).

Figure 3- 10 Temperature dependence of magnetization in the zero-field-cooling (ZFC) and field-cooling (FC) regime at magnetic field of 100 Oe, and remnant magnetization measurements (RM) of the prepared catalyst. The different catalyt shown are (a) $MnFe_2O_4$ 10PVA, (b) $MnFe_2O_4$ 15PVA, (c) $MnFe_2O_4$ 20PVA, (d) $Mn_{0.5}Fe_{2.5}O_4$ 15PVA, (e) $Mn_{2.5}Fe_{0.5}O_4$ 15PVA

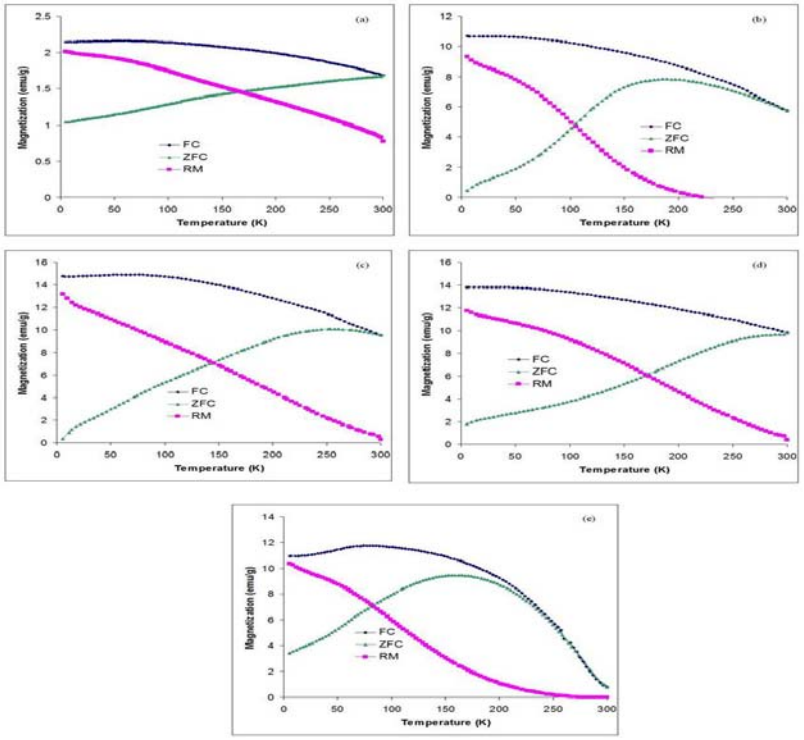

No hysteresis has been found at 300K for the catalysts. Generally such behavior is attributed to the formation of ferro/ferri-magnetic nanoparticles. The $MnFe_2O_4$ 10PVA catalyst shows a hysteresis at 5K with coercive field 520 Oersted (Oe) (Figure 3-11).

According to AC measurements of the $MnFe_2O_4$ 15PVA samples the data indicates that it contains one type of nanoparticles with blocking temperature at about 200K. This is clearly visible from the peak at about 200K on temperature dependent AC susceptibility plot and a maximum on ZFC curve. The sample also shows a hysteresis at 5K with coercive field 520 Oe.

The AC measurements of the $MnFe_2O_4$ 20PVA catalyst, indicates that it contains three types of nanoparticles with blocking temperature 10K, 100K and over 300K. This is clearly visible as two peaks at about 10 and 100K on temperature dependent AC susceptibility and continual increase of χ" over 300K. Non-zero remnant magnetization and non-superposition of FC and ZFC curves also indicate the existence of nanoparticles with blocking temperature over 300K. The sample shows a hysteresis at 5K with coercive field 500 Oe.

The $Mn_{0.5}Fe_{2.5}O_4$ 15PVA contains one type of nanoparticles with blocking temperature over 300K. There is no peak observed on the temperature dependent AC susceptibility, but just a continual increase of χ" over 300K. Non-zero remnant magnetization and non-superposition of FC and ZFC curves also indicate the existence of nanoparticles with blocking temperature over 300K.The sample shows a hysteresis at 5K with coercive field 400 Oe.

Figure 3- 11 Hysteresis at 5K of the prepared catalysts. The different catalyst shown are (a) $MnFe_2O_4$ 10PVA, (b) $MnFe_2O_4$ 15PVA, (c) $MnFe_2O_4$ 20PVA, (d) $Mn_{0.5}Fe_{2.5}O_4$ 15PVA, and (e) $Mn_{2.5}Fe_{0.5}O_4$ 15PVA

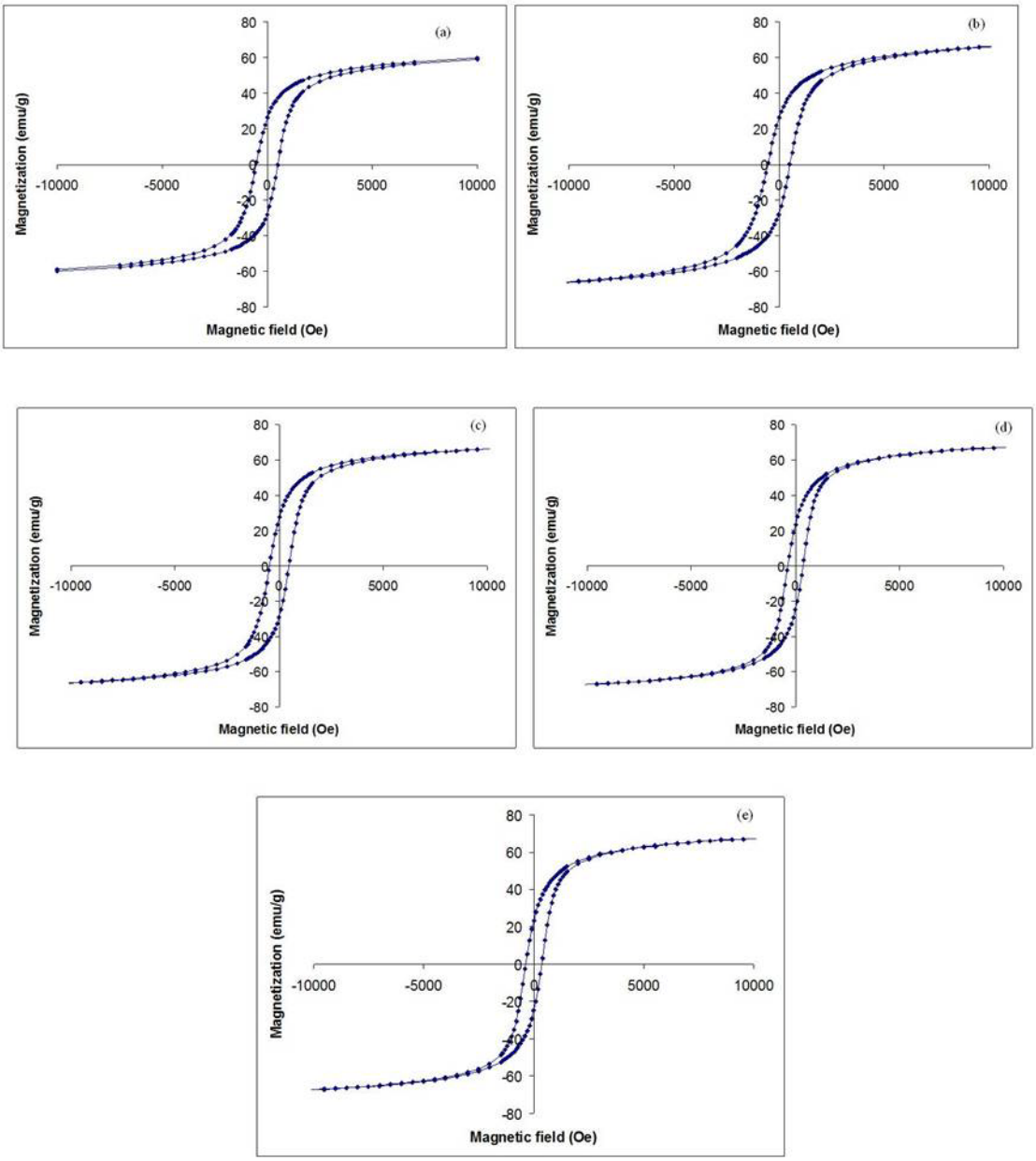

The $Mn_{2.5}Fe_{0.5}O_4$ 15PVA particles contain one type of nanoparticles with blocking temperature at about 200K. This is clearly visible from the peak at about 200K on temperature dependent AC susceptibility and a round maximum on ZFC curve. The sample shows a hysteresis at 5K with coercive field 400 Oe.

3.4 Conclusions

A simple combustion method was developed and verified to create magnetic manganese ferrite. It was clear that only above total nitrates: PVA ratios of 1:1, a total conversion of particles to manganese ferrites is observed. Moreover PVA is essential in making the particles magnetic. The created manganese ferrites were thoroughly characterized using XRD, SEM, TEM techniques. BET suraface area, carbon content and, pH_{zpc} of the particles were also determined. The magnetic property of the prepared catalysts has been obtained by field dependent magnetization measurements. The particles were created for the purpose of creating reactive surfaces that could easily be separated within by a magnetic field when used within water and water treatment processes. The simplified combustion method used to make managenese ferrites results in the creation of reactive surfaces that offer a wide range of applications while being easily scalable.

4. MAGNETIC MANGANESE FERRITES AS OZONATION CATALYSTS (TOPIC 3)

4.1 Introduction

Ozonation has been widely used for disinfection purposes over the past two decades. Recent observations indicate ozonation is also effective for treating trace organics in aqueous systems; which has renewed interest in the technology. However, ozone by itself is selective in nature and many trace organics are recalcitrant to molecular ozone alone. Therefore, catalytic ozonation processes were developed to increase the removal of recalcitrant organics by promoting ·OH radical formation during ozonation. Both homogeneous and heterogeneous ozonation catalysts are reported in the literature. Homogeneous catalysis, including Mn(II), Fe(III), Fe(II), Co(II), Cu(II), Zn(II), and Cr(III), enhance ozone decomposition into hydroxyl radicals or form complexes that easily decompose into hydroxyl radicals (*83-86*). Heterogeneous catalytic systems, including metal oxides (MnO_2, TiO_2, Al_2O_3, FeOOH, and CeO_2), metals (Cu, Ru, Pt, and Co) on supports (SiO_2, Al_2O_3, TiO_2, CeO_2, and activated carbon), zeolites modified with metals, and activated carbon are also effective ozonation catalysts (*18, 19, 87-98*).

Manganese based catalysts rapidly enhance hydroxyl radical production during ozonation. The use of Mn(II) as an ozonation catalyst was first reported by Tyupalo *et al.* (*99*). In an investigation of Mn(II) catalyzed ozonation of oxalic acid in aqueous solution Andreozzi and co-workers found that manganese formed an intermediate

product with ozone which was easier to degrade (*29*). Gracia *et al.* (*18*), in their work on catalytic ozonation of humic acid using various transition metals, showed that Mn(II) most effective in reducing TOC in drinking water. Their study also demonstrated the ability of Mn(II) catalytic ozonation to eliminate chlorination byproducts. Gracia *et al.* proposed that oxidation of Mn(II) to Mn(IV) during catalytic ozonation results in a MnO_2 structural analog that could be easily removed from treatment plants in subsequent stages using precipitation, sorption or coagulation. Ma and Graham (*21*) demonstrated that Mn(II) facilitiated the catalytic removal of atrazine during ozonation due to hydroxyl radical formation. In-situ formed hydrous manganese oxides were determined to be the active catalysts in the Ma and Graham study.

Heterogeneous (solid) manganese based catalysts are also effective ozonation catalysts. Manganese loaded activated carbon removed 1.5-2 times more nitrobenzene compared to activated carbon alone during ozonation (*25*). von Gunten *et al.(27)* prepared manganese doped carbon aerogels that showed higher hydroxyl radical production compared to carbon aerogels alone. Zhao *et al.* (*26*) prepared manganese based honeycomb catalysts and demonstrated their use to remove nitrobenzene from aqueous systems. Martins *et al.* (*100*) produced Mn-Ce bimetallic oxides for use as ozonation catalysts, testing several commercially available and laboratory prepared manganese based mixed oxides. Mn-Ce based mixed oxides were identified as the most promising in treatment of phenolic effluents.

Pereira and co-workers (*93*) synthesized manganese based catalysts on activated carbon, Mn-Ce mixed oxides, Mn-Co mixed oxides, and manganese oxide-carbon

composites for the effective removal of organics including oxalic acid. A number of pharmaceuticals have also been treated using manganese based ozonation catalysts. Pharmaceutical removal is reported for ciprofloxacin removal on carbon nanotube supported manganese oxides (*101*); phenazone, ibuprofen, diphenhydramine, phenytoin, and diclofenac sodium using mesoporous alumina supported manganese oxide (*33*); and fenofibric acid using alumina supported manganese oxide (*102*).

A major challenge in using catalytic ozonation for water/wastewater treatment is catalyst recovery. Designing magnetic catalysts overcomes this challenge. While magnetic catalysts are widely applied in biotechnology and biomedicine, only a few studies have examined the application of magnetic catalysts for contaminant removal during water and wastewater treatment. Lv *et al.* (*103*) tested cobalt and manganese doped γ-Fe_2O_3 for degradation of 2,4-dichlorophenol. Ren and colleagues (*104*) explored the use of magnetic ferrospinels in form of $NiFe_2O_4$ for the removal of di-*n*-butyl phthalate. These early reports demonstrate the remarkable structural, electronic, magnetic and catalytic properties of manganese-iron mixed oxides for catalytic ozonation.

This research further investigates the use of manganese-iron based ferrites for catalytic ozonation by studying magnetic manganese ferrospinels created using a novel combustion method. The developed catalysts blend the catalytic properties of manganese with the magnetic and structural properties of ferrospinels. The objective of this study was to test the efficacy of the new catalysts to enhance hydroxyl radical production during ozonation. Catalyst effectiveness was determined by measuring R_{ct}; a

concept developed by Elovitz and von Gunten (*105*) which is defined as the ratio of ·OH exposure to the O_3 exposure [$\frac{\int[\cdot OH]dt}{\int[O3]dt}$] during ozonation. Para-chlorobenzoic acid (pCBA) was used as a hydroxyl radical probe to investigate effect of catalyst type, catalyst dosage, pre-ozonation, pH and presence of DOM on hydroxyl radical production during catalytic ozonation.

4.2 Methods

4.2.1 Reagents

Reagent grade iron nitrate, manganese nitrate, poly(vinyl) alcohol, phosphoric acid, indigo trisulfonate, para-chlorobenzoic acid (pCBA), sodium hydroxide, hydrochloric acid, dipotassium phosphate, potassium dihydrogen phosphate, potassium tertraborate, and tert-butanol were purchased from Sigma-Aldrich (St. Louis, MO). Stock solutions were prepared in ultrapure de-ionized (DI) water (>18 MΩ-cm) produced using a laboratory Millipore DI water system. The ozone stock solution was prepared by dissolving ozone produced by an Ozone Solutions TG-10 ozone generator (Hull, IA) in DI water. All ozone stock solutions were prepared in an ice bath inside a chemical fume hood.

4.2.2 Catalyst preparation

Magnetic manganese ferrite ($MnFe_2O_4$) was prepared by a 'combustion synthesis' method described in Desai *et al. (106)*. Briefly, manganese nitrate ($Mn(NO_3)_2$) and iron nitrate ($Fe(NO_3)_3$) were mixed together to achieve a 1:2 Mn:Fe ratio with 10 grams of total nitrate. 10, 15, or 20 grams of poly-vinyl alcohol (PVA) was added to nitrates mixture and the solution was heated in a muffle furnace for a period of 1 hour. A complete and detailed characterization of each produced catalyst is reported in Desai *et al. (106)*. X-ray Photospectroscopy (XPS) analysis was used to analyze the fresh (unused) catalyst as well as catalyst after ozonation experiments (spent). A Surface Science Labs SSX-100 instrument was used to perform the XPS analysis. Each sample for analysis was prepared by distributing a small amount of the powder on a piece of copper adhesive tape so as to achieve uniform and complete coverage. The nominal x-ray beam diameter for this analysis was 600 µm. Two spots were analyzed on each sample.

4.2.3 Experimental system

A sacrificial reactor approach was used throughout the experiments. This approach prevented ozone degassing from solution by eliminating headspace in the reactor and maintained a constant solid:liquid ratio within each reactor. Full details of the experimental approach including the number of replicates sampled at each time point, the total number of samples, and timing of sampling are found in the Quality

Assurance Project Plan governing this research (*107*). Briefly, catalyst performance was investigated using individual time series experiments designed to determine the effect of: catalysts PVA content and Mn mass percentage; catalytic and non-catalytic ozonation; catalyst dosage; ozone dosage; pre-ozonation; DOM; and pH on catalytic enhancement of hydroxyl radical generation. All experiments were performed in a 40 mL glass vial capped with septa caps.

For ozone only experiments, individual reaction vials were filled with 10 mM borate or phosphate pH buffered DI water. The vials were then spiked to a final concentration of 2 μM pCBA and 100 μM tert-butanol. The reaction was initiated by spiking a known amount of ozone into each vial, which varied depending upon the experiment. For experiments containing a catalyst, a known amount of catalyst was added to each vial and the vial was filled with DI water. The vials were then spiked to a final concentration of 2 μM pCBA and 100 μM tert-butanol. Because preliminary studies indicated that both borate and phosphate salts interacted with the catalyst, pH buffering could not be used to maintain a desired pH. Preliminary experiments without the buffers showed that the nascent pH of most catalyst, DI, pCBA and tert-butanol systems was ~8.5-8.8 depending on the catalyst type and dose. Addition of ozone typically resulted in a pH drop of 0.3 to 0.7 pH units depending on catalyst type and dose. Through trial and error it was determined a requisite amount of 0.01 N NaOH or HCl to be added to the reactors prior to ozone addition such that upon ozone addition the initial pH would be 8.3. As detailed later, this addition of NaOH or HCl only established an initial pH upon ozone addition required to bring the initial pH within the reactor to

8.3 for each catalyst. The same amount of NaOH or HCl was then added to the reactors used within the experiment. Finally, a known amount of ozone was added to initiate the experiment.

It should be noted here that the tert-butanol is a radical scavenger ($k_{O3} = 0.003\ M^{-1}s^{-1}$; $k_{\cdot OH} = 5.9 \times 10^8\ M^{-1}s^{-1}$). The addition of excess of tert-butanol with respect to pCBA ensures that all of the pCBA added does not disappear within the time-frame of our experiment. Table 4- 1 shows the selected second-order rate constants for the relevant reaction species and the total calculated first-order ·OH scavenging rates ($k_{\cdot OH}$ [S]) for reaction at pH 8 and room temperature ($\approx 23^o$ C). The bicarbonate/carbonate scavenging rates are shown at the two different pH's where we ran our experiments.

For the pre-ozonation experiments, a known amount of catalyst was first taken in the vial and filled with a pre-specified amount of DI water. The sample was then dosed with a given dosage of ozone (3 mg/L or 20 mg/L as required) and the vial capped. After 24 hours the ozone concentration was confirmed to be exhausted. Thereafter, each vial was spiked with pCBA and tert-butanol and the pH adjusted with 0.01 M NaOH or HCl. The reaction is then initiated by spiking the ozone into the vials. For the NOM experiments, the NOM used in the experiments was collected from the Ohio River and concentrated in the laboratory as described in Pressman (*108*). A working stock solution was prepared by diluting the NOM in DI water mixing on a magnetic stirrer and raising the pH close to a value of 10 by adding 0.01M NaOH. This ensures that the NOM

dissolves in the water. For the ozonation experiments, the pH of this solution is brought down to get a final value of pH 8.3 and the solution filtered to remove any precipitate.

All vials were placed on a rotary shaker. At a specified time point a vial was pulled from the shaker and sacrificed. 3 mL samples were drawn from each vial using a gas-tight syringe. The sample was then passed through a Teflon filter into a vial containing 200 µL of indigo dye to quench the reaction. Preliminary experiments demonstrated that filtering had no effect on the ozone or pCBA determination.

Table 4- 1 Scavenging capacities of model compounds and scavengers

Compound	k_{O3} ($M^{-1}s^{-1}$)	k_{OH} ($M^{-1}s^{-1}$)	[S] (M)	Scavenging Capacity: $k_{OH}[S]$ (s^{-1})	
tert-butanol	0.003	5.9×10^{8}	1.0×10^{-4}	5.9×10^{4}	
pCBA	0.15	5.0×10^{9}	2.0×10^{-6}	1.0×10^{4}	
DOC		2.5×10^{4} L/mg/s	2.6 mg/L	6.5×10^{4}	
HCO_3^-/CO_3^{2-}	<<0.01/<0.01	8.5×10^{6}/ 4×10^{8}	3.16×10^{-5}/ 1.12×10^{-8}	2.7×10^{2}	pH 6.8
			1.0×10^{-3}/ 1.12×10^{-5}	1.3×10^{4}	pH 8.3

4.2.4 Analytical measurements and R_{ct} determination

One aspect of catalyst efficiency is determined by calculating R_{ct} within the system. R_{ct} is the ratio of ·OH exposure to the O_3 exposure during ozonation. Therefore, calculating R_{ct} requires simultaneous measurement of hydroxyl radical (used to

determine ·OH exposure) and molecular ozone concentrations (used to determine ozone exposure) within the reaction system. Dissolved ozone was analyzed using the indigo method (Bader and Hoigne´, 1982). pCBA was analysed using a HPLC (Agilent 1200 series) equipped with a diode-array UV detector operating at a wavelength of 234 nm equipped with a Discovery C18 HPLC column (5µm; 2.1 mm x 100 mm). 250 µL of the quenched sample was injected into the head of the column and eluted with 30:70 of acetonitrile: reagent water containing 0.1% glacial acetic acid at a flow rate 0.5 mL/min under isocratic conditions. Quantitation of ozone concentration and pCBA was achieved using a five point external calibration curve.

Ozone exposure at each time point ($O_{3_{CT}}$) is calculated according to the trapezoidal rule based upon the average concentration of ozone measured in each replicate at two successive time points and contributions from previous time points as shown in the following equation:

$$O_{3_{CTi}} = \frac{O_{3_{t=i-1}} + O_{3_{t=i}}}{2}(t_i - t_{i-1}) + O_{3_{CTi-1}} \quad (4\text{-}1)$$

A plot of $\ln\left(\frac{[pCBA_t]}{[pCBA_0]}\right)$ versus $O_{3_{CT}}$ at each time point results in a straight line. The slope of the resulting line is divided by the rate constant for pCBA reaction with hydroxyl radical ($k = 5.2 \times 10^9\ M^{-1}s^{-1}$). The result of this calculation is the R_{ct}.

4.3 Results and Discussion

One important aspect of these reaction systems is the use of tert-butanol to provide a constant background scavenger capacity. tert-butanol is frequently used in this capacity as it has low reactivity with ozone, but moderate reactivity with hydroxyl radicals ($k_{O3} = 0.003\ M^{-1}s^{-1}$; $k_{\cdot OH} = 5.9 \times 10^{8}\ M^{-1}s^{-1}$) (*105*). Moreover tert-butanol is thought to behave predominantly as an inhibitor in the ozone decomposition cycle, though some promotion via H_2O_2 production is possible (*109*). The addition of excess tert-butanol with respect to pCBA ensures that all of the pCBA added does not disappear within the time-frame of our experiment.

The addition of this synthetic hydroxyl radical scavenger will affect the absolute value of R_{ct} of any system. Together with the ambient carbonate species (HCO_3^- and CO_3^{2-}) the overall scavenging capacity of the system is dictated by the concentration of these constituents. Calculation of the total initial kinetic scavenging capacity (e.g. the Da^I values) of both tert-butanol and pCBA show that tert-butanol out-competes pCBA by a factor of 6, and both outcompete carbonate by a factor of 5 at pH 8.3 and 218 at pH 6.3 (Table 4-1). The loss of both tert-butanol and pCBA during the course of the reaction will result in a change in the overall scavenging capacity of the system. The degree of change depends on the magnitude of loss of tert-butanol and pCBA, assuming no change in carbonate scavenging, and no contribution to scavenging from tert-butanol or pCBA reaction products. For example, we see that when pCBA C/C_o drops to 0.6 the total loss in scavenging is about 10.9% and about 33% when C/C_o drops to 0.1 (Table 4-2).

Table 4- 2 Percent loss of scavenging capacities

C/C_0		% loss of total scavenging
pCBA	tert-butanol	
0.6	0.94	10.9
0.5	0.92	14.1
0.25	0.85	23.7
0.1	0.76	33.3

It is important to point out that tert-butanol and pCBA were added at the same concentrations in each reaction vial. Therefore, by using the same total scavenging capacity for each reaction, R_{ct} values can be compared in a relative sense between experiments. Table 4-1 also provides estimated bicarbonate or DOC concentrations that would achieve similar ·OH scavenging capacity. The concentrations of DOC in natural waters range from < 1 mg/L to > 50 mg/L (*110*). The bicarbonate ion concentrations of natural waters lie largely within the range 1×10^{-3} to 5×10^{-3} M (*111*). Thus the scavenging capacity used in our systems is representative of natural waters which have DOC and bicarbonate/carbonate scavengers.

Finally, tests were performed to evaluate the degree of pCBA sorption on the catalysts; and it was found to sorb negligibly at all experimental conditions performed based upon preliminary studies. The negative charge of the deprotonated pCBA and the fact that pH range in this study was above the pH_{pzc} (below) suggests charge repulsion limiting sorption.

Experiments involving catalyst were run without the use of any pH buffers, as both borate and phosphate buffers were shown to affect the system within the pH region investigated (data not shown). The reaction matrix pH prior to ozone addition was established with mineral acid/base addition, such that upon ozone addition the initial pH of the system was approximately 8.3. Due to the lack of pH buffers, the pH of systems run with catalyst drifted downward (towards neutral), typically 0.3 to 0.7 pH units. It is uncertain the exact influence of the pH depression on pCBA removal. Elovitz *et al.* (*105*) showed that within the bulk aqueous phase, a lower pH decreases the rate of ozone decomposition to ·OH via the classical decomposition model, and hence pCBA loss is slower, R_{ct} values are smaller, but overall, the same amount of pCBA removal is achieved (*112*). However, those studies were performed in the absence of carbonate, whose contribution to scavenging capacity changes dramatically with pH. The pH effect on the chemistry occurring at the surface of the catalyst (e.g. ozone reaction with surface sites to produce ·OH, potential reactions of ·OH, and any redox cycling within the catalyst metal centers) is not known due to the unknown nature of the surface sites and the complexity of mixed metal species. However, pH experiments discussed later demonstrate that lower pH leads to slower and overall less pCBA removal in both ozone-alone and catalytic ozone systems. This discussion is relevant in that it suggests that under the impact of pH depression, the pCBA loss observed in the unbuffered systems is likely conservative relative to that which would be achieved if pH remained constant. pH buffering achieved from natural constituents may, however, impact the

system in other ways (for example the negative effect of the presence of DOM). As such full catalyst evaluation is best done in the specific system of interest.

The BET surface area and pH_{zpc} for each catalyst are reported in Table 4-3. pH_{zpc} is the pH where the net surface charge is zero. When the aqueous solution pH is below the pH_{zpc} then we have the condition $[\equiv MOH_2^+] > [\equiv MO^-]$, the net surface charges being positive. At pH's above pH_{zpc} we have $[\equiv MO^-] > [\equiv MOH_2^+]$, the net surface charges being negative.

One general observation made in all catalytic systems is the presence of both a fast initial phase, corresponding to rapid loss of O_3 and pCBA, and second phase with slower loss of both. This phenomenon is frequently seen in systems of natural waters containing various O_3 and ·OH reactive species. The observation of the fast initial phase in these catalyst systems is interesting and is discussed later. However, it is mentioned now such that its presence can be noted in the subsequent figures.

Table 4- 3 BET surface area and pH_{zpc} of the catalysts

Catalyst	BET Area (m^2/g)	pH_{zpc}
$MnFe_2O_4$ 10PVA	48.8	3.1
$MnFe_2O_4$ 15PVA	57.4	3.8
$MnFe_2O_4$ 20PVA	39.9	3.6
$Mn_{0.5}Fe_{2.5}O_4$ 15PVA	46.4	3.0
$Mn_{2.5}Fe_{0.5}O_4$ 15PVA	50.9	3.7

4.3.1 Effect of catalyst dosage

Experiments were conducted at three different dosages of $MnFe_2O_4$ 15PVA catalyst to observe the effect of catalyst dosage on hydroxyl radical production. Catalyst dosages of 75 mg/L, 150 mg/L and 250 mg/L were investigated with an ozone dosage of 3 mg/L. Figure 4-1 indicates that presence of the catalyst resulted in increased removal of pCBA compared to ozone alone. However, increasing the catalyst dose did not result in an observed increase in pCBA removal within the first 5.5 minutes (~ 67% removal). Higher catalyst dosages resulted in faster ozone decay rate. It took 4.5 minutes at a catalyst dose of 250 mg/L to decompose 92% of ozone in the system as compared to 6.5 minutes for a 150 mg/L dose and 10 minutes for a 75 mg/L dose. If we compare the pCBA removal at this same extent of ozone decay (92% O_3 loss), we see that the pCBA removals were 63%, 66% and, 71% with catalyst dosages of 250 mg/L, 150 mg/L and, 75 mg/L, respectively. If it is assumed that there is the same stoichiometric conversion of O_3 to ·OH at the catalyst surface in all three systems, then the lower effective ·OH - CT in the bulk phase (where the reaction is presumed to take place) seemingly suggests greater quenching of ·OH at the catalyst surface with increasing catalyst dose. Hence, it could be as simple as the catalyst itself adds to the scavenging ·OH capacity of the system, and a larger catalyst dose adds a larger scavenging capacity. Alternatively, higher ·OH formation with increased catalyst dose (consistent with the higher rate of O_3 decay) could allow for ·OH -·OH quenching to take place. Finally, with the assumption that the catalyst itself does not quench radicals, there could be a shift in the stoichiometry of O_3 to ·OH conversion, with the higher catalyst dose having a less

efficient stoichiometry. This finding implies that either there is an additional generation of radicals being quenched in the system (likely on the catalyst surface) or the effective yield for hydroxyl radicals is lower at a higher catalyst dosage.

Figure 4- 1 Effect of catalyst dosage. Conditions: pH= 8.3; [O_3] = 3mg/L; [pCBA] = 2µM; [t-BuOH] = 100µM; T=25°C

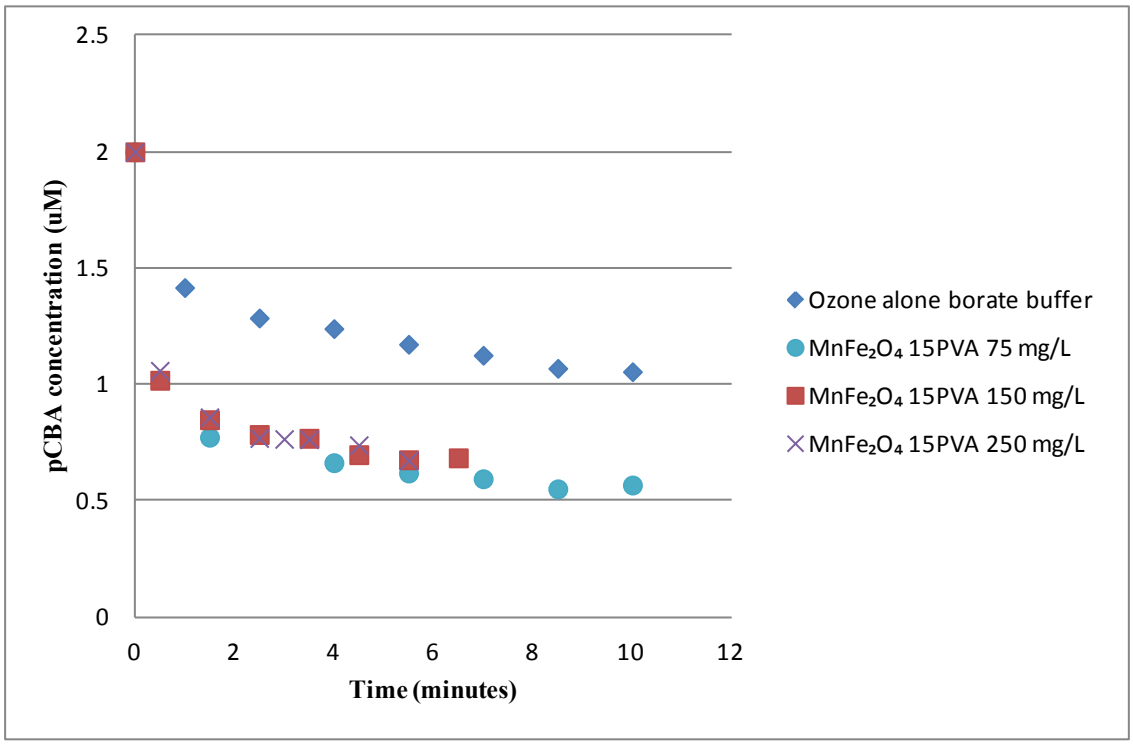

Additionally, the data indicate that the number of active catalytic sites at the lowest dosage (75 mg/L) is sufficient to decay the 3 mg/L of ozone dosage to its maximum hydroxyl radical yield within the three dosages tested.

Figure 4- 2 R_{ct} values for different catalyst dosages

Condition	R_{ct}	R^2
Ozone alone borate buffer	6.9×10^{-9}	0.99
$MnFe_2O_4$ 15PVA 75 mg/L	1.3×10^{-8}	0.97
$MnFe_2O_4$ 15PVA 150 mg/L	2.2×10^{-8}	0.97
$MnFe_2O_4$ 15PVA 250 mg/L	3.6×10^{-8}	0.95

R_{ct} values for different catalyst dosages are shown in Figure 4-2. Ozone decay was then fitted as a pseudo-first order reaction in order to gain further insight into the reaction system (Figure 4-3). The plot clearly showed two reaction phases. Such an observance is common in wastewaters as well as natural waters which contain dissolved organic matter (DOM) that has multiple reaction sites for ozone. The initial phase is often referred to as the 'instantaneous ozone demand (IOD)' and this rate does not follow apparent first-order kinetics (*113*). The second phase follows first-order kinetics and proceeds at a slower rate. It is generally considered that the fast reacting sites of DOM (and potentially some inorganic compounds) correspond to the IOD, and the less reactive sites of DOM combine to demonstrate first-order behavior (*114*). Given the presence of a two-phase behavior in the absence of DOM in our system, in analogy to a DOM system, it appears that there are limited number of fast reacting sites on the catalyst surface, and a larger number of less reactive sites.

Comparing the ozone decay rate (k_d) as a function of catalyst dose for the second phase of the reaction, the pseudo-first order ozone decay rate increases as the catalyst dosage increases which is consistent with literature which reports increasing DOM or catalyst dose result in increasing k_d. When we normalize the k_d by the dose we see the values ranging from (1.06 ± 0.11) x 10^{-3} $min^{-1}mg^{-1}$ for a dose of 250 mg/L to (1.74 ± 0.17) x 10^{-3} $min^{-1}mg^{-1}$ for a dose of 75 mg/L (Table 4-4). A one-way ANOVA test showed that the normalized k_d values did not differ significantly (p=0.13). A calculation for dose normalized k_d for catalytic ozonation of Lake Zurich waters using carbon aerogels from data provided in their paper by von Gunten *et al* showed that their values were also constant (*27*).

Figure 4- 3 Ozone decay rate

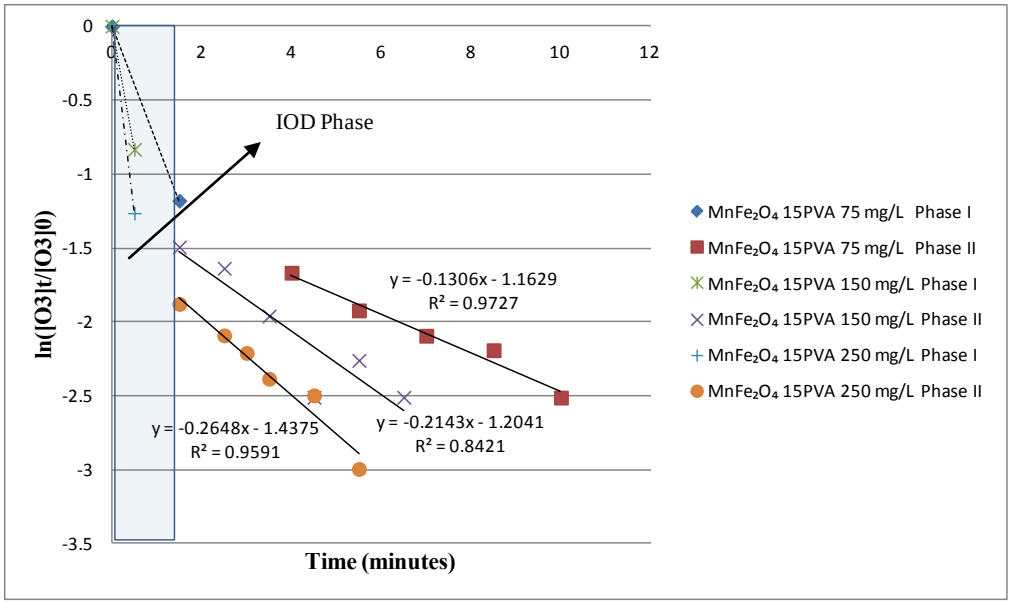

Table 4- 4 Ozone decay (k_d) per catalyst dose

Catalyst	$\frac{k_d}{catalyst\ dose}$ ($min^{-1}mg^{-1}$)
$MnFe_2O_4$ 15PVA 75mg/L	$(1.74 \pm 0.17)\ X\ 10^{-3}$
$MnFe_2O_4$ 15PVA 150mg/L	$(1.43 \pm 0.31)\ X\ 10^{-3}$
$MnFe_2O_4$ 15PVA 250mg/L	$(1.06 \pm 0.11)\ X\ 10^{-3}$

Thus conversion of O_3 to ·OH may not lead to ·OH exposure that is effective in reacting with pCBA.

4.3.2 Effect of PVA variation

Experiments were conducted at three different PVA contents to determine the impact of PVA on the resulting catalyst efficiency. PVA: nitrate ratios of 1:1 ($MnFe_2O_4$ 10PVA); 1.5:1 ($MnFe_2O_4$ 15PVA) and 2:1 ($MnFe_2O_4$ 20PVA) were investigated at a total catalyst dosage of 250 mg/L. All three compositions of the catalyst resulted in improved removal of pCBA when compared to ozone alone (Figure 4-4). pCBA removal during the first 5.5 minutes of the reaction trended from $MnFe_2O_4$ 20PVA (68%) ≅ $MnFe_2O_4$ 15PVA (66%) > $MnFe_2O_4$ 10PVA (49%) and no PVA (41%).

Mean pCBA loss observed for $MnFe_2O_4$ 20PVA and $MnFe_2O_4$ 15PVA was not statistically different ($p=0.35$ at 95% C.I) indicating that these two PVA compositions

Figure 4- 4 Effect of PVA variation. Conditions: pH= 8.3; [O_3] = 3mg/L; [pCBA] = 2µM; [t-BuOH] = 100µM; T=25°C

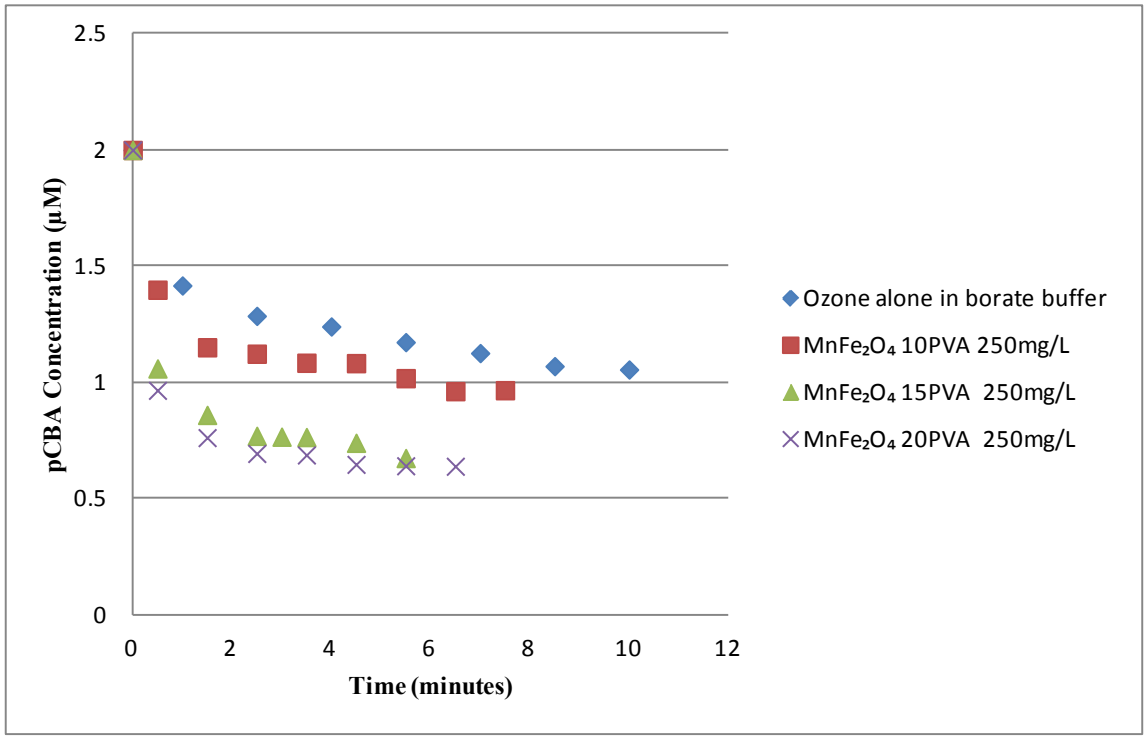

had the same hydroxyl exposure. Ozone decay and the R_{ct} of the secondary phase in each system followed the same trend observed in pCBA removal. The observed ozone decay rate constants ranged from 1.07 x 10^{-3} $min^{-1}mg^{-1}$ for $MnFe_2O_4$ 20PVA and $MnFe_2O_4$ 15PVA to 0.67 x 10^{-3} $min^{-1}mg^{-1}$ for $MnFe_2O_4$ 10PVA. R_{ct} ranged from 3.0 x 10^{-8} for $MnFe_2O_4$ 20PVA and $MnFe_2O_4$ 15PVA to 1.05 x 10^{-8} for $MnFe_2O_4$ 10PVA, and 0.69 x 10^{-8} for ozone alone.

Interestingly, the decreasing trend observed as a function of PVA content for pCBA removal, ozone decay, and R_{ct} was not correlated to BET surface. While increasing PVA content from $MnFe_2O_4$ 10PVA to $MnFe_2O_4$ 15PVA did enhance

hydroxyl radical production, an observed increase of carbon content within the catalyst also resulted from increasing PVA content. Therefore, the observed trend may reflect the presence of increased carbon (shown in Section 3) instead of an impact of changes to the structure of Mn and Fe on the surface of the catalyst. In order to examine the impact of Mn and Fe composition on the surface in more detail, the next set of experiments were investigated.

4.3.3 Effect of Mn:Fe stoichiometric ratio

Three different compositions with varying Mn:Fe ratios were synthesized and tested for their activity to enhance hydroxyl radical production within the ozonation system (Figure 4-5). Differences in catalyst performance were immediately observed when stoichiometric ratios of Mn and Fe were varied while producing the catalyst. Following an ozone dosage of 3mg/L, greater than 90% of the ozone decomposed within 1 minute for the $Mn_{2.5}Fe_{0.5}O_4$ 15PVA composition (Figure 4-5). The same level of ozone decomposition spanned 3.5 minutes for the $MnFe_2O_4$ 15PVA composition. For the $Mn_{0.5}Fe_{2.5}O_4$ 15PVA composition, only 80% of ozone was degraded during the entire 14 minute reaction duration (Figure 4-5).

Figure 4- 5 Ozone consumptions as a function of time

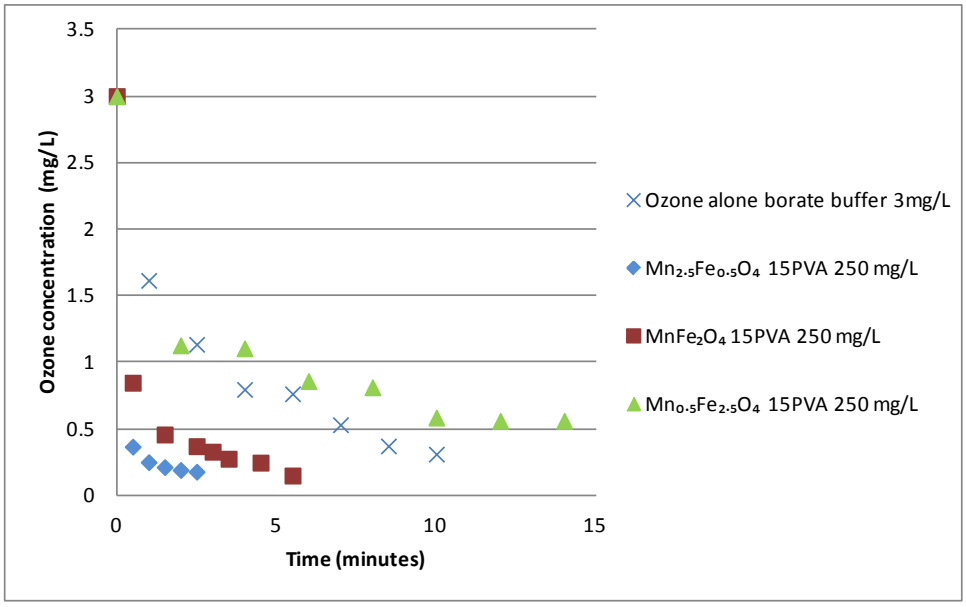

Examining pCBA removal for each Mn:Fe composition provided additional insight into the complicated relationship between ozone exposure, R_{ct}, and organic removal (Figure 4-6).

While >90% of ozone degraded in the first minute for the $Mn_{2.5}Fe_{0.5}O_4$ 15PVA composition, pCBA removal was only 18%. For $MnFe_2O_4$ 15PVA, 3.5 minutes was required to achieve >90% ozone decomposition within the system. However, 61.7% of pCBA removal occurred. The highest pCBA removal was observed with the $Mn_{0.5}Fe_{2.5}O_4$ 15PVA catalyst where 72% pCBA removal occurred in 14 minutes although only 80% of ozone decomposed. The data indicate that lower Mn:Fe ratios

promote greater pCBA removal despite having lower R_{ct} values and ozone decay rates (Table 4-5).

Figure 4- 6 Effect of Mn:Fe stoichiometric variation on pCBA removal. Conditions: pH= 8.3; [O_3] = 3 mg/L; [pCBA] = 2 µM; [tert-butanol] = 100 µM; T=25°C

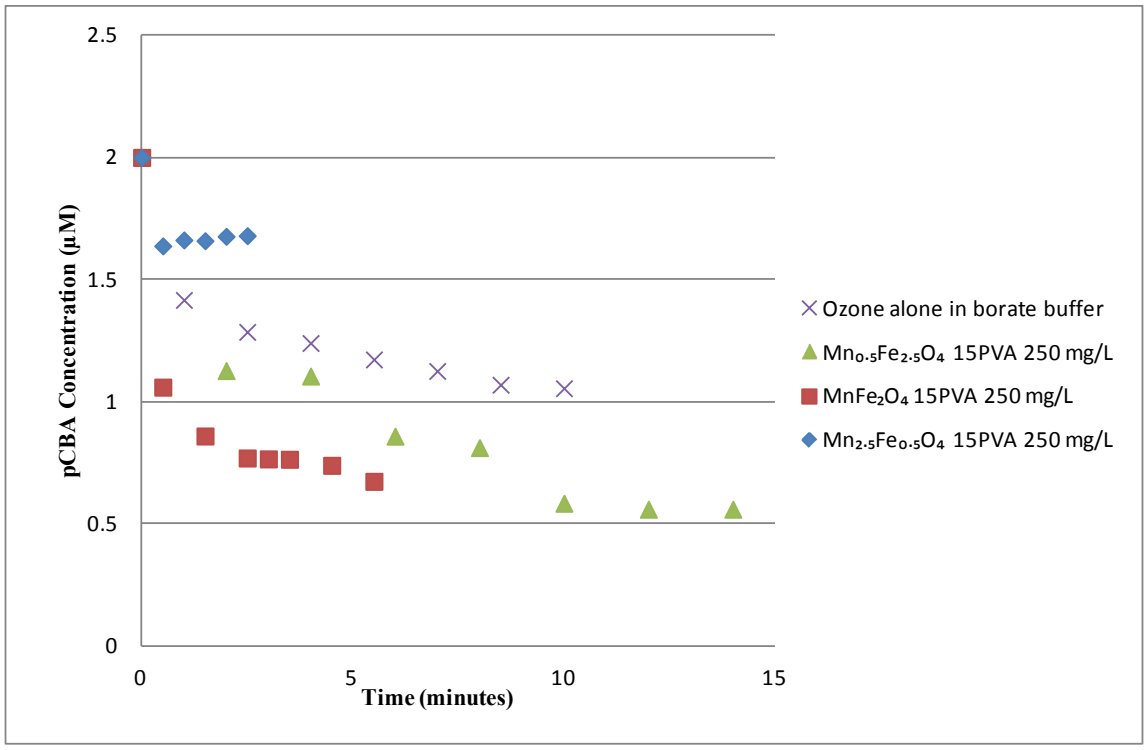

Because system conditions were constant except for the Mn:Fe ratio of the catalysts, catalysts with a higher Mn percentage are hypothesized to contain a higher number of fast reacting surface sites that rapidly decompose ozone and quench the generated hydroxyl radicals on the surface of the catalyst. Also, because of potentially higher concentration of hydroxyl radicals from the rapid decomposition of O_3, there

could be greater radical-radical interactions leading to more radical quenching rather than pCBA reaction.

Table 4- 5 Ozone decay rates and R_{ct} values

Catalyst	k_d (s^{-1})	Rct	R^2
Ozone alone	$(3.01 \pm 0.18) \times 10^{-3}$	6.9×10^{-9}	0.99
$Mn_{0.5}Fe_{2.5}O_4$ 15PVA	$(1.14 \pm 0.14) \times 10^{-3}$	5.8×10^{-9}	0.93
$MnFe_2O_4$ 15PVA	$(5.14 \pm 0.50) \times 10^{-3}$	3.6×10^{-8}	0.95
$Mn_{2.5}Fe_{0.5}O_4$ 15PVA	$(5.68 \pm 0.12) \times 10^{-3}$	2×10^{-8}	0.89

These results exemplify several different points regarding AOP design and the description of a system's efficacy. The general goal of an ozone-based AOP is the conversion of O_3 to ·OH. However, the rate at which ·OH exposure is generated may be a consideration when the reaction time (residence time) in the reactor is limited. Comparing short reaction times of < 5 min for the $MnFe_2O_4$ 15PVA and $Mn_{0.5}Fe_{2.5}$ O_4 15PVA catalysts shows that the $MnFe_2O_4$ 15PVA catalyst was more effective at eliminating pCBA (there are insufficient data for < 1 minute to compare the results for the $Mn_{2.5}Fe_{0.5}O_4$ 15PVA catalyst). On the other hand, given long enough reaction times, the $Mn_{0.5}Fe_{2.5}$ O_4 15PVA formulation is more effective.

R_{ct} value may be another way to assess an AOP. However, R_{ct} alone only informs on the ratio of ·OH exposure to O_3 exposure, and not on the absolute value of the ·OH exposure. Moreover, R_{ct} does not provide any measurement of a stoichiometric

conversion of O_3 to ·OH. That is, higher R_{ct} values for a given ozone dose does not necessarily result in greater ·OH exposure in the bulk phase. This aspect of stoichiometric efficiency may not be the most important design criterion, but the concept of the stoichiometry of O_3 conversion to ·OH may explain some of the results.

An interesting observation from the above experiments is that rapid decay of ozone (i.e. with higher Mn:Fe ratios) does not lead to commensurately higher ·OH exposure in the bulk phase. AOPs may be designed with the goal of rapid conversion of O_3 to ·OH. If the stoichiometric ratio of the conversion of O_3 to ·OH remains the same under the influence of this accelerating factor, then one would observe faster loss of pCBA with fast O_3 decomposition but equal overall loss of pCBA, in all systems. Such effects were putatively observed in Elovitz *et al.* (*112*) for pH and temperature variations. In the case of a peroxone AOP, relative to a system with no peroxide, there is faster decomposition of ozone and both faster and greater pCBA loss due to a more favorable stoichiometric conversion of O_3 to ·OH (*115*). The experiments described above demonstrate yet a different trend of enhanced ozone decomposition, but lower overall pCBA loss. Whether this is a result of the quenching of ·OH at the catalyst surface (·OH -catalyst interactions, or ·OH -·OH interactions), or a change in O_3-to-·OH stoichiometry with changes in Mn:Fe formulations is not certain.

Additionally, the varied Mn:Fe compositions could produce different stoichiometric yields of hydroxyl radicals based upon differences in structural composition. The latter concept has some theoretical backing from various literature

reports. Brillas *et al.(116)* explored the reactivity of Fe^{2+} with ozone as presented in the following reactions:

$$O_3 + Fe^{2+} \longrightarrow FeO^{2+} + O_2\cdot \quad (4\text{-}2)$$

$$FeO^{2+} + H_2O \longrightarrow Fe^{3+} + OH\cdot + OH^- \quad (4\text{-}3)$$

$$FeO^{2+} + Fe^{2+} + 2H^+ \longrightarrow Fe^{3+} + H_2O \quad (4\text{-}4)$$

The authors hypothesize that at lower Fe^{2+} concentrations reaction (5) is predominant. However, at higher Fe^{2+} concentrations reaction (6) becomes predominant. Therefore, an increase in Fe^{2+} concentration limits hydroxyl radical production. Similar chemistry has also been observed with Mn^{2+} ions as shown below (*117*):

$$O_3 + Mn^{2+} \longrightarrow MnO^{2+} + O_2 \quad (4\text{-}5)$$

$$MnO^{2+} + H_2O \longrightarrow Mn^{3+} + OH\cdot + OH^- \quad (4\text{-}6)$$

$$2Mn^{3+} + 2H_2O \longrightarrow MnO_2 + Mn^{2+} + 4H^+ \quad (4\text{-}7)$$

Additionally, based on the redox potentials the following reactions can take place (*118*)

$$Fe^{3+} + e^{-} \longrightarrow Fe^{2+} \quad (E^0 = 0.77V) \qquad (4\text{-}8)$$

$$Mn^{3+} + e^{-} \longrightarrow Mn^{2+} \quad (E^0 = 1.51V) \qquad (4\text{-}9)$$

Thus thermodynamically the following reaction is possible:

$$Mn^{3+} + Fe^{2+} \longrightarrow Fe^{3+} + Mn^{2+} \quad (E^0 = 0.73V) \qquad (4\text{-}10)$$

A redox cycle between the Mn and Fe may thus also occur in the system. XPS analysis performed to understand the oxidation state of the Mn and Fe on the surface of the catalyst showed that both the metals were present in multiple oxidation states both before and after ozonation (Table 4-6). The peaks of Mn^{2+}/Mn^{3+} and Fe^{2+}/Fe^{3+} differ by just 1eV. Thus, it is hard to state conclusively from the data which oxidation changes took place in the ozonation process.

As stated earlier, the distribution of manganese in the tetrahedral and octahedral sites governs the capability of the catalyst. A number of reports have found the tetrahedral sites to be inactive and attribute the octahedral sites as responsible for any catalytic activity. Moreover, the tetrahedral sites are not accessible to the reactants (*74*).

Table 4- 6 Peak binding energy values as determined from high resolution XPS scans

After ozonation

Sample	Fe $2p_{3/2}$ (eV)	Mn $2p_{3/2}$ (eV)
$Mn_{2.5}Fe_{0.5}O_4$		
- 1	710.9	642.5
- 2	711.0	642.5
$Mn_{0.5}Fe_{2.5}O_4$		
- 1	711.0	642.2
- 2	710.8	642.1
$MnFe_2O_4$ PVA10		
- 1	710.7	642.0
- 2	710.7	641.9
$MnFe_2O_4$ PVA15		
- 1	710.9	642.0
- 2	711.0	642.3
$MnFe_2O_4$ PVA20		
- 1	710.9	642.0
- 2	710.8	642.0
FeO	**709.8 ± 0.7**[1]	
Fe_2O_3	**711.0 ± 0.2**[1]	
MnO		**641.0 ± 0.5**[1]
MnO_2		**642.0 ± 0.2**[1]

Before ozonation

Sample	Fe $2p_{3/2}$ (eV)	Mn $2p_{3/2}$ (eV)
$Mn_{2.5}Fe_{0.5}O_4$		
- 1	710.6	642.2
$Mn_{0.5}Fe_{2.5}O_4$		
- 1	710.6	641.7
$MnFe_2O_4$ PVA10		
- 1	710.9	641.8
$MnFe_2O_4$ PVA15		
- 1	710.8	641.9
$MnFe_2O_4$ PVA20		
- 1	710.4	642.1

1. Values from Handbook of X-Ray Photoelectron Spectroscopy, Perkin-Elmer Corp., Eden Prairie MN (1979)

Thus it can be said that the octahedral sites are the actual surface sites where the reaction takes place. Hence, it is the distribution of Mn and Fe in the octahedral sites that will govern the reaction chemistry. Given the very presumed similar chemistry of Fe and Mn it should have made no difference in the reactivity given the distributions based on stoichiometry. The differences in reactivity observed in our experiments are hard to explain with the given data and we need to do a detailed catalyst characterization in order to understand the distribution of the metals in the octahedral sites to explain the particular trend for pCBA removal.

4.3.4 Effect of ozone dosage

Two different dosages of ozone (3mg/L and 5mg/L) were evaluated for their impact on the catalytic activity of the PVA15 catalysts at a dosage of 150 mg/L (Figure 4-7). As could be expected data indicate that pCBA removal is enhanced by increasing ozone dosage. Additionally, pCBA removal is enhanced in the presence of the catalysts compared to when ozone is present alone.

Without the catalyst pCBA removal increased from 47.2% to 62.3% with an increase in ozone dosage from 3mg/L to 5mg/L within first 10 minutes. In presence of the catalyst at an ozone dosage of 3mg/L, 66.1% of pCBA was removed in 5.5 minutes compared to ozonation alone which removed 41.3% pCBA. The same trend was observed at an ozone dosage of 5mg/L in presence of the catalyst 81.2% removal of pCBA was observed in the first 14 minutes as compared to 64.4% in absence of any catalyst within the same time frame.

Figure 4- 7 Effect of ozone dosage. Conditions: pH= 8.3; [pCBA] = 2µM; [tert-butanol] = 100µM; T=25°C

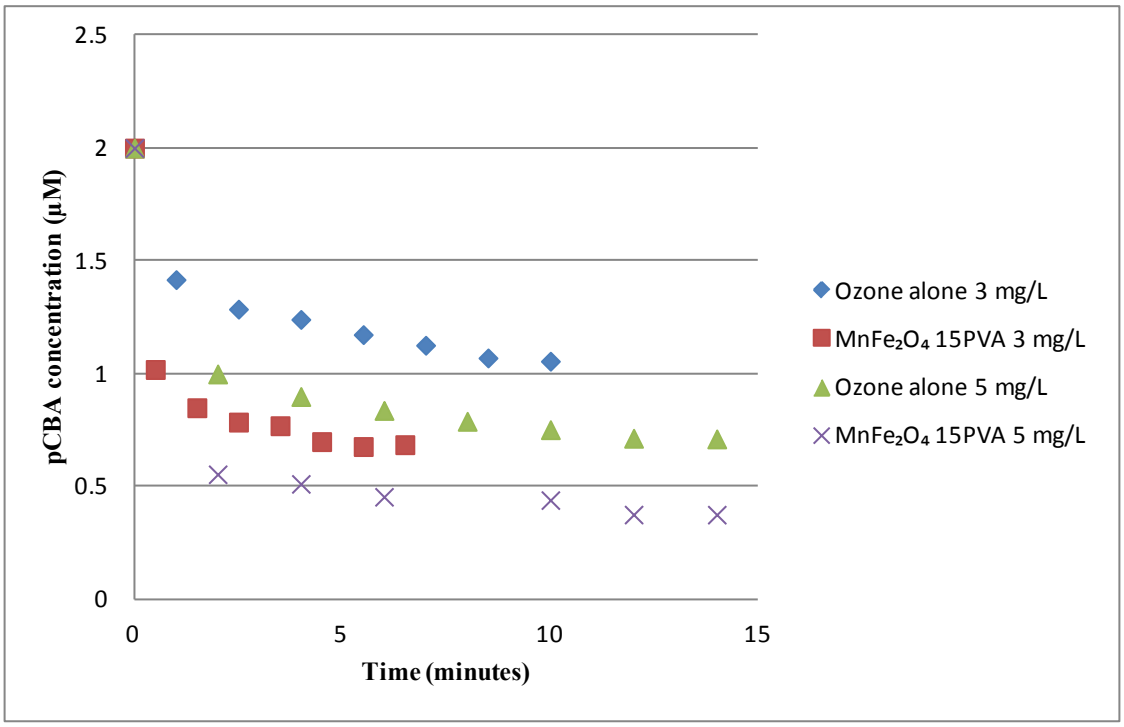

4.3.5 Effect of pre-ozonation and NOM

Experiments were conducted to examine the effect of pre-ozonating the catalyst ($MnFe_2O_4$ 15PVA at a dose of 150 mg/L). The catalyst was first ozonated with either an ozone dose of 3 mg/L or 20 mg/L. The dissolved ozone in the system was allowed to decompose completely (24 h), and then pCBA and tert-butanol were spiked into the system. The system pH was then adjusted so that after addition of the second ozone dose, the system pH would initially be 8.3. A second dose of 3 mg/L ozone was added and pCBA and ozone concentrations monitored. Pre-ozonating the catalyst with 3mg/L had no discernible effect on pCBA removal compared to the same system without pre-

ozonation (Figure 4-8). However, a pre-ozonation dose of 20mg/L had a marked effect on the rate of removal of pCBA. In fact the removal of pCBA within the first 10 minutes was less with the 20 mg/L pre-dose compared to the single dose ozone-only system (29.2% compared to 47.2%). Around 48.5% of pCBA with a pre-ozonation of 20 mg/L system was observed in about 24 minutes. Thus a 20 mg/L pre-ozonation dose could have completely eliminated the active sites which could not be regenerated by adjusting the pH to 8.3 as opposed to a pre-ozonation dose of 3 mg/L.

Figure 4- 8 Effect of pre-ozonation and NOM on pCBA removal. Conditions: pH= 8.3; [pCBA] = 2µM; [tert-butanol] = 100µM in all experiments except NOM study where no tert-butanol is added; Final ozone dose = 3mg/L; T=25°C

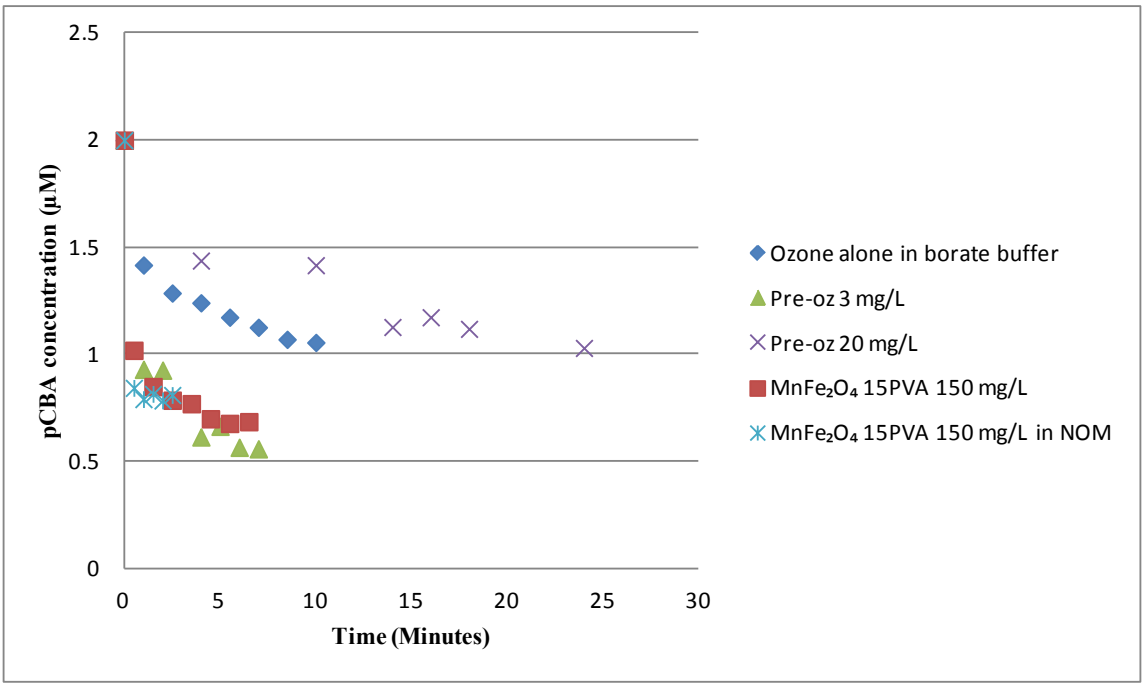

One of the more curious results of the pre-ozonation tests at a dose of 3 mg/L is the fact that the two-phase kinetics of both ozone decomposition and pCBA loss were observed for the second O_3 dose. As mentioned previously, two-phase kinetics are frequently observed in natural systems containing DOM. There is a general theory that the DOM contains a variety of reactive moieties. There is a low concentration of O_3-reactive moieties that leads to fast (sometimes referred to as instantaneous ozone demand, IOD) consumption of ozone and high yields of ·OH ((*105, 113*)). There is a larger concentration of moderately O_3-reactive sites that combine to show a log-linear decrease in time (first-order kinetics). (There is likely another fraction of sites that are very unreactive and are not relevant under the time ranges of most ozonation processes). Under this presumption, an initial dose of ozone would consume the IOD sites. The second ozone dose would therefore involve only the remaining second phase sites, and as such the IOD phase would not be observed.

The presence of a fast IOD phase in our catalyst systems could be due to either reactive low concentration (relative to the ozone dose) of highly reactive catalyst sites that get consumed as would reactive DOM moieties. Alternatively, there could be impurities due to the PVA, or Fe or Mn that was not incorporated into the catalyst structure. In either case one would suspect that these impurities would also get consumed with the first dose, as the single dose results show two phases. The presence of the two-phase kinetics that mirrors the first dose results suggests that the highly reactive sites were regenerated over the course of the experiment. If they regenerate on short time-scales similar to the IOD time-scales, the system would be regenerating the

reactive sites as they are being consumed, and hence two phase kinetics would not be as evident. If there is a slower regeneration process (e.g. >1 h<t<24hr), then it is possible the reactive sites regenerated overnight and were available for the second O_3 dose that was added 24 hours after the first dose. The results of the 20 mg/L pre-dose suggests that the regeneration process is either destroyed or greatly retarded due to high exposure to O_3 and ·OH. Extending these observations to predictions of catalyst longevity is difficult. More experiments are needed. However, there is some suggestion of catalyst regeneration.

Experiments were also conducted in presence of 2.6 mg/L of dissolved organic carbon (DOC) to determine the impact of NOM on radical production. It should be noted here that in these set of experiments we did not add any tert-butanol to the system that we were adding in our earlier set of experiments. As it is evident from Table 4-1, a DOC of 2.6 mg/L has a comparable scavenging capacity (6.5×10^4 s^{-1}) as the tert-butanol (5.9×10^4 s^{-1}). The primary interest in conducting this experiment was to see if the DOM which is mainly thought to be a scavenger in natural systems has the same effect as tert-butanol which primarily acts as a scavenger too (it can act as a promoter too). Not surprisingly, the presence of NOM reduced the catalyst efficiency. In fact a comparison with tert-butanol system suggests that these two systems were similar. At a time point of 2.5 minutes both the systems gave a 60% removal of pCBA within the system. In theory, NOM may affect the system is different manners. For example, NOM may sorb to the active sites on the surface of the catalyst and thus block the sites from O_3. In addition, as

mentioned NOM serves as a hydroxyl radical scavenger competing with pCBA for ·OH in the bulk phase ·OH.

Figure 4- 9 Ozone decomposition kinetics under different pre-ozonation and NOM conditions

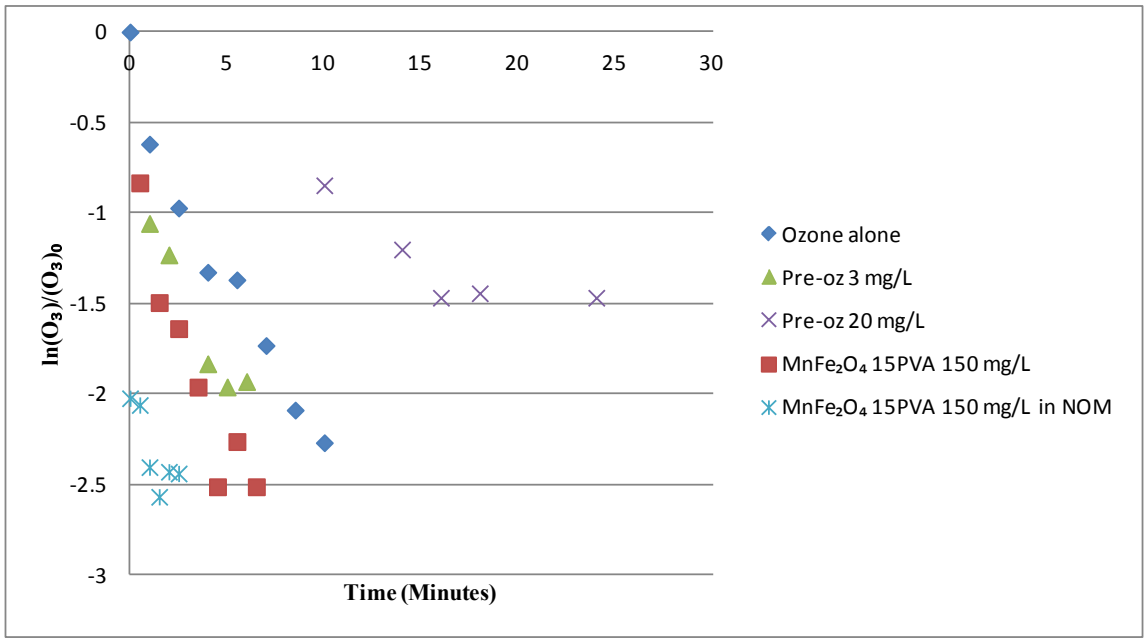

4.3.6 Effect of pH

Two initial pH conditions (pH 8.3 and pH 6.8) were evaluated to determine the effect of system pH on catalyst performance (Figure 4-10). It is important to mention here that for the pH 6.8 experiments with the catalyst, no buffers were used (just like the pH 8.3 experiments as discussed earlier). The downward drift in pH during the pH 6.8

experiments was more pronounced than with the pH 8.3 experiments; the pH dropped as much as 1-1.2 pH units for some of the samples in the time series.

Figure 4- 10 Removal of pCBA under different pH conditions

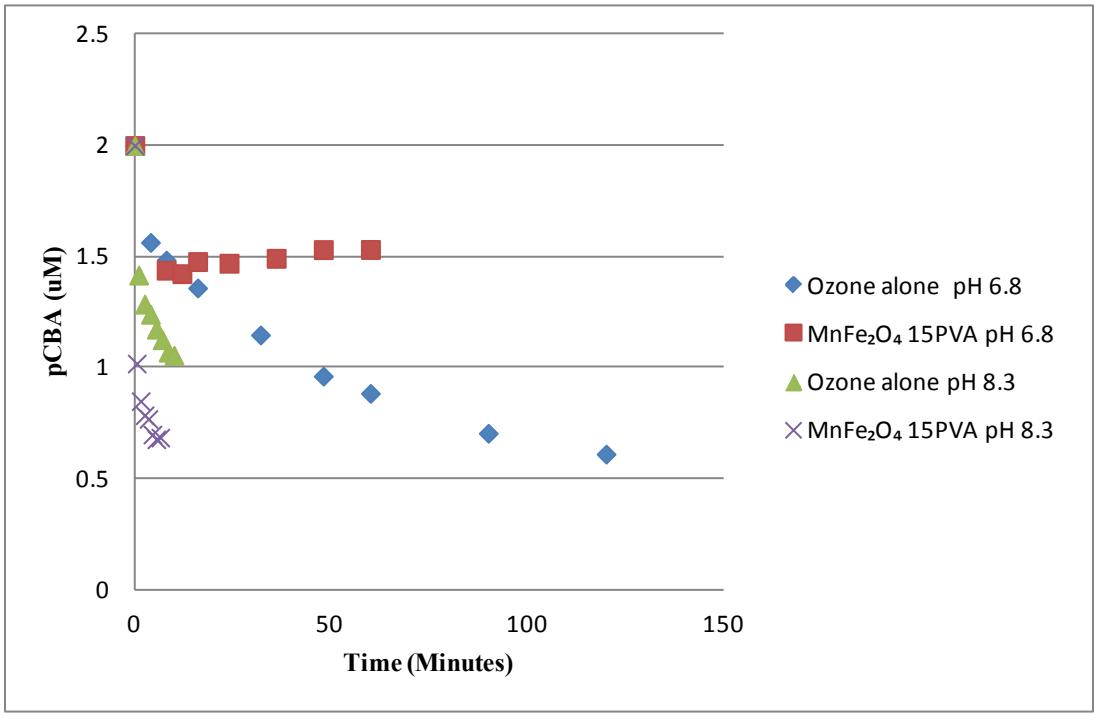

Comparing systems without the catalyst at pH 8.3 (10 mM borate buffer) and pH 6.8 (10 mM phosphate buffer) indicates that the decay of pCBA was faster at higher pH. Examining the ozone decomposition kinetics (Figure 4-11) showed that the decay of ozone was also faster at higher pH. It is a well known fact that in natural waters, under

the second phase of ozonation, a higher pH favors the autocatalytic chain reaction which results in faster ozone decomposition (*113*). Since the scavenging capacities used in our experiments are comparable to natural waters such a trend is expected. Also it should be noted that the changes in bicarbonate/carbonate concentrations at different pH's can also have marked effects on the pCBA removal since bicarbonate/carbonate species act as a scavenger. Comparing the data for the catalyst experiments at different pH's, it is easily seen that pCBA removal was enhanced at pH 8.3 compared to pH 6.8. Interestingly the catalyst performance in the system at pH 6.8 was poorer than the ozone-alone system at the same pH. The ozone decomposition data (Figure 4-11) indicate that the ozone decay was in fact faster in presence of the catalyst when compared to ozone alone as one would have expected. But strangely, lower pCBA removal (Figure 4-12) indicates that the available ·OH radical in the bulk phase was limited. In fact ·OH radicals are generated in the initial phase but barely any pCBA removal is seen in the second phase.

Since the pK_a value of pCBA is close to 3.9, and the reaction between ·OH and pCBA is with the deprotonated form of pCBA, the pCBA is almost completely dissociated at both pH 6.8 and 8.3. Hence, changes in reactivity of pCBA are not a plausible explanation of the pH effects. There could be an effect of decreasing pH leading to the increased concentration of protonated (neutral) pCBA sorbing to the catalyst surface, and acting as a site blocker similar to the effect described for DOM above. The pH_{zpc} of the catalyst $MnFe_2O_4$ 15PVA is about 3.8. The changes in interaction between the organic and the catalyst could result into more ·OH being

quenched by the catalyst itself thus decreasing the yield of the available radicals in the bulk solution.

The final consideration for the effect of pH involves the change in bulk-phase ·OH scavenging due to changes in carbonate speciation. Elovitz *et al* (*112*) showed that, for homogeneous phase systems, lower pH would slow down the rate of ozone decay and pCBA degradation, but for the same extent of O_3 consumption, the overall pCBA degradation was the same. This is in contrast to the non-catalyst experiments here. However, Elovitz et al purposefully decarbonated the systems, thus removing the effects of carbonate scavenging. In that these systems were not expressly controlled for carbonate, if we assume that each system was at atmospheric equilibrium with respect to total inorganic carbon, an open system speciation calculation can estimate the HCO_3^- and CO_3^{2-} concentrations at pH 6.8 and 8.3, and subsequently the scavenging capacity due to those species. With the lower pH 6.8, there is lower scavenging capacity of the whole bulk-phase system due to the large decrease in carbonate scavenging (Table 4-1). Examining the ozone-alone experiments, as expected there is a slower ozone and pCBA decay at pH 6.8. However, the effect of the diminished carbonate scavenging at pH 6.8 will result in greater overall pCBA degradation compared to pH 8.3. Thus the involvement of the carbonate species leads to a different conclusion than reported by Elovitz et al (*112*). The lower pCBA removal at lower pH in presence of catalyst could be due to changes on the mineral surface at a lower pH thus resulting into more scavenging effect. Also a possible shift in ozone decay mechanism could lead to ozone still decaying in the system slowly but no pCBA removal being observed.

Figure 4- 11 Ozone decomposition kinetics at different pH conditions

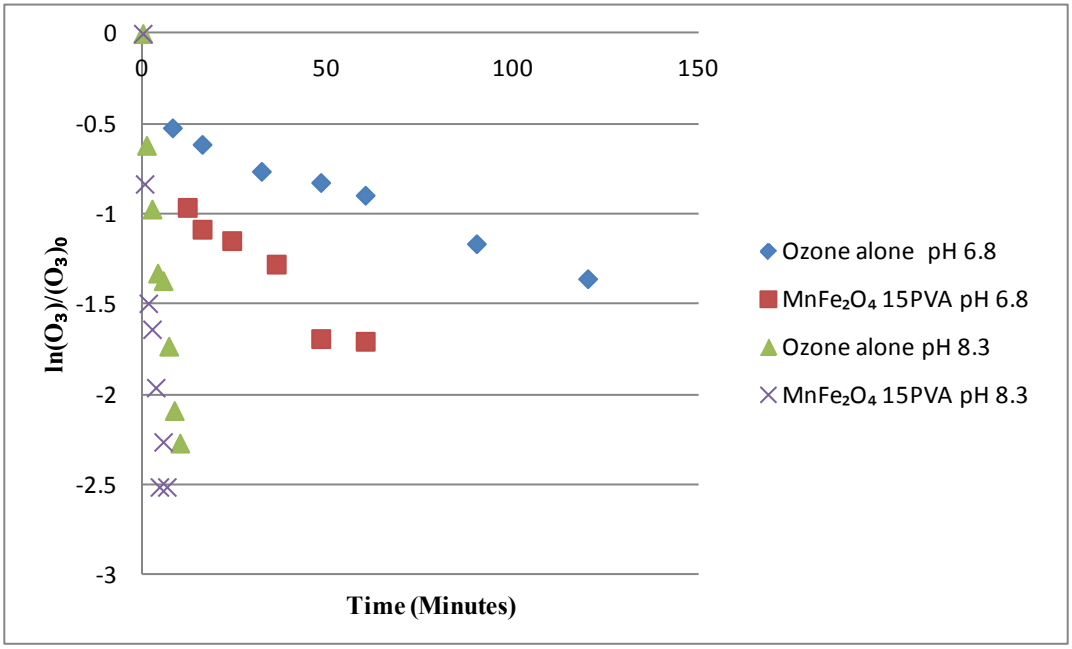

Figure 4- 12 Oxidation of pCBA as a function of ozone exposure

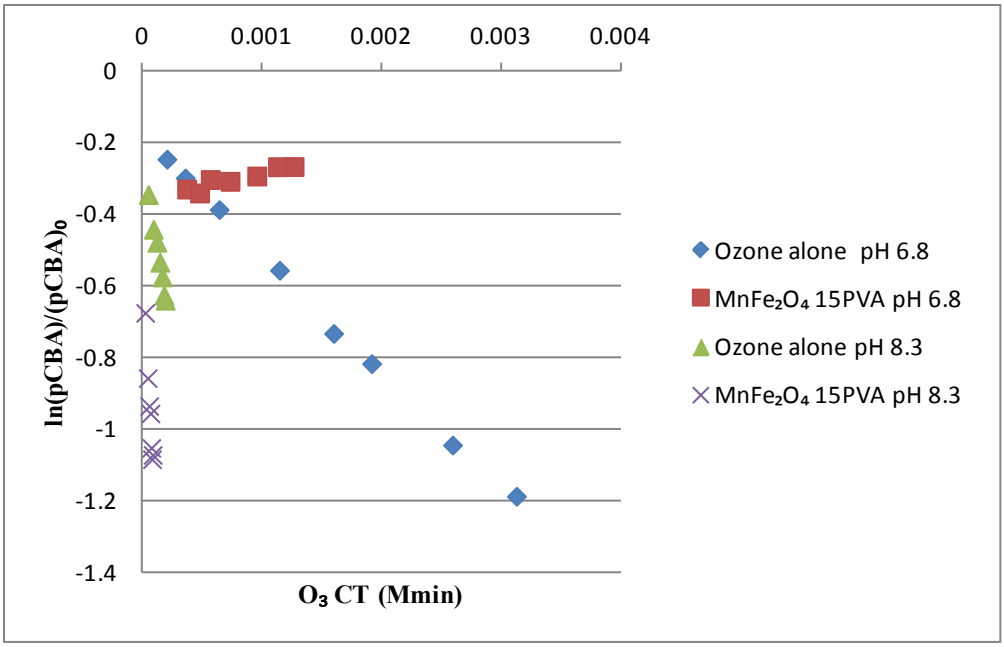

4.4 Conclusions

Manganese ferrites were demonstrated for their use as ozonation catalysts. While all catalysts dosages examined within this research enhanced hydroxyl radical production, the lowest dosage (75 mg/L) was sufficient to decay the 3 mg/L of ozone dosage to its maximum hydroxyl radical yield. However, A PVA content above 1:1.15 PVA:nitrates was required to enhance hydroxyl radical production. Hyrdroxyl radical production was increased with increasing ozone dosage, and reduced with decreasing system pH and by the presence of NOM. Pre-ozanation did not have an effect on the system at low ozone dosages, indicating potential for the reuse of the catalysts.

Ozone decay demonstrated a two phase behavior indicating that ozone is reacting with the fast reacting sites on the manganese ferrite surface leading to an observed IOD pattern. The initial reaction was followed by a second phase, which follows a pseudo-first order kinetics during the reaction of ozone with the larger concentration of slower acting surface sites. The two phase behavior finding was also observed when the ratio of Mn:Fe was increased. Higher Mn content catalysts resulted in decreased pCBA removal observed in the system due to increased ozone decomposition and likely uptake of produced hydroxyl radicals on the surface.

Overall, we did not find a direct correlation between R_{ct} and organic removal as we had expected. The data instead points to the complicated relationship between ozone exposure, R_{ct}, and organic removal. When ozone decomposition is promoted too rapidly, ozone exposures decrease and pCBA removal drops. Therefore, additional parameters other than R_{ct} should be considered when assessing catalyst performance to

enhance organic removal. Developing ozonation catalysts that balance ozone decomposition while enhancing organic removal are required to improve treatment capacity within catalytic ozonation systems.

5. CONCLUSION

5.1 Research Summary

This presented dissertation research verified that catalytic and non-catalytic heterogeneous managenese based oxidative treatment technologies can be developed to oxidize trace organics present in aqueous systems. Laboratory prepared manganese oxide demonstrated high surface area (BET surface area = 355 m^2/g) and reactivity to degrade OP in aqueous systems. The research results confirmed the hypothesis that manganese oxide removed OP from aqueous systems through oxidation. The hypothesis is supported by the reaction pathway determined through identification of the primary reaction byproduct observed in the system. Oxidation was promoted with decreasing system pH and increasing oxide concentration. Oxidation was inhibited in the presence of metal and humic acid co-solutes due to the interaction of the co-solutes with the surface.

Novel magnetic manganese ferrites were also capable of enhancing the removal of pCBA (a surrogate organic) during ozonation. Magnetic catalysts were developed in order to aid their recovery from treatment systems using a magnetic retrieval system. Magnetic manganese ferrites were prepared by mixing manganese nitrate and iron nitrate in a stoichiometric ratio of 1:2. PVA contents above 1:1 PVA:nitrate composition were required to create pure manganese ferrites. Lower PVA contents resulted in impure reaction products. The hypothesis that PVA is required to create magnetic manganese ferrites was supported based upon the full characterization of the resulting catalysts

using X-Ray diffraction (XRD) and X-ray photoelectron spectroscopy (XPS). Use of additional characterization tools, including BET surface analysis, scanning electron microscope (SEM), tunneling electron microscope (TEM), and Ultraviolet–Visible spectroscopy (UV/Vis) provided additional insight into the surface features of the developed catalysts.

The surface area of the developed manganese ferrite catalysts ranged from 39.9 to 57.4 m^2/g with carbon contents ranging from non-detectable to 0.2% by weight. XRD analysis confirmed that the resulting catalyst structures are manganese ferrites and SEM-EDX identified $Mn_{2.5}Fe_{0.5}O_4$, $MnFe_2O_4$, and $Mn_{0.5}Fe_{2.5}O_4$ as the exact form of the manganese ferrites.

The developed catalysts were successfully demonstrated to effectively remove pCBA from aqueous solutions. While the hypothesis that the magnetic manganese ferrites increase R_{ct} was true in comparison to an ozone alone system, the link between R_{ct} and organic removal between catalysts presented a more complicated system. All catalysts dosages examined within this research enhanced hydroxyl radical production. Hyrdroxyl radical production was observed to increase with increasing ozone dosage and PVA content, but reduced with decreasing system pH and by the presence of NOM. Pre-ozonation at lower dosages did not have an effect on the system, indicating potential for the reuse of the catalysts.

Overall, the created heterogeneous manganese surfaces are active sites where oxidation occurs in natural and engineered systems. The active surfaces can be successfully employed to remove trace organics in catalytic and non-catalytic water

treatment system. Manganese ferrite use in catalytic ozonation offers the promising ability to facilitate oxidation across a range of operational parameters while being easily recovered due to the catalysts magnetic properties.

5.2 Future Work

One of the lingering questions we did not address within this research is what happens if a contaminant sorbs to the surface of the manganese ferrites. We specifically picked a probe compound (pCBA) that did not sorb to the catalyst surface because we were interested in studying hydroxyl radical production. However, we can design a study to see what happens within the system if examine contaminants that are likely to interact with the catalyst via sportive processes. Selecting contaminants that weakly, moderately, and strongly sorb to the manganese ferrite surface would allow us to understand how the system could be used practically.

In a general sense I am most interested in continuing to work on catalyst synthesis and application. The development of heterogeneous catalysts with magnetic properties is of particular interest to me because of recovery opportunities. However, I have always enjoyed synthesizing novel materials in a laboratory environment and would enjoy branching out into developing other types of heterogeneous catalysts systems. Developing working knowledge of catalysts supported on organic backbones would be enjoyable and rewarding.

Over the past four years I have also developed an interest in understanding fate and transport of trace organics in the environment. I am more interested in developing treatment technologies, but within treatment technology development there are a lot of opportunities for clarifying reaction mechanisms. My background in chemical and environmental engineering will allow me to contribute within reaction pathway determination, which is generally missing from the literature that currently seems to focus more on applications.

REFERENCES

1. Post, J. E. (1999) Manganese oxide minerals: crystal structures and economic and environmental significance, *Proceedings of the National Academy of Sciences 96*, 3447-3454.
2. Stone, A. T. (1987) Reductive dissolution of manganese (III/IV) oxides by substituted phenols, *Environmental Science & Technology 21*, 979-988.
3. Laha, S., and Luthy, R. G. (1990) Oxidation of aniline and other primary aromatic amines by manganese dioxide, *Environmental Science & Technology 24*, 363-373.
4. Zhang, H., and Huang, C.-H. (2003) Oxidative transformation of triclosan and chlorophene by manganese oxides, *Environmental Science & Technology 37*, 2421-2430.
5. Zhang, H., and Huang, C.-H. (2005) Oxidative transformation of fluoroquinolone antibacterial agents and structurally related amines by manganese oxide, *Environmental Science & Technology 39*, 4474-4483.
6. Zhang, H., and Huang, C.-H. (2004) Reactivity and transformation of antibacterial N-oxides in the presence of manganese oxide, *Environmental Science & Technology 39*, 593-601.
7. Hwang, S., Lee, D.-I., Lee, C.-H., and Ahn, I.-S. (2008) Oxidation of 17[alpha]-ethinylestradiol with Mn(III) and product identification, *Journal of Hazardous Materials 155*, 334-341.

8. Jiang, L., Huang, C., Chen, J., and Chen, X. (2009) Oxidative transformation of 17β-estradiol by MnO_2 in aqueous solution, *Archives of Environmental Contamination and Toxicology 57*, 221-229.

9. Chen, W.-R., Ding, Y., Johnston, C. T., Teppen, B. J., Boyd, S. A., and Li, H. (2010) Reaction of lincosamide antibiotics with manganese oxide in aqueous solution, *Environmental Science & Technology 44*, 4486-4492.

10. Shin, J. Y., and Cheney, M. A. (2004) Abiotic transformation of atrazine in aqueous suspension of four synthetic manganese oxides, *Colloids and Surfaces A: Physicochemical and Engineering Aspects 242*, 85-92.

11. Lin, K., Liu, W., and Gan, J. (2009) Oxidative removal of bisphenol A by manganese dioxide: efficacy, products, and pathways, *Environmental Science & Technology 43*, 3860-3864.

12. Lin, K., Liu, W., and Gan, J. (2009) Reaction of tetrabromobisphenol A (TBBPA) with manganese dioxide: kinetics, products, and pathways, *Environmental Science & Technology 43*, 4480-4486.

13. Rubert, and Pedersen, J. A. (2006) Kinetics of oxytetracycline reaction with a hydrous manganese oxide, *Environmental Science & Technology 40*, 7216-7221.

14. Xu, L., Xu, C., Zhao, M., Qiu, Y., and Sheng, G. D. (2008) Oxidative removal of aqueous steroid estrogens by manganese oxides, *Water Research 42*, 5038-5044.

15. Ulrich, H. J., and Stone, A. T. (1989) The oxidation of chlorophenols adsorbed to manganese oxide surfaces, *Environmental Science & Technology 23*, 421-428.

16. Zhao, L., Yu, Z., Peng, P. a., Huang, W., Feng, S., and Zhou, H. (2006) Oxidation kinetics of pentachlorophenol by manganese dioxide, *Environmental Toxicology and Chemistry 25*, 2912-2919.

17. Zhao, L., Yu, Z., Peng, P. a., Huang, W., and Dong, Y. (2009) Oxidative transformation of tetrachlorophenols and trichlorophenols by manganese dioxide, *Environmental Toxicology and Chemistry 28*, 1120-1129.

18. Gracia, R., Aragües, J. L., and Ovelleiro, J. L. (1996) Study of the catalytic ozonation of humic substances in water and their ozonation byproducts, *Ozone: Science & Engineering 18*, 195-208.

19. Cortés, S., Sarasa, J., Ormad, P., Gracia, R., and Ovelleiro, J. L. (2000) Comparative efficiency of the systems O_3/High pH and O_3/catalyst for the oxidation of chlorobenzenes in water, *Ozone: Science & Engineering 22*, 415-426.

20. Andreozzi, R., Insola, A., Caprio, V., Marotta, R., and Tufano, V. (1996) The use of manganese dioxide as a heterogeneous catalyst for oxalic acid ozonation in aqueous solution, *Applied Catalysis A: General 138*, 75-81.

21. Ma, J., and Graham, N. J. D. (1997) Preliminary investigation of manganese-catalyzed ozonation for the destruction of atrazine, *Ozone: Science & Engineering 19*, 227-240.

22. Xiao, H., Liu, R., Zhao, X., and Qu, J. (2008) Enhanced degradation of 2,4-dinitrotoluene by ozonation in the presence of manganese(II) and oxalic acid, *Journal of Molecular Catalysis A: Chemical 286*, 149-155.

23. Xiao, H., Liu, R., Zhao, X., and Qu, J. (2008) Effect of manganese ion on the mineralization of 2,4-dichlorophenol by ozone, *Chemosphere 72*, 1006-1012.

24. Tong, S.-P., Liu, W.-P., Leng, W.-H., and Zhang, Q.-Q. (2003) Characteristics of MnO_2 catalytic ozonation of sulfosalicylic acid and propionic acid in water, *Chemosphere 50*, 1359-1364.

25. Ma, J., Sui, M.-H., Chen, Z.-L., and Wang, L.-N. (2004) Degradation of refractory organic pollutants by catalytic ozonation—activated carbon and Mn-loaded activated carbon as catalysts, *Ozone: Science & Engineering 26*, 3-10.

26. Zhao, L., Ma, J., Sun, Z.-z., and Zhai, X.-d. (2008) Catalytic ozonation for the degradation of nitrobenzene in aqueous solution by ceramic honeycomb-supported manganese, *Applied Catalysis B: Environmental 83*, 256-264.

27. Sánchez-Polo, M., Rivera-Utrilla, J., and von Gunten, U. (2006) Metal-doped carbon aerogels as catalysts during ozonation processes in aqueous solutions, *Water Research 40*, 3375-3384.

28. Andreozzi, R., Marotta, R., and Sanchirico, R. (2000) Manganese-catalysed ozonation of glyoxalic acid in aqueous solutions, *Journal of Chemical Technology & Biotechnology 75*, 59-65.

29. Andreozzi, R., Insola, A., Caprio, V., and D'Amore, M. G. (1992) The kinetics of Mn(II)-catalysed ozonation of oxalic acid in aqueous solution, *Water Research 26*, 917-921.

30. Andreozzi, R., Caprio, V., Insola, A., Marotta, R., and Tufano, V. (1998) The ozonation of pyruvic acid in aqueous solutions catalyzed by suspended and dissolved manganese, *Water Research 32*, 1492-1496.

31. Ma, J., Sui, M., Zhang, T., and Guan, C. (2005) Effect of pH on MnO_x/GAC catalyzed ozonation for degradation of nitrobenzene, *Water Research 39*, 779-786.

32. Rivas, J., Rodríguez, E., Beltrán, F. J., García-Araya, J. F., and Alvarez, P. (2001) Homogeneous catalyzed ozonation of simazine: effect of Mn(II) and Fe(II), *Journal of Environmental Science and Health, Part B 36*, 317-330.

33. Yang, L., Hu, C., Nie, Y., and Qu, J. (2009) Catalytic ozonation of selected pharmaceuticals over mesoporous alumina-supported manganese oxide, *Environmental Science & Technology 43*, 2525-2529.

34. Villaseñor, J., Reyes, P., and Pecchi, G. (2002) Catalytic and photocatalytic ozonation of phenol on MnO_2 supported catalysts, *Catalysis Today 76*, 121-131.

35. Sharma, V. K., Anquandah, G. A. K., Yngard, R. A., Kim, H., Fekete, J., Bouzek, K., Ray, A. K., and Golovko, D. (2009) Nonylphenol, octylphenol, and bisphenol-A in the aquatic environment: a review on occurrence, fate, and treatment, *Journal Of Environmental Science And Health. Part A, Toxic/Hazardous Substances & Environmental Engineering 44*, 423-442.

36. Ying, G.-G., Williams, B., and Kookana, R. (2002) Environmental fate of alkylphenols and alkylphenol ethoxylates--a review, *Environment International 28*, 215-226.

37. Renner, R. (1997) European bans on surfactant trigger transatlantic debate, *Environmental Science & Technology 31*, 316A-320A.

38. White, R., Jobling, S., Hoare, S. A., Sumpter, J. P., and Parker, M. G. (1994) Environmentally persistent alkylphenolic compounds are estrogenic, *Endocrinology 135*, 175-182.

39. Arnold, S. F., Robinson, M. K., Notides, A. C., Guillette, L. J., Jr., and McLachlan, J. A. (1996) A yeast estrogen screen for examining the relative exposure of cells to natural and xenoestrogens, *Environmental Health Perspectives 104*, 544-548.

40. Gronen, S., Denslow, N., Manning, S., Barnes, S., Barnes, D., and Brouwer, M. (1999) Serum Vitellogenin Levels and Reproductive Impairment of Male Japanese Medaka (Oryzias latipes) Exposed to 4-tert-Octylphenol, *Environmental Health Perspectives 107*, 385-390.

41. Blake, C. A., and Boockfor, F. R. (1997) Chronic administration of the environmental pollutant 4-tert-octylphenol to adult male rats interferes with the secretion of luteinizing hormone, follicle-stimulating hormone, prolactin, and testosterone, *Biology of Reproduction 57*, 255-266.

42. Sweeney, T., Nicol, L., Roche, J. F., and Brooks, A. N. (2000) Maternal exposure to octylphenol suppresses ovine fetal follicle-stimulating hormone secretion, testis size, and sertoli cell number, *Endocrinology 141*, 2667-2673.

43. Mikkilä, T. F. M., Toppari, J., and Paranko, J. (2006) Effects of neonatal exposure to 4-tert-octylphenol, diethylstilbestrol, and flutamide on steroidogenesis in Infantile Rat Testis, *Toxicological Sciences 91*, 456-466.

44. Yoshida, M., Katsuda, S.-i., Takenaka, A., Watanabe, G., Taya, K., and Maekawa, A. (2001) Effects of neonatal exposure to a high-dose p-tert-octylphenol on the male reproductive tract in rats, *Toxicology Letters 121*, 21-33.

45. Sharpe, R. M., Fisher, J. S., Millar, M. M., Jobling, S., and Sumpter, J. P. (1995) Gestational and lactational exposure of rats to xenoestrogens results in reduced testicular size and sperm production, *Environmental Health Perspectives 103*, 1136-1143.

46. Gray, M. A., Teather, K. L., and Metcalfe, C. D. (1999) Reproductive success and behavior of Japanese medaka (Oryzias latipes) exposed to 4-tert-octylphenol, *Environmental Toxicology and Chemistry 18*, 2587-2594.

47. Ahel, M., and Giger, W. (1993) Partitioning of alkylphenols and alkylphenol polyethoxylates between water and organic solvents, *Chemosphere 26*, 1471-1478.

48. Ahel, M., and Giger, W. (1993) Aqueous solubility of alkylphenols and alkylphenol polyethoxylates, *Chemosphere 26*, 1461-1470.

49. Ning, B., Graham, N. J. D., and Zhang, Y. (2007) Degradation of octylphenol and nonylphenol by ozone - Part I: Direct reaction, *Chemosphere 68*, 1163-1172.

50. Ning, B., Graham, N. J. D., and Zhang, Y. (2007) Degradation of octylphenol and nonylphenol by ozone - Part II: Indirect reaction, *Chemosphere 68*, 1173-1179.

51. Neamtu, M., Popa, D.-M., and Frimmel, F. H. (2009) Simulated solar UV-irradiation of endocrine disrupting chemical octylphenol, *Journal of Hazardous Materials 164*, 1561-1567.

52. Mazellier, P., and Leverd, J. (2003) Transformation of 4-tert-octylphenol by UV irradiation and by an H_2O_2/UV process in aqueous solution, *Photochemical & Photobiological Sciences 2*, 946-953.

53. Brand, N., Mailhot, G., Sarakha, M., and Bolte, M. (2000) Primary mechanism in the degradation of 4-octylphenol photoinduced by Fe(III) in water-acetonitrile solution, *Journal of Photochemistry and Photobiology A: Chemistry 135*, 221-228.

54. Yamazaki, S., Mori, T., Katou, T., Sugihara, M., Saeki, A., and Tanimura, T. (2008) Photocatalytic degradation of 4-tert-octylphenol in water and the effect of peroxydisulfate as additives, *Journal of Photochemistry and Photobiology A: Chemistry 199*, 330-335.

55. Anquandah, G. A. K., and Sharma, V. K. (2009) Oxidation of octylphenol by ferrate(VI), *Journal Of Environmental Science And Health. Part A, Toxic/Hazardous Substances & Environmental Engineering 44*, 62-66.

56. Zhao, L., Yu, Z., Peng, P., Huang, W., Feng, S., and Zhou, H. (2006) Oxidation kinetics of pentachlorophenol by manganese dioxide, *Environ. Toxicol. Chem. 25*, 2912-2919.

57. Klausen, J., Haderlein, S. B., and Schwarzenbach, R. P. (1997) Oxidation of substituted anilines by aqueous MnO_2: effect of co-solutes on initial and quasi-steady-state kinetics, *Environmental Science & Technology 31*, 2642-2649.

58. Rudder, J. D., Wiele, T. V. D., Dhooge, W., Comhaire, F., and Verstraete, W. (2004) Advanced water treatment with manganese oxide for the removal of 17[alpha]-ethynylestradiol (EE2), *Water Research 38*, 184-192.

59. Daniel Sheng, G., Xu, C., Xu, L., Qiu, Y., and Zhou, H. (2009) Abiotic oxidation of 17[beta]-estradiol by soil manganese oxides, *Environmental Pollution 157*, 2710-2715.

60. Murray, J. W. (1974) The surface chemistry of hydrous manganese dioxide, *Journal of Colloid and Interface Science 46*, 357-371.

61. Yost, E. C., and Anderson, M. A. (1984) Absence of phenol adsorption on goethite, *Environmental Science & Technology 18*, 101-106.

62. Connors, K. A. (1990) *Chemical Kinetics: The Study of Reaction Rates in Solution*, Wiley-VCH.

63. Anquandah, G. A. K., and Sharma, V. K. (2008) Oxidation of octylphenol by ferrate(VI), *Journal of Environmental Science and Health, Part A 44*, 62-66.

64. Haun, J. B., Yoon, T.-J., Lee, H., and Weissleder, R. (2010) Magnetic nanoparticle biosensors, *Wiley Interdisciplinary Reviews: Nanomedicine and Nanobiotechnology 2*, 291-304.

65. Ahmed, S., Ogale, S., Papaefthymiou, G., Ramesh, R., and , and Kofinas, P. (2002) Magnetic properties of $CoFe_2O_4$ nanoparticles synthesized through a block copolymer nanoreactor route *Appl. Phys. Lett. 80*, 1616-1618.

66. Brigger, I., Dubernet, C., and Couvreur, P. (2012) Nanoparticles in cancer therapy and diagnosis, *Advanced Drug Delivery Reviews 64, Supplement*, 24-36.

67. Goodarz Naseri, M., Saion, E. B., Ahangar, H. A., Hashim, M., and Shaari, A. H. (2011) Synthesis and characterization of manganese ferrite nanoparticles by thermal treatment method, *Journal of Magnetism and Magnetic Materials 323*, 1745-1749.

68. Amighian, J., Mozaffari, M., and Nasr, B. (2006) Preparation of nano-sized manganese ferrite ($MnFe_2O_4$) via coprecipitation method, *Physica Status Solidi (C) 3*, 3188-3192.

69. Li, J., Yuan, H., Li, G., Liu, Y., and Leng, J. (2010) Cation distribution dependence of magnetic properties of sol–gel prepared $MnFe_2O_4$ spinel ferrite nanoparticles, *Journal of Magnetism and Magnetic Materials 322*, 3396-3400.

70. Zhang, D., Zhang, X., Ni, X., Song, J., and Zheng, H. (2006) Low-temperature fabrication of $MnFe_2O_4$ octahedrons: Magnetic and electrochemical properties, *Chemical Physics Letters 426*, 120-123.

71. Nishamol, K. (2002) Surface properties and catalytic activity of manganese ferrospinels, In *Department of Applied Chemistry*, Cochin University of Science And Technology, Kochi, India.

72. Rozman, M., and Drofenik, M. (1995) Hydrothermal synthesis of manganese zinc ferrites, *Journal of the American Ceramic Society 78*, 2449-2455.

73. Christmann, H., and Teel, P. (1975) Manganese ferrite catalyzed oxidative dehydrogenation Petro-Tex Chemical Corporation, United States.

74. Oliveira, L. C. A., Lago, R. M., Rios, R. V. R. A., Augusti, R., Sousa, P. P., Mussel, W. N., and Fabris, J. D. (2000) The effect of Mn substitution on the catalytic properties of ferrites, In *Studies in Surface Science and Catalysis* (Avelino Corma, F. V. M. S. M., and José Luis, G. F., Eds.), pp 2165-2170, Elsevier, Spain.

75. Lahiri, P., and Sengupta, S. (1995) Physico-chemical properties and catalytic activities of the spinel series $Mn_xFe_{3-x}O_4$ towards peroxide decomposition, *J. Chem. Soc., Faraday Trans., 91*, 3489-3494.

76. Menini, L., Pereira, M. C., Parreira, L. A., Fabris, J. D., and Gusevskaya, E. V. (2008) Cobalt- and manganese-substituted ferrites as efficient single-site heterogeneous catalysts for aerobic oxidation of monoterpenic alkenes under solvent-free conditions, *Journal of Catalysis 254*, 355-364.

77. Mohapatra, J., Mitra, A., Bahadur, D., and Aslam, M. (2013) Surface controlled synthesis of MFe2O4 (M= Mn, Fe, Co, Ni and Zn) nanoparticles and their magnetic characteristics, *CrystEngComm 15*, 524-532.

78. Zeng, H., Rice, P. M., Wang, S. X., and Sun, S. (2004) Shape-controlled synthesis and shape-induced texture of $MnFe_2O_4$ nanoparticles, *Journal of the American Chemical Society 126*, 11458-11459.

79. Liu, G., Han, C., Pelaez, M., Zhu, D., Liao, S., Likodimos, V., Ioannidis, N., Kontos, A. G., Falaras, P., and Dunlop, P. S. (2012) Synthesis, characterization and photocatalytic evaluation of visible light activated C-doped TiO_2 nanoparticles, *Nanotechnology 23*, 294003.

80. Phani, A., Manorama, S., and Rao, V. (2000) The nature of surface behavior of tin oxide doped sensors: X-ray photoelectron spectroscopy studies before and after exposure to liquid petroleum gas, *Journal of Physics and Chemistry of Solids 61*, 985-993.

81. Yamashita, T., and Hayes, P. (2008) Analysis of XPS spectra of Fe^{2+} and Fe^{3+} ions in oxide materials, *Applied Surface Science 254*, 2441-2449.

82. Nesbitt, H., and Banerjee, D. (1998) Interpretation of XPS Mn (2p) spectra of Mn oxyhydroxides and constraints on the mechanism of MnO_2 precipitation, *American Mineralogist 83*, 305-315.

83. Hu, J., Lo, I. M., and Chen, G. (2005) Fast removal and recovery of Cr (VI) using surface-modified jacobsite ($MnFe_2O_4$) nanoparticles, *Langmuir 21*, 11173-11179.

84. Beltrán, F. J., Rivas, F. J., and Montero-de-Espinosa, R. (2005) Iron type catalysts for the ozonation of oxalic acid in water, *Water Research 39*, 3553-3564.

85. Pi, Y., Ernst, M., and Schrotter, J.-C. (2003) Effect of Phosphate Buffer upon CuO/Al2O3 and Cu (II) Catalyzed Ozonation of Oxalic Acid Solution, *Ozone: Science & Engineering 25*, 393-397.

86. El-Raady, A. A. A., and Nakajima, T. (2005) Decomposition of Carboxylic Acids in Water by O_3, O_3/H_2O_2, and O_3/Catalyst, *Ozone: Science & Engineering 27*, 11-18.

87. Beltrán, F. J., Rivas, F. J., and Montero-de-Espinosa, R. (2003) Ozone-Enhanced Oxidation of Oxalic Acid in Water with Cobalt Catalysts. 1. Homogeneous Catalytic Ozonation, *Industrial & Engineering Chemistry Research 42*, 3210-3217.

88. Leitner, N. K. V., Delanoë, F., Acedo, B., and Legube, B. (2000) Reactivity of various Ru/CeO2 catalysts during ozonation of succinic acid aqueous solutions, *New J. Chem. 24*, 229-233.

89. Gracia, R., Cortes, S., Sarasa, J., Ormad, P., and Ovelleiro, J. (2000) Heterogeneous catalytic ozonation with supported titanium dioxide in model and natural waters, *Ozone: Science & Engineering 22*, 461-471.

90. Pines, D. S., and Reckhow, D. A. (2003) Solid Phase Catalytic Ozonation Process for the Destruction of a Model Pollutant, *Ozone: Science & Engineering 25*, 25-39.

91. Ping, T. S., Hua, L. W., Qing, Z. J., and Nan, C. C. (2002) Catalytic ozonation of sulfosalicylic acid, *Ozone: Science & Engineering 24*, 117-122.

92. Yunrui, Z., Wanpeng, Z., Fudong, L., Jianbing, W., and Shaoxia, Y. (2007) Catalytic activity of Ru/Al_2O_3 for ozonation of dimethyl phthalate in aqueous solution, *Chemosphere 66*, 145-150.

93. Ernst, M., Lurot, F., and Schrotter, J.-C. (2004) Catalytic ozonation of refractory organic model compounds in aqueous solution by aluminum oxide, *Applied Catalysis B: Environmental 47*, 15-25.

94. Faria, P. C. C., Órfão, J. J. M., and Pereira, M. F. R. (2008) A novel ceria–activated carbon composite for the catalytic ozonation of carboxylic acids, *Catalysis Communications 9*, 2121-2126.

95. Kasprzyk-Hordern, B., Andrzejewski, P., Dąbrowska, A., Czaczyk, K., and Nawrocki, J. (2004) MTBE, DIPE, ETBE and TAME degradation in water using perfluorinated phases as catalysts for ozonation process, *Applied Catalysis B: Environmental 51*, 51-66.

96. Park, J.-S., Choi, H., and Cho, J. (2004) Kinetic decomposition of ozone and para-chlorobenzoic acid (pCBA) during catalytic ozonation, *Water Research 38*, 2285-2292.

97. Valdés, H., and Zaror, C. A. (2006) Heterogeneous and homogeneous catalytic ozonation of benzothiazole promoted by activated carbon: Kinetic approach, *Chemosphere 65*, 1131-1136.

98. Kasprzyk-Hordern, B., Raczyk-Stanisławiak, U., Świetlik, J., and Nawrocki, J. (2006) Catalytic ozonation of natural organic matter on alumina, *Applied Catalysis B: Environmental 62*, 345-358.

99. Zhang, T., and Ma, J. (2008) Catalytic ozonation of trace nitrobenzene in water with synthetic goethite, *Journal of Molecular Catalysis A: Chemical 279*, 82-89.

100. Tyupalo, N. F., and Yakobi, Y. A. (1980) The reactions of ozone with manganese(II) and manganese(III) ions in sulfuric acid, *Russian Journal of Inorganic Chemistry 25*, 865-868.

101. Martins, R. C., and Quinta-Ferreira, R. M. (2009) Manganese-based catalysts for the catalytic remediation of phenolic acids by ozone, *Ozone: Science & Engineering 31*, 402-411.

102. Sui, M., Xing, S., Sheng, L., Huang, S., and Guo, H. (2012) Heterogeneous catalytic ozonation of ciprofloxacin in water with carbon nanotube supported manganese oxides as catalyst, *Journal of Hazardous Materials 227–228*, 227-236.

103. Rosal, R., Gonzalo, M. S., Rodríguez, A., and García-Calvo, E. (2010) Catalytic ozonation of fenofibric acid over alumina-supported manganese oxide, *Journal of Hazardous Materials 183*, 271-278.

104. Lv, A., Hu, C., Nie, Y., and Qu, J. (2010) Catalytic ozonation of toxic pollutants over magnetic cobalt and manganese co-doped γ-Fe2O3, *Applied Catalysis B: Environmental 100*, 62-67.

105. Ren, Y., Dong, Q., Feng, J., Ma, J., Wen, Q., and Zhang, M. (2012) Magnetic porous ferrospinel $NiFe_2O_4$: A novel ozonation catalyst with strong catalytic property for degradation of di-n-butyl phthalate and convenient separation from water, *Journal of Colloid and Interface Science 382*, 90-96.

106. Elovitz, M. S., and von Gunten, U. (1999) Hydroxyl Radical/Ozone Ratios During Ozonation Processes. I. The Rct Concept, *Ozone: Science & Engineering 21*, 239-260.

107. Desai, I., Mills, M., Nadagouda, M., Elovitz, M., and Boulanger, B. (2013) Characterization of Manganese Ferrites Synthesized Using a Combustion Method, *TechConnect World*, Washington D.C.

108. Desai, I., and Mills, M. (2011) Advanced oxidation of some chemicals of concern using catalytic ozonation, (USEPA/ORD/NRMRL/LRPCD/SSMB, Ed.), Cincinnati.

109. McCurry, D., Speth, T., and Pressman, J. (2012) Lyophilization and Reconstitution of Reverse-osmosis concentrated natural organic matter from a drinking water source, *Journal of Environmental Engineering 138*, 402-410.

110. Flyunt, R., Leitzke, A., Mark, G., Mvula, E., Reisz, E., Schick, R., and von Sonntag, C. (2003) Determination of •OH, O2•-, and hydroperoxide yields in ozone reactions in aqueous solution, *The Journal of Physical Chemistry B 107*, 7242-7253.

111. Evans, C. D., Monteith, D. T., and Cooper, D. M. (2005) Long-term increases in surface water dissolved organic carbon: observations, possible causes and environmental impacts, *Environmental Pollution 137*, 55-71.

112. Stiff, M. J. (1971) Copper/bicarbonate equilibria in solutions of bicarbonate ion at concentrations similar to those found in natural water, *Water Research 5*, 171-176.

113. Elovitz, M. S., von Gunten, U., and Kaiser, H.-P. (2000) Hydroxyl radical/ozone ratios during ozonation processes. II. the effect of temperature, pH, alkalinity, and DOM properties, *Ozone: Science & Engineering 22*, 123-150.

114. Buffle, M.-O., Schumacher, J., Meylan, S., Jekel, M., and von Gunten, U. (2006) Ozonation and advanced oxidation of wastewater: effect of O_3 dose, pH, DOM and HO•-scavengers on ozone decomposition and HO• generation, *Ozone: Science & Engineering 28*, 247-259.

115. Buffle, M.-O., and von Gunten, U. (2006) Phenols and amine induced HO• generation during the initial phase of natural water ozonation, *Environmental Science & Technology 40*, 3057-3063.

116. Rosenfeldt, E. J., Linden, K. G., Canonica, S., and von Gunten, U. (2006) Comparison of the efficiency of OH radical formation during ozonation and the advanced oxidation processes O_3/H_2O_2 and UV/H_2O_2, *Water Research 40*, 3695-3704.

117. Sauleda, R., and Brillas, E. (2001) Mineralization of aniline and 4-chlorophenol in acidic solution by ozonation catalyzed with Fe^{2+} and UVA light, *Applied Catalysis B: Environmental 29*, 135-145.

118. Nawrocki, J., and Kasprzyk-Hordern, B. (2010) The efficiency and mechanisms of catalytic ozonation, *Applied Catalysis B: Environmental 99*, 27-42.

119. Costa, R. C. C., Lelis, M. F. F., Oliveira, L. C. A., Fabris, J. D., Ardisson, J. D., Rios, R. R. V. A., Silva, C. N., and Lago, R. M. (2006) Novel active heterogeneous Fenton system based on $Fe_{3-x}M_xO_4$ (Fe, Co, Mn, Ni): The role of

M^{2+} species on the reactivity towards H_2O_2 reactions, *Journal of Hazardous Materials 129*, 171-178.